

A denoising algorithm for surface EMG decomposition

Robert I. Kumar, B.Kin

A thesis submitted in partial completion of the requirements for the degree of Master of
Science in Applied Health Sciences (Kinesiology)

Supervised by Dr. David A. Gabriel, PhD

Faculty of Applied Health Sciences

Brock University

St. Catharines, ON

Robert Kumar © 2019

TABLE OF CONTENTS

ABSTRACT	I
ACKNOWLEDGEMENTS	II
LIST OF FIGURES	IV
LIST OF TABLES	VIII
CHAPTER 1: Introduction	1
1.1 Development of the Problem	1
1.2 Statement of the Problem	4
1.3 Purpose of the Research	5
1.4 Approach to the Problem	5
1.5 Hypotheses	6
1.6 Significance of the Study	7
1.7 Assumptions.....	8
1.8 Delimitations	9
1.9 Limitations	9
CHAPTER 2: Review of the Related Literature	11
2.1 Anatomy.....	11
2.1.1 Flexor Carpi Radialis	11
2.2 Surface Electromyography.....	14
2.2.1 Muscle Fiber Action Potential	14
2.2.2 Motor Unit Action Potential	16
2.2.3 Motor Unit Action Potential Train and Interference Pattern	18
2.3 Variability in MUP Shape.....	20
2.3.1 Jiggle	20
2.3.2 Variance Ratio.....	22
2.3.3 Signal-to-Noise Ratio.....	25
2.4 Motor Unit Behaviour	27
2.4.1 Henneman’s Size Principle	27
2.4.2 Phenomenon Known as Onion Skin Scheme.....	27
2.5 Muscle Force Regulation	32
2.5.1 Recruitment Range.....	32
2.5.2 Common Drive.....	33
2.5.3 Synchronization	34
2.5.4 Doublets	34

2.6	Factors That Affect the Surface Electromyographic Signal	37
2.6.1	Subcutaneous Tissue	37
2.6.2	Architectural Properties of Muscle	39
2.6.3	Muscle Fiber Conduction Velocity	40
2.6.4	Cross-talk	42
2.6.5	Electrode Placement.....	46
2.6.6	Movement Artifact.....	49
2.6.7	Temperature and EMG.....	49
2.6.8	Muscular Fatigue.....	51
2.7	Electromyographic Decomposition.....	53
2.7.1	Delsys Decomposition EMG System.....	54
2.7.2	High-density sEMG Decomposition.....	59
2.7.3	Decomposition-based Quantitative EMG	62
2.8	Validation Techniques	67
2.8.1	Reconstruct & Test Method	67
2.8.2	Two-Source Method of Validation	70
2.8.3	Spike Triggered Averaging.....	71
2.8.4	The Gap Statistic.....	72
2.8.5	Debate on the Accuracy and Validation of the dEMG System.....	73
CHAPTER 3: Methods.....		78
3.1	Participants.....	78
3.2	Experimental Task	78
3.3	Apparatus and Instrumentation	79
3.4	Data Reduction.....	81
3.5	Editing of Motor Unit Potential Trains	83
3.6	Statistics	85
CHAPTER 4: Results		90
CHAPTER 5: Discussion.....		94
5.1	Conclusion	100
5.2	Future Work	100
References		102
Appendix 1 – Piloting the Denoising Algorithm.....		134
Appendix 2 – Ethics Clearance		171

ABSTRACT

The goal of the present thesis was to investigate a novel motor unit potential train (MUPT) editing routine, based on decreasing the variability in shape (variance ratio, VR) of the MUP ensemble. Decomposed sEMG data from 20 participants at 60% MVC of wrist flexion was used. There were two levels of denoising (relaxed and strict) criteria for removing discharge times associated with waveforms that did not decrease the VR and increase its signal-to-noise ratio (SNR) of the MUP ensemble. The peak-to-peak amplitude and the duration between the positive and negative peaks for the MUP template were dependent on the level of denoising (p 's < 0.05). The error-filtered estimation (EFE) algorithm was used to calculate the inter-discharge interval (IDI) for the denoised MUPTs. In total, VR decreased 24.88% and the SNR increased 6.0% (p 's < 0.05). The standard error of estimate (3.2 versus 3.69%) in mean IDI before and after denoising using the relaxed criteria, was very similar ($p > 0.05$). The same was true between denoising criteria ($p > 0.05$). Editing the MUPT based on MUP shape resulted in significant differences in measures extracted from the MUP template, with trivial difference between the standard error of estimate for mean IDIs between the complete and denoised MUPTs.

ACKNOWLEDGEMENTS

Few are provided the opportunities that I have been *lucky* enough to have. Words cannot sum the gratitude that is owed to Dr. David Gabriel. You have been unrelenting in your support and mentorship for me over the past three and a half years. Without you, none of this would be possible. I have learned plenty about the field of electromyography, but most importantly I have learned about what is required to grow as a researcher. Dr. Gabriel, you have consistently shown me patience, taught me the importance of independence and most importantly, shown me the articulate nature of science. These are lessons that I will carry with me forward into my future in science. Thank you, Dr. Gabriel – for everything. I am hopeful that we will continue to work on projects together while I am at Brock.

To my committee members, Dr. Anita Christie and Dr. Michael Holmes, thank you for your contributions to my thesis. Your comments, questions and criticisms are greatly appreciated. The great contribution from Dr. Dan Stashuk must also not go unmentioned, as he was involved in this project from very early on, and the project would not have been possible otherwise – thank you for everything.

To my science mates: Dr. Greig Inglis, for your contributions to my writing, Dr. Lara Green, for helping me improve my teaching, Dr. Gary Hodges, for your honesty and perspective and of course, Matt Mallette, for showing me the way to research and continually pushing me to strive to be better. You have all shown me what it means to improve and become the best version of ourselves. Thank you.

I must extend a massive thanks to some of the greatest gentlemen I've been fortunate enough to get to know: Brad Baranowski, Garrick Forman, Tom Hoshizaki,

Alex Watson, Kyle Johnson, James Hall and Jake Scott. I have had the pleasure of getting to know all of you and learning from each of you. I hope to stay in touch and that our paths intersect in the future. Brad and Garrick, I am looking forward to the next few years at Brock with you both as we conquer our PhDs!

To my family: my mother, my father, my sister and my grandparents. Somehow, you've managed to all deal with me talking about science and accepted that this is the route that I want to take. Your support and love help keep me going every single day. Thank goodness you guys accept this path I've taken, since it truly has barely begun. I love you all.

To the one who I love so dearly, Bridget Baskett. You've seen the best and absolute worst of me over the past three years, and yet you still stand by me. Your kind heart, your unique perspective, and the amount you've cared for me when I needed it most will always be appreciated. Thank you for listening to me practice my presentations, for watching me mark 4P10 Labs, listening to me yell at MATLAB, and for always believing in me. I love you.

There are many others I want to thank, but I must say a collective *Thank You*.

LIST OF FIGURES

- Figure 1. Muscles of the lower arm, the flexor carpi radialis (FCR) is highlighted. Luttgens, K., Wells, K. (1982). *Kinesiology: scientific basis of human motion. Saunders College Pub.* 13
- Figure 2. Electrochemical events at the cellular level of a muscle fiber and the ensuing waveform as seen from electrode recordings. Loeb, G. E., Gans, C. (1986). *Electromyography for experimentalists. University of Chicago Press.* 15
- Figure 3. One motor unit is depicted here with only 6 of its muscle fibers. The signal that propagates along the muscle fiber is recorded by an electrode in a unipolar or bipolar fashion. Griep, P. A. M., Boon, K. L., Stegeman, D. F. (1978). A study of the motor unit action potential by means of computer simulation. *Biological cybernetics.* 17
- Figure 4. Trains of motor unit action potentials (top) summate together to make up the recorded EMG signal (bottom). Basmajian, J. V., De Luca, C. J. (1985). *Muscles alive: their function revealed by electromyography. Williams & Wilkins.* 19
- Figure 5. Difference in jiggle can be seen visually here, as depicted by the variability in the overlaid MUAPs. In a normal motor unit, there is a low CAD and high CCC value. In the amyotrophic lateral sclerosis (ALS) motor unit, the CAD is much higher and the CCC is substantially lower. Stålberg, E. V., Sonoo, M. (1994). Assessment of variability in the shape of the motor unit action potential, the “jiggle” at consecutive discharges. *Muscle & Nerve.* 21
- Figure 6. M-waves from the biceps brachii overlaid from two different subjects. One is depicting a low VR (0.02) and the other a higher VR (0.62). Calder, K. M., Hall, L., Lester, S. M., Inglis, J. G., Gabriel, D. A. (2005). Reliability of the biceps brachii M-wave. *Journal of NeuroEngineering and Rehabilitation.* 24
- Figure 7. Two samples of motor unit shimmer plots (thin grey lines) with their respective mean templates (black line): (a) clear, unambiguous event against background noise (as denoted by the clear peak and thick band around the mean), (b) an unclear event against background noise (noticeable by the dispersion of the shimmer in the background and unclear template). Both examples have dashed vertical lines to denote where the 15 ms of signal and 5+5 ms of noise is calculated from. 26
- Figure 8. Coloured lines: Mean firing rate of individual motor units identified in the first dorsal interosseous muscle relating to the Y-axis. Black line: force paradigm relating to the right Y-axis. All events are bound by time. De Luca, C. J., Adam, A., Wotiz, R., Gilmore, D. L., Nawab, S. H. (2006). Decomposition of Surface EMG Signals. *Journal of Neurophysiology.* 29
- Figure 9. Motor units are recruited in a hierarchical manner with an increase in force output. The lowest threshold motor units are recorded first and the highest threshold motor units are recruited last. The max tension that a motor unit can generate occurs after

- a short period of time after recruitment. Motor units will summate to generate maximal muscle tension. Winter, D. A. (1990). *Biomechanics and motor control of human movement* (2nd Ed.). *John Wiley & Sons*. 30
- Figure 10. Catch-like properties of muscle as shown through 3 separate situations. In A and B the muscle is stimulated by a doublet pulse immediately. In B, a single drop-out of a pulse reduced the force. In C, an additional firing occurred immediately after another to enhance the force. Kamen G., Gabriel, D.A. (2010). *Essentials of Electromyography. Human Kinetics*. 36
- Figure 11. Double-differential amplification, where electrodes are in-line and V_a and V_b are differentiated, then V_b and V_c are differentiated. IA_1 and IA_2 are the single differentiations and IA_3 is the differentiation of IA_1 and IA_2 , therefore IA_3 is a double differential. Guerrero, F. N., Spinelli, E. M., Haberman, M. A. (2016). *IEEE Transactions on Biomedical Circuits and Systems*. Figure 1, page 787. 45
- Figure 12. This is an example of an EMG signal that was recorded with a linear electrode array. The electrode array was placed longitudinally with the vastus medialis muscle and it was placed over the innervation zone. There is a clear attenuation of signal amplitude (A), and the phases are reversed for B1 and B2. Rainoldi, A., Melchiorri, G., Caruso, I. (2004). A method for positioning electrodes during surface EMG recordings in lower limb muscles. 48
- Figure 13. Visual depiction of the surface EMG decomposition algorithm. De Luca, C. J., Adam, A., Wotiz, R., Gilmore, L. D., Nawab, S. H. (2006). Decomposition of surface EMG signals. *Journal of Neurophysiology*. 56
- Figure 14. Diagram of the PD-IPUS and PD-IGAT stages of MU decomposition. The PD-IPUS is used for template creation, template matching and updating templates. The PD-IGAT is used to discriminate MUPs that have led to a superposition in the signal. Nawab, S. H., Chang, S., De Luca, C. J. (2010). High-yield decomposition of surface EMG signals. *Clinical Neurophysiology*. 57
- Figure 15. Sample of motor unit firing statistics as observed from the dEMG system. From top to bottom: MUDR of each identified MU respectively; inter-pulse interval for each identified MU; the mean firing rate for each identified; templates of the MUs identified from the decomposition. De Luca, C. J., Adam, A., Wotiz, R., Gilmore, L. D., Nawab, S. H. (2006). Decomposition of surface EMG signals. *Journal of Neurophysiology*. 58
- Figure 16. A 192-electrode high-density sEMG grid with an inter-electrode distance of 10 mm. Pan, L., Zhang, D., Jiang, N., Sheng, X., Zhu, X. (2015). Improving robustness against electrode shift of high density EMG for myoelectric control through common spatial patterns. *Journal of NeuroEngineering and Rehabilitation*. 60
- Figure 17. Surface EMG signals that was recorded from the biceps brachii using a 61-electrode grid array. Each individual waveform within each column represents a double-differentially amplified signal. Gazzoni, M., Farina, D., Merletti, R. (2004). A new

method for the extraction and classification of single motor unit action potentials from surface EMG signals. *Journal of Neuroscience Methods*. 61

Figure 18. (a) Manually decomposed EMG signals with the (a) MUP template, (b) the MUP shimmer plot and (c) the firing times for the respective firings. Stashuk, D. W. (2001). EMG signal decomposition: how can it be accomplished and used? *Journal of Electromyography and Kinesiology*. 65

Figure 19. (b) Clustering algorithm results, with the (a) MUP template, (b) the MUP shimmer plot and (c) the firing times for the respective firings. Stashuk, D. W. (2001). EMG signal decomposition: how can it be accomplished and used? *Journal of Electromyography and Kinesiology*. 66

Figure 20. Decompose-synthesize-decompose-compare visual outline. The sEMG signal is decomposed into its constituent MUAPTs. The decomposed MUAPTs are then resynthesized and Gaussian noise equal to the residual from the first decomposition is redistributed across the signal. The resynthesized signal is then decomposed again and is compared to the original decomposition. Nawab, S. H., Chang, S., De Luca, C. J. (2010). High-yield decomposition of surface EMG signals. *Clinical Neurophysiology*. 69

Figure 21. Comparison of the MUs obtained through decomposition of the original sEMG signal and the reconstructed signal. *Top*: the individual MUs that were identified in both decompositions. *Bottom*: a short epoch of the firings from the detected MUs, errors were marked with an oval. De Luca, C. J., Hostage, E. C. (2010). Relationship between firing rate and recruitment threshold of motoneurons in voluntary isometric contractions. 75

Figure 22. Participant seated comfortably their hand comfortably placed in the jig. The dEMG sensor is secured to the skin surface over the FCR with tape. The force paradigm is viewable on the monitor with direct feedback of the participant's applied force. 80

Figure 23. The shimmer plots. The gray waveforms are the individual motor unit (MU) potentials with the motor unit potential train. The thick black line is the MU template for each channel. The total number of discharges is presented in the top right corner of channel 1. The variance ratio (VR) and signal-to-noise-ratio (SNR) are also presented in the top left corner, and they represent the mean across channels. 82

Figure 24. Representative example of denoising a motor unit potential train (MUPT) using relaxed criteria. The top panels are the shimmer plots, one for each channel. The shimmer plots include the MU templates calculated before (black) and after (red) denoising. The waveforms removed from each channel are plotted immediately below it, indicating the percent decrease in discharge times (Δ FIR). Beneath the residuals plots are the frequency-distributions curves of the inter-discharge intervals (IDIs) before (left) and after (right) denoising. The variance ratio (VR), the signal-to-noise ratio (SNR), and the cross-correlation coefficient (R_{xy}) for the MU template before and after denoising. The bottom graphs plot the isometric wrist flexion force-time curves and instantaneous motor unit discharge rate (MUDR) before (left) and after (right) denoising. After denoising, the

mean and standard deviation of the IDIs was calculated using the Error Filtered Estimation algorithm. 87

Figure 25. Representative example of denoising a motor unit potential train (MUPT) using strict criteria. The top panels are the shimmer plots, one for each channel. The shimmer plots include the MU templates calculated before (black) and after (red) denoising. The waveforms removed from each channel are plotted immediate below it, indicating the percent decrease in discharge times (Δ FIR). Beneath the residuals plots are the frequency-distributions curves of the inter-discharge intervals (IDIs) before (left) and after (right) denoising. The variance ratio (VR), the signal-to-noise ratio (SNR), and the cross-correlation coefficient (R_{xy}) for the MU template before and after denoising. The bottom graphs plot the isometric wrist flexion force-time curves and instantaneous motor unit discharge rate (MUDR) before (left) and after (right) denoising. After denoising, the mean and standard deviation of the IDIs was calculated using the Error Filtered Estimation algorithm. 88

Figure 26. Representative example of superposition of two motor unit potential trains (MUPTs) using strict criteria. The top panels are the shimmer plots, one for each channel. The shimmer plots include one MU templates calculated after denoising (black). The waveforms removed from each channel are plotted immediate below it, indicating the percent decrease in discharge times (Δ FIR). A portion of the MUPs from a second MUPTs appears in the residuals, sufficient to generate a second MU template. Note the shadow peak in the top panels at approximately 7 ms, which is also present in the MU template in the residuals. Additional tuning is possible if greater separation is desired. . 89

Figure 27. Regression analysis of IDIs calculated on the original motor unit discharge times versus those obtained using the Error Filtered Estimation (EFE) algorithm on the denoised data using the relaxed and strict criteria. The difference in the number of sampled motor units was due the removal of discharge times relative to the requirement for an absolute minimum. While the percent decrease was constrained to 50%, the minimum absolute number was 30% of discharge times within a motor unit potential train. 93

LIST OF TABLES

Table 1. Means (M) and standard deviations (S) for the motor unit template peak-to-peak (P-P) amplitude, the duration between the P-P amplitudes, variance ratio (VR), and the signal-to-noise ratio (SNR) for the original and denoise MU discharge times.....	92
---	----

CHAPTER 1: Introduction

1.1 Development of the Problem

The main advantage of indwelling recordings is that they bypass the fascia, fat, and skin which alter the electrical signals to obtain direct and clear motor unit action potentials (MUPs) (Perry, Easterday, & Antonelli, 1981). Indwelling electrodes have been criticized because the needle or wire has a limited pickup area compared to its surface electrode counterpart (Farina & Holobar, 2016). Thus, to obtain a more representative sample throughout the muscle, the needle must be reinserted in multiple locations and at different depths (Podnar, 2004). Therein lays the main disadvantage in that the procedure is invasive and can be painful to the patient or study participant (Strommen & Daube, 2001). There is a low risk for infection or disease transmission, but the needle may still cause minor damage to muscle fibers which could cause changes in MUP shapes (De Luca et al., 2006). The MUP shape is a critical variable used to identify motor units (MUs) and study the health status of the neuromuscular system (Mambrito & De Luca, 1984). Another limitation is that it is difficult to obtain reliable recordings of the same MU from one session to the next, because it is nearly impossible to place an indwelling electrode in the same location within the muscle (Perry et al., 1981).

The limitations outlined above are more problematic for kinesiological investigation as needle examinations are more commonly performed within the clinical setting as part of electrodiagnostic testing by a physician (Daube & Rubin, 2009). Advances in biomedical instrumentation and signal processing techniques now allow researchers to record MUPs from the skin surface to investigate the neuromuscular system non-invasively (De Luca, Adam, Wotiz, Gilmore, & Nawab, 2006; Farina &

Holobar, 2016; Holobar & Farina, 2014; Nawab, Chang, & De Luca, 2010). In addition to being non-invasive, surface electrodes can record from 25 MUs or more (De Luca, Adam, Wotiz, Gilmore, & Nawab, 2006; Farina & Holobar, 2016; Holobar & Farina, 2014; Nawab, Chang, & De Luca, 2010). Surface electrodes can be placed and replaced on the skin at the same location over the muscle to reliably track the same MU over multiple sessions to determine the effects of various interventions (Martinez-Valdes et al., 2017) but, unfortunately the validity of the surface detected MUs is challenged due to the sEMG decomposition technique (Enoka, 2019; Farina & Enoka, 2011).

The two-source technique is the gold-standard for validating MUPs that have been obtained by decomposition of the surface electromyographic (sEMG) signal (Farina & Enoka, 2011). The procedure involves inserting a needle into the muscle and a surface electrode on the skin, immediately over the needle (Conwit et al., 1997). Once an indwelling MUP has been identified on an oscilloscope (or, computer screen), the analogue-to-digital (A/D) data collection system is set to trigger based on the peak-to-peak (P-P) amplitude of spikes from an identified indwelling motor unit action potential train (MUPT). The result is hundreds, or even thousands of epochs of EMG waveforms detected from the skin surface, when that particular MU discharged during the contraction. The waveforms are then averaged to decrease the random noise and increase the signal-to-noise (SNR) as a function of the \sqrt{N} (N represents the number of waveforms), revealing the underlying deterministic MUP shape from the skin surface (Boe, Stashuk, Brown, & Doherty, 2005; Conwit et al., 1997). The technique is termed 'spike triggered averaging' (STA), and the MUP shape that is revealed is termed a

‘template’. Each MU is identified by its own template should be unique in shape, with unambiguous discharge times.

Hu, Suresh and Rymer (2013a) used the two-source technique to validate MU discharge times obtained by sEMG decomposition (dEMG, version 4.1.1.0, Delsys, Natick, MA) up to 15% MVC. The same research group more recently demonstrated that even slight errors in MU discharge times result in an unrecognizable template (Hu, Rymer, & Suresh, 2013b). As a result, STA of the sEMG signal using only the MU discharge times obtained by sEMG decomposition has been used to validate MU data up to 50% MVC (Hu et al., 2013b). In this case, a number of different MUPs were identified from the skin surface, and their templates were compared to those provided by the dEMG decomposition system. The criteria for a match was that coefficient of variation in P-P amplitude between the two templates had to be less than 0.3, and the average cross-correlation coefficient had to be greater than 0.7.

The purpose of this thesis was to extend the approach of Hu and colleagues (2013a, 2013b), by editing the individual motor unit potential trains (MUPTs), retaining only those MU discharge times for which there is ‘high confidence’ (Enoka, 2019). The term ‘high confidence’ is derived from the notion that all MUPs within a MUPT having the same shape, confer a degree of validity to the discharge times (Parsaei & Stashuk, 2009, 2011). While edited trains may result in MUP quantification with greater precision, the calculation of motor unit discharge rates (MUDRs) on MUPTs with missing and/or erroneous discharge times can also be problematic (Stashuk & Qu, 1996a; Stashuk, 1999a, 2001). To this end, this thesis also compared the inter-discharge intervals (IDIs) obtained by the original sEMG composition to that of edited MUPTs, as determined by

the error-filtered estimation (EFE) algorithm. The EFE algorithm is a robust statistical method for estimation of the mean and standard deviation of IDIs, which has already been validated for use in quantitative needle EMG (Stashuk & Qu, 1996a).

1.2 Statement of the Problem

The discharge times of a MU are the most critical measure to extract from the decomposition process because they are used to calculate MUDR and quantify the MUP as a means to understand the neural control of muscle and assess the health status of the neuromuscular system (Castronovo et al., 2018; Contessa, Letizi, De Luca, & Kline, 2018; Piasecki et al., 2018).

Hu et al. (2013a; 2013b) have demonstrated that if the discharge times are correctly obtained from the indwelling MUP, they can be used to obtain a sufficient number of epochs of EMG data to reveal its respective surface motor unit potential. The investigators have more recently shown that the firing times obtained by the Delsys (dEMG, version 4.1.1.0, Natick, MA) decomposition algorithm can be used in isolation to obtain epochs of data from the surface EMG signal, to validate MUP templates external to the commercially available propriety program (McManus, Hu, Rymer, Suresh, & Lowery, 2017). The critical assumption is that incorrect discharge times will not allow the signal averaging of random noise to cancel-out and reveal a deterministic shape. It could reasonably be argued that, since the protocol involved relatively low force level (<30% MVC) isometric contractions, decomposition of the surface EMG signal was easily unambiguous. High intensity contractions (>50% MVC) would, however, involve greater numbers of MUs, more MUPs in superposition, leading to a more complex interference pattern, which would have a greater probability of error (Nawab et al., 2010).

Editing the MUPTs based on the shape of contributing MUPs would provide a greater degree of confidence in the remaining MU discharge times (Parsaei & Stashuk, 2009, 2011).

1.3 Purpose of the Research

This thesis determined the efficacy of a semi-automated routine for editing the MU discharge times within a MUPT from the flexor carpi radialis (FCR) during isometric contractions at 60% MVC. The IDIs obtained by the original sEMG decomposition were then compared to that of edited MUPTs, as determined by the error-filtered estimation (EFE) algorithm.

1.4 Approach to the Problem

Participants performed two isometric contractions of the wrist flexors, held at 60% MVC for 15 seconds. Motor unit potentials were recorded in the flexor carpi radialis (FCR). The MU discharge times obtained from the dEMG decomposition were then used to STA the sEMG signal. A custom graphical user interface (GUI) in MATLAB (MathWorks Inc., Natick, MA) was used to edit the MU discharge times from the dEMG system, based on how well the MUP shape fits the overall MU template derived from STA. The algorithm for inclusion of an individual motor unit potential (MUP) and its associated discharge time was: (1) a correlation greater than or equal to $r=0.0$ (relaxed) or $r=0.3$ (strict) between any MUP and its respective template; (2) a signal-to-noise ratio (SNR) of root-mean-square (RMS) amplitudes greater than 0.0 (relaxed) or 0.3 (strict); (3) a peak that was located within the 95% (relaxed) or 68% (strict) confidence interval for the MU template peak location; (4) and (5) relaxed and strict values were multiplied

with the MUP template peak to create a range that the MUPs must fall within.

Waveforms falling outside the boundaries of these three criteria were considered as noise and the erroneous discharge time was removed. The process was termed ‘denoising’.

The following criteria was used to assess the impact of denoising. First, it was expected that there would be a decrease in the variance ratio (VR) which measures the variability in the shape of MUP waveforms contributing to the MU template. Decreases in the VR should also be accompanied by an increase in the SNR of individual MUPs underlying the MU template. Motor unit action potentials that have a lower variability in shape are easier to isolate and classify, ultimately creating a better template (Parsaei & Stashuk, 2009). The peak-to-peak (P-P) amplitude and duration of the MU template were also monitored for changes, but a case could be made for either increases or decreases these measures, depending on the amplitude nature of the waveforms that were removed. Since MUDRs cannot be calculated on denoised MUPTs, the EFE algorithm (Stashuk & Qu, 1996a) estimated the mean and standard deviation of the IDIs as a function of the level of denoising based on ‘relaxed’ and ‘moderate’ exclusion criteria, for less or more removal of MU firings, respectively. The statistically estimated mean and standard deviation IDIs were then compared to the original, complete MUPTs from the dEMG system decomposition. The goal was to determine if the level of denoising has an impact on the outcome measures outlined above.

1.5 Hypotheses

1. Noise reduction will result in a significant decrease in the VR of remaining MUPs that constitute the extracted MUP template.

2. Noise reduction will result in significant increase in the SNR of MUPs that constitute the extracted MU template.
3. There will be a significant difference in MUP P-P amplitude and duration after noise reduction. There are no predictions for direction of change (increase or decrease) in these measures, as it would depend on the amplitude nature of the ‘noise’ waveforms that have been removed.
4. There will be a significant correlation between the original IDIs from the dEMG system and those calculated from the denoised MUPTs. However, previous work on the EFE algorithm suggests that the correlation may degrade as the level of denoising increases and more MU discharge time are removed (Stashuk & Qu, 1996a).

1.6 Significance of the Study

Advances in biomedical instrumentation and signal processing techniques have resulted in an increase of commercially available devices that have facilitated EMG investigation of the neuromuscular system by the non-expert (De Luca, 1997). Despite the ease of use, understanding the various factors that affect the EMG signal requires in-depth knowledge of physiological signals so that results are not misinterpreted (De Luca, 1997). As a result, misinterpretation of the surface EMG signal has been cited as one of the main obstacles to understanding the neuromuscular system (Enoka & Duchateau, 2015).

It is now possible for investigators to record MUPTs from the skin surface and make inferences about the neural control of muscle without being able to independently validate the data from proprietary software (De Luca & Nawab, 2011; Nawab et al.,

2010). Validation of surface EMG decomposition algorithms has been the subject of much debate, with the two-source method as the gold-standard (Farina, Merletti, & Enoka, 2015). Routine validation by the two-source method is invasive, which is contrary to the main goal of surface EMG detection. This thesis proposed to extend the method of using only the discharge times identified by surface EMG decomposition, but for higher intensity contractions. The challenge is significantly greater with high intensity contractions because the interference is more complex and MU activity is more variable (Nawab et al., 2010). A simple method, as proposed here, that can be used by any investigator to facilitate the extraction of surface detected MUPTs for further validation will help to limit the misinterpretation of surface EMG signals that plagues the field (Enoka, 2019).

1.7 Assumptions

The following is a list of assumptions that must be made for the study:

1. Participants were able to successfully complete a trapezoidal contraction profile that achieved a truly representative 60% MVC.
2. The study participants were healthy and did not have any neuromuscular disorders.
3. When asked to flex at the wrist, the flexor carpi radialis was the greatest contributor to this joint action.
4. Minimal coactivation of antagonist muscles of the wrist (extensor carpi radialis) occurred.

5. The EMG data recorded from the surface through the dEMG sensor was from the flexor carpi radialis with minimal cross-talk from surrounding musculature.
6. The data collection did not impose fatigue in the participants' muscles during the study.

1.8 Delimitations

The following is a list of delimitations placed upon the study:

1. Only isometric contractions of the flexor carpi radialis were used in this study.
2. Only 60% MVC was used during this study.
3. Participants were university/college aged.
4. Participants had no neuromuscular abnormalities.
5. A single joint action was considered for this study, which is flexion for the wrist.

1.9 Limitations

The following is a list of limitations that correspond to the study delimitations:

1. Since only isometric contractions of the flexor carpi radialis were used for this study, the results can only be directly applied to contractions of the same type from these muscles. The findings may not be applied to other muscles or contraction types.
2. Since only contractions of 60% MVC were used for this study, the results can only be applied to 60% MVC intensity contractions, or lower.

3. Since our participants were university/college aged population, the findings may not apply to individuals with age-related differences in muscle size, body composition, or MU behaviour.
4. The findings also do not necessary apply to individuals with neuromuscular abnormalities that would have greater variability in MUP shape and MU activity patterns.
5. Due to the single joint action at the wrist, the findings may not accurately represent the applicability to muscle during multi-joint actions.

CHAPTER 2: Review of the Related Literature

2.1 Anatomy

2.1.1 *Flexor Carpi Radialis*

The flexor carpi radialis (FCR) is a flexor and abductor of the hand, at the wrist joint. The FCR originates on the medial epicondyle of the humerus and inserts on the base of the second metacarpal (Figure 1). The FCR is innervated by the median nerve and is supplied blood from the ulnar artery. The FCR muscle fibers that insert along the midline of the tendon are oriented longitudinally and muscle fibers originating along the sides of the tendon are oriented at oblique angles (Segal, Wolf, DeCamp, Chopp, & English, 1991). Cadaveric work has demonstrated that the FCR has an approximated length of 164 mm to 197 mm, a pennation angle that varied considerably between 3.1° to 13.25° and a physiological cross-sectional area of 166 mm^2 to 250 mm^2 (Lieber, Fazeli, & Botte, 1990; Liu et al., 2014). These differences are likely due to the inherent interindividual variability between cadavers, also Liu and colleagues (2014) split the FCR into two neuromuscular compartments to isolate the neurovascular supply, where Lieber and associates (1990) did not. According to results of a study where investigators used biopsies and phosphorus-31 nuclear magnetic resonance to determine fiber-type distribution, the FCR has approximately 40% Type I fibers and 60% Type II fibers (Mizuno, Secher, & Quistorff, 1994). Due to the proximal, longitudinally arranged muscle fibers of the FCR, it is easy to instrument with surface electrodes to record EMG data. There is minimal subcutaneous fat tissue over the FCR, which also facilitates the use of the FCR for neuromuscular investigations (Imanishi, Nakajima, & Aiso, 2000).

Recent cadaveric work has suggested that the motor endplates of the innervating alpha motoneurons are located in the proximal quarter of the FCR (Song et al., 2014). This evidence provides insight into appropriate placement of the dEMG electrode, since it is suggested that innervation zones are avoided in the dEMG user's manual. Based on evidence from Zaheer et al. (2012) and Roy et al. (1986), it is ideal to detect the motor point before placing the electrode, thus minimizing chances of EMG amplitude cancellation, which will be further discussed in a later section.

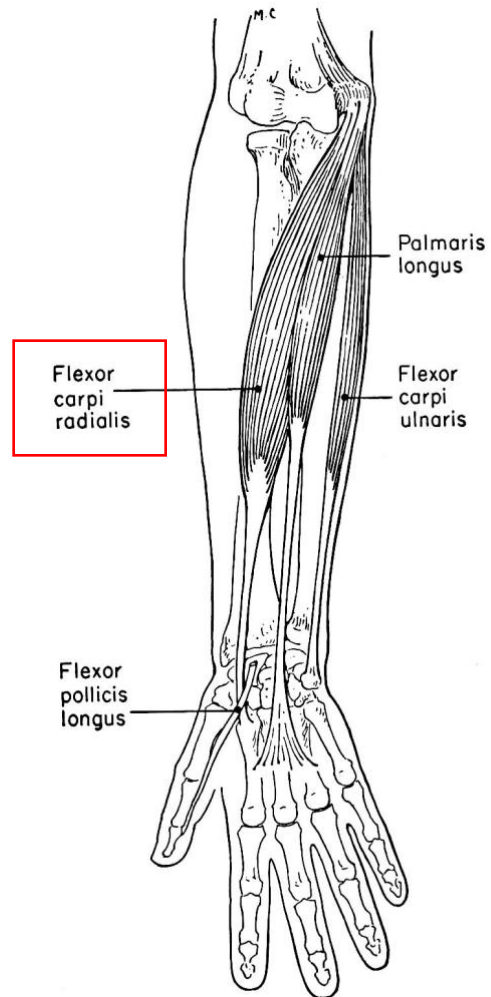


Figure 1. Muscles of the lower arm, the flexor carpi radialis (FCR) is highlighted.
Luttgens, K., Wells, K. (1982). Kinesiology: scientific basis of human motion. *Saunders College Pub.*

2.2 Surface Electromyography

2.2.1 *Muscle Fiber Action Potential*

The electrochemical activity can be recorded as voltage changes using electrodes placed on the skin surface or intramuscularly via a needle or fine wire (see Figure 2). The electrochemical activity is a result of membrane potential changes at the cellular level. The propagation of the action potential arises from a cascade of events that begins with the depolarization of an alpha motoneuron cell axon. The axonal terminal of the alpha motoneuron then releases acetylcholine. This neurotransmitter crosses the synaptic cleft and attaches to the nicotinic receptor which propagates the action potential across the neuromuscular junction. This then causes the sarcolemma around the myofibril to begin the depolarization cascade by increasing the permeability to sodium (Na^+) through the opening of voltage-gated Na^+ channels as a result of a 10 mV increase in positive membrane potential. Subsequently, Na^+ rushes into the cell, generating a polarity reversal inside the cell. The polarity reversal in the cell can be seen from an electrode as the active depolarization where there is a current sink (see Figure 2a). The inactivation gate on the Na^+ channel closes shortly after the Na^+ rushes into the cell. The adjacent local area to the initial site of depolarization then undergoes the same change due to the polarity reversal from the Na^+ . The depolarization propagates axially and radially toward the following adjacent areas due to the Na^+ ions moving towards the negatively charged inner membrane of the sarcolemma. This can be seen from an electrode as the passive depolarization where there is a weak source of electrical potential (see Figure 2b). The new relative positivity that exists in the cell then causes potassium (K^+) ions to leave the cell and repolarize the cell, bringing it to the baseline -70 mV resting potential. The

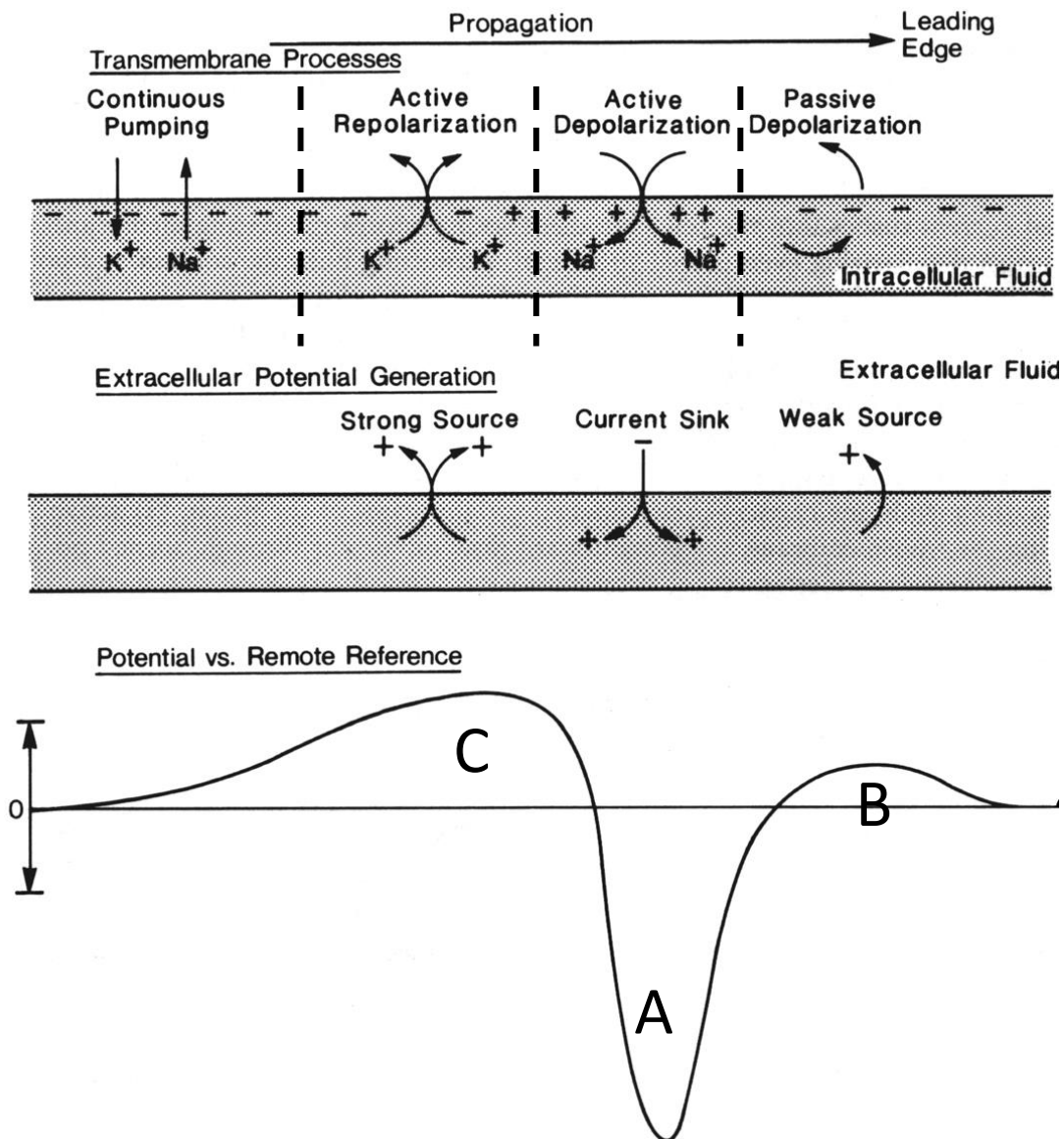


Figure 2. Electrochemical events at the cellular level of a muscle fiber and the ensuing waveform as seen from electrode recordings. Loeb, G. E., Gans, C. (1986). Electromyography for experimentalists. *University of Chicago Press*.

repolarization is seen from an electrode as the strong source of electrical potential (see Figure 2c) (Sherwood, Kell, & Ward, 2013). These events are what give rise to a muscle fiber action potential (MFP).

2.2.2 *Motor Unit Action Potential*

A motor unit (MU) is defined as a single alpha motoneuron and all of the muscle fibers it innervates and is the smallest functional unit of the neuromuscular system (see Figure 3). The individual MFPs which occur very close in time ($\sim 10 \mu\text{s}$) summate at the electrode to create a motor unit action potential (Griep, Boon, & Stegeman, 1978; Stålberg, Ekstedt, & Broman, 1971). The motor unit action potential (MUP) generated from an alpha motoneuron propagates along a muscle membrane. Motor neurons branch out from the spinal cord through various pathways, which are routed throughout the body to innervate muscle fibers. Each individual motor neuron innervates a different number of muscle fibers, and this ratio is termed the innervation ratio (Enoka & Fuglevand, 2001). Using a 14-lead multi-electrode, investigators identified that there are approximately 329 muscle fibers per MU in the tibialis anterior (Gath & Stålberg, 1981). While there are no available studies on an innervation ratio estimation for the flexor carpi radialis, investigators have found an innervation ratio of 1:165 for a similar muscle, the extensor longus digitorum (Clark, 1931). Figure 3 shows that depolarization begins a cascade that propagates along the axon of the motor neuron, then bidirectionally along the muscle fibers it innervates. From the neuromuscular junction of the motoneurons towards the tendons to then cause a muscle twitch that occurs after a delay of a few milliseconds (De Luca, 1979; Kamen & Gabriel, 2010). The narrow region of motor

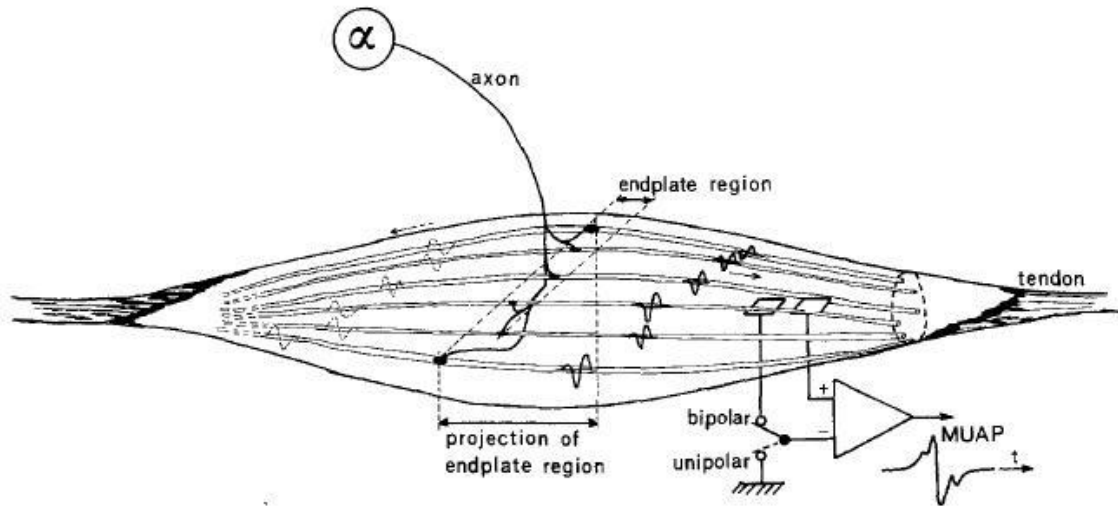


Figure 3. One motor unit is depicted here with only 6 of its muscle fibers. The signal that propagates along the muscle fiber is recorded by an electrode in a unipolar or bipolar fashion. Griep, P. A. M., Boon, K. L., Stegeman, D. F. (1978). A study of the motor unit action potential by means of computer simulation. *Biological cybernetics*.

endplates near the muscle belly is termed the innervation zone (Rainoldi, Melchiorri, & Caruso, 2004; Rodriguez-Falces, 2017).

2.2.3 Motor Unit Action Potential Train and Interference Pattern

A series of discharges from a single motor unit is termed a motor unit action potential train (MUPT). Figure 4 shows the MUPTs from many MUs. Note that the firings for each MU are separated by a non-uniform inter-pulse interval (IPI). An electrode placed either within the muscle itself or on the skin surface can record the electrical potentials from a population of MUs as they summate (De Luca, 1979; Stashuk, 2001). The composite EMG signal can be described as an interference pattern (IP) as depicted in the bottom panel of Figure 4. Depending on the type of electrode, the IP will appear different due to variations in conductance from the surrounding tissues. The signal also undergoes wave cancellation due to the summation of positive and negative potentials from neighbouring MUs occurring at the same time (Christie, Inglis, Kamen, & Gabriel, 2009; Keenan, Farina, Maluf, Merletti, & Enoka, 2005). Both volume conduction and cancellation hinder the detection of MUPs from the surface EMG signal. Indwelling electrodes, with a smaller recording volume, allow investigators to record from individual MUPTs (Andreassen & Rosenfalck, 1978), and there is less chance for wave cancellation due to the selectivity of the electrode. Superposition and synchronization may occur due to the temporal characteristics of various MU firings occurring at the same time (Defreitas, Beck, Ye, & Stock, 2014; Stashuk, 2001).

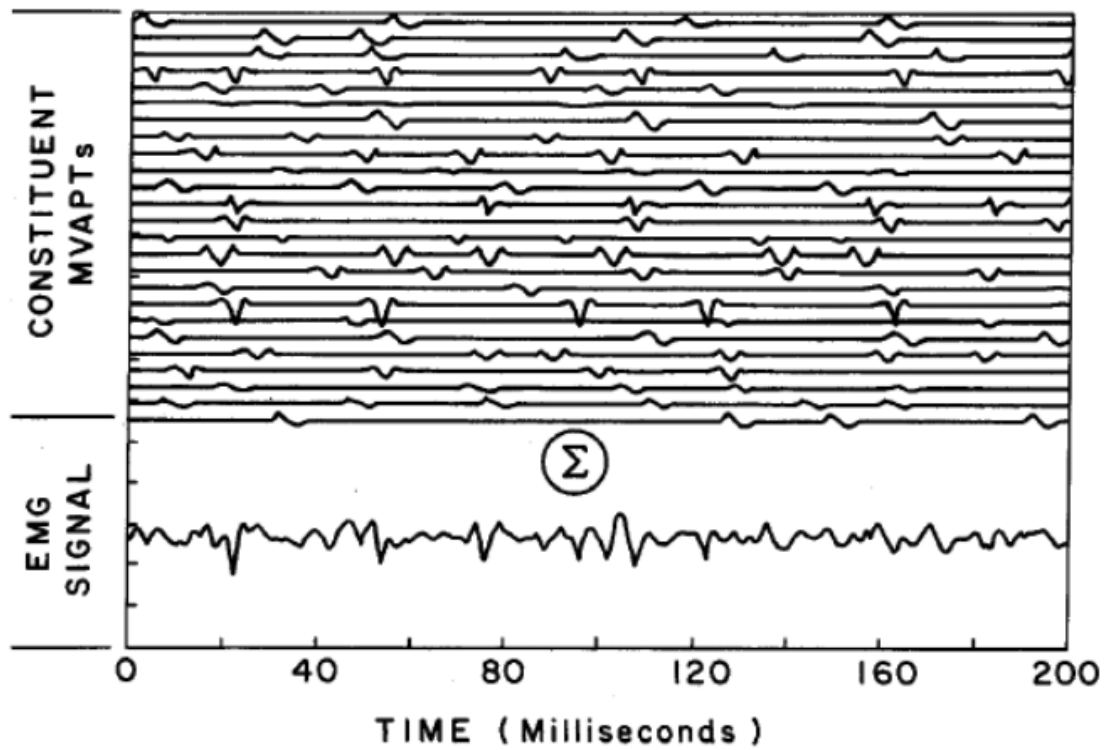


Figure 4. Trains of motor unit action potentials (top) summate together to make up the recorded EMG signal (bottom). Basmajian, J. V., De Luca, C. J. (1985). *Muscles alive: their function revealed by electromyography*. Williams & Wilkins.

2.3 Variability in MUP Shape

2.3.1 *Jiggle*

Motor unit potential jiggle is defined as the variability of MUP shape. The jiggle was originally measured by Stålberg and Sonoo (1994) to quantify the amount the variability of MUP shape as an electrodiagnostic measure. A higher jiggle value is representative of greater MU shape variability and a lower jiggle value is representative of lower MU shape variability (Stålberg & Sonoo, 1994). As reported by Stålberg and Sonoo (1994) the jiggle is represented by calculations of consecutive amplitude difference (CAD) and the cross-correlational coefficient (CCC) of the consecutive discharges. Inspection of Figure 5 shows that greater consecutive amplitude difference values and lower cross-correlational coefficient of the consecutive discharge times are associated with a greater jiggle. It is expected that jiggle increases with an increase in jitter, which is formally defined as the random arrival times of single fiber action potentials at the electrode (Stålberg & Sonoo, 1994). Boyd and colleagues (1979) noted four major mechanisms for jitter and jiggle: variance in propagation time in the terminal nerve endings; neuromuscular transmission delays at the motor end plate; positions of the motor end plates on the muscle fibers, giving rise to an unequal distance for the potentials to travel to the electrode. Changes in jitter and jiggle are characteristic of neuromuscular disorders (Campos et al., 2000). A change has been suggested to modify the jiggle measurement, which includes the estimation of baseline fluctuation from segments of the recording that are free from secondary MU firings, and alignment of the consecutive discharges using a correlation maximization (Campos et al., 2000). Campos and

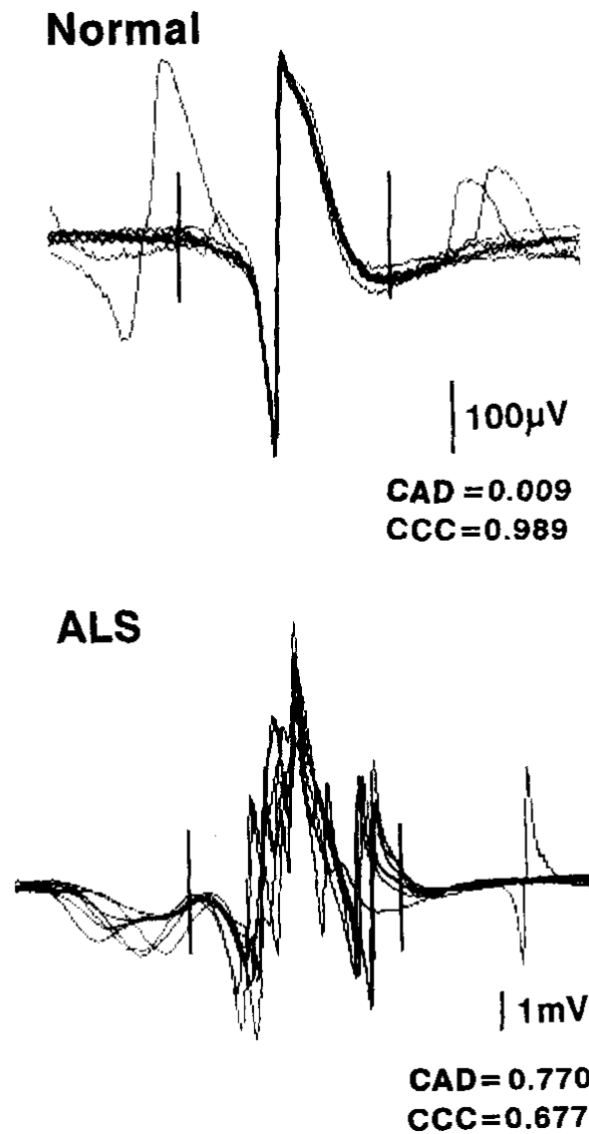


Figure 5. Difference in jiggle can be seen visually here, as depicted by the variability in the overlaid MUAPs. In a normal motor unit, there is a low CAD and high CCC value. In the amyotrophic lateral sclerosis (ALS) motor unit, the CAD is much higher and the CCC is substantially lower. Stålberg, E. V., Sonoo, M. (1994). Assessment of variability in the shape of the motor unit action potential, the “jiggle” at consecutive discharges. *Muscle & Nerve*.

colleagues (2000) noted that there was an 18.8% improvement upon the jiggle measures, which indicates that the modifications using correlation maximization were beneficial.

2.3.2 Variance Ratio

The variance ratio (VR) is a measure that quantifies the reproducibility of a waveform and it is similar to the measurement of jiggle. Reproducibility and variability are interrelated. The less variability in the shape of a waveform, the more reproducible it is. Conversely, the more variability in waveform shape, the less reproducible it is. Variability may be affected by both physiological and technical factors associated with recording EMG. The VR was originally used by Hershler and Milner (1978) to quantify the reproducibility of EMG waveforms during gait. Kadaba and colleagues (1985) later used the VR to compare the variability in the shape of muscle activity recorded by surface versus indwelling wire electrodes. Calder et al. (2005) employed VR to study the reproducibility of an evoked compound muscle action potential (CMAP) from the biceps brachii (see Figure 6). The VR is represented by the following formula:

$$VR = \frac{\frac{\sum_{t=1}^T \sum_{n=1}^N (y_{t,n} - \bar{y}_t)^2}{T(N-1)}}{\frac{\sum_{t=1}^T \sum_{n=1}^N (y_{t,n} - \bar{y})^2}{TN-1}}$$

where T = the number of time points, N = the number of waveforms and $y_{t,n}$ is the value of the n^{th} waveform at time point t , \bar{y}_t is the average of the waveform values at the time point t , averaged over N waveforms and \bar{y} is the grand mean of all the waveforms. As the observation for \bar{y}_t approaches \bar{y} the VR starts to approach one (1), which is the

maximum value for VR. The inverse is also true, the numerator approaches zero (0) if $y_{t,n}$ approaches \bar{y}_t the VR approaches zero (0).

A higher VR is representative of waveforms that are loosely grouped, and a lower VR is representative of a VR that is tightly grouped. The VR is ultimately a ratio of the mean squared differences between waveforms divided by the total sum of squares of the waveforms (Hershler & Milner, 1978; Kamen & Gabriel, 2010). For the purpose of the present study, the VR will be used to evaluate the reproducibility of a MUP over the duration of its entire train.

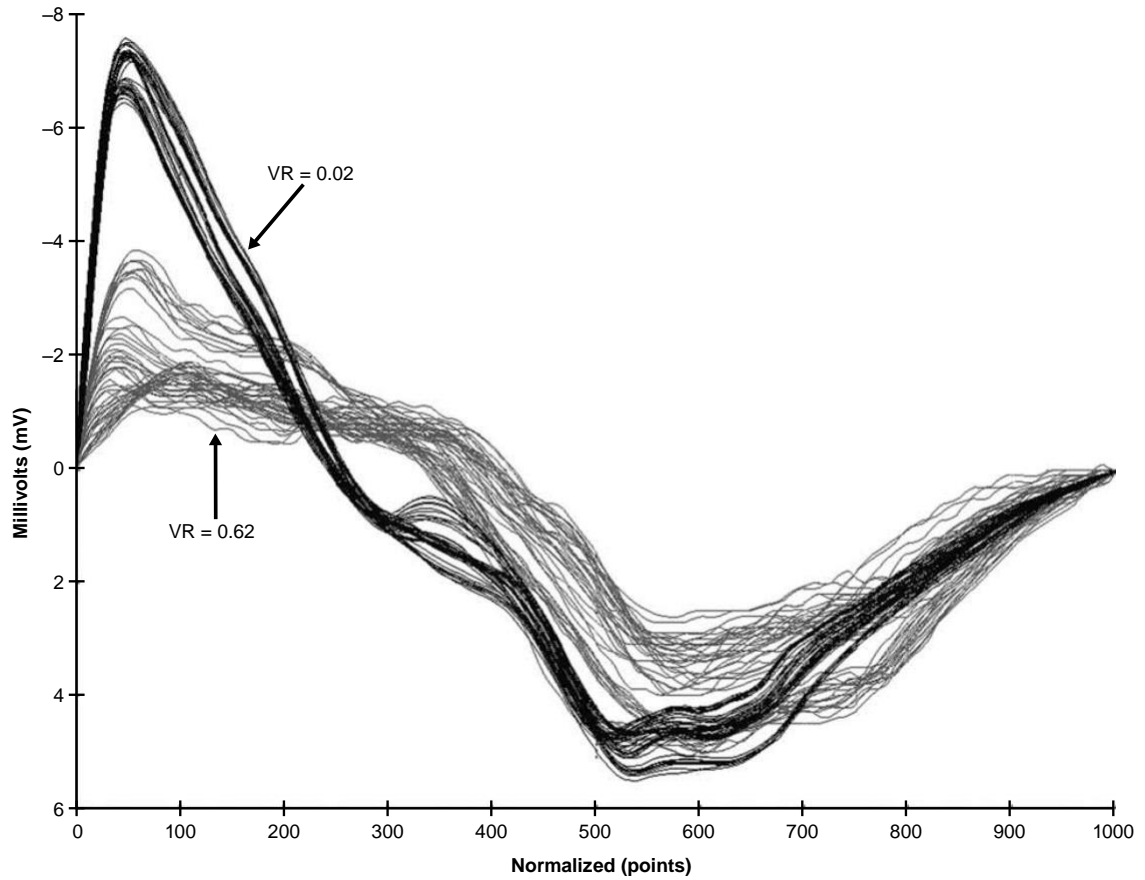


Figure 6. M-waves from the biceps brachii overlaid from two different subjects. One is depicting a low VR (0.02) and the other a higher VR (0.62). Calder, K. M., Hall, L., Lester, S. M., Inglis, J. G., Gabriel, D. A. (2005). Reliability of the biceps brachii M-wave. *Journal of NeuroEngineering and Rehabilitation*.

2.3.3 *Signal-to-Noise Ratio*

The SNR is a classic signal processing measure to quantify the amount of signal energy of interest versus unwanted noise. The SNR is calculated by dividing the signal power (P_S) by the noise power (P_N), which provides the investigator with a gain ratio in decibels (dB). One method that the SNR is represented is by the following formula:

$$SNR = 10 \log \left(\frac{P_S}{P_N} \right)$$

To conduct this calculation effectively, the noise is often a portion of the EMG signal that is taken from a quiescent period before the subject begins contracting. The signal is often taken from the middle of the isometric contraction. A higher SNR is representative of well-defined MU events, while a lower SNR is representative of less-defined MU events (see Figure 7). The SNR is dependent on the contact of the electrode with the skin, the muscles around the muscle of interest and other sources of noise such as computer monitors and lights, and the recording equipment itself (Clancy, Morin, & Merletti, 2002). Recommendations have been made to minimize the difficulties around SNR, such as carefully preparing the skin by using alcohol, using a mild abrasive to remove superficial layers of the skin and by using a conductive electrolyte gel (Clancy et al., 2002). The decomposition algorithm developed by Delsys requires a signal-to-baseline noise ratio of at least 2 dB. Within the context of the present study, the signal will be considered the innermost 15 ms of the MUPT window, while the noise will be considered the outermost 5 ms from either side of the MUPT window. The reason for these windowed values is to be as selective as possible in exclusively capturing the signal against the noise.

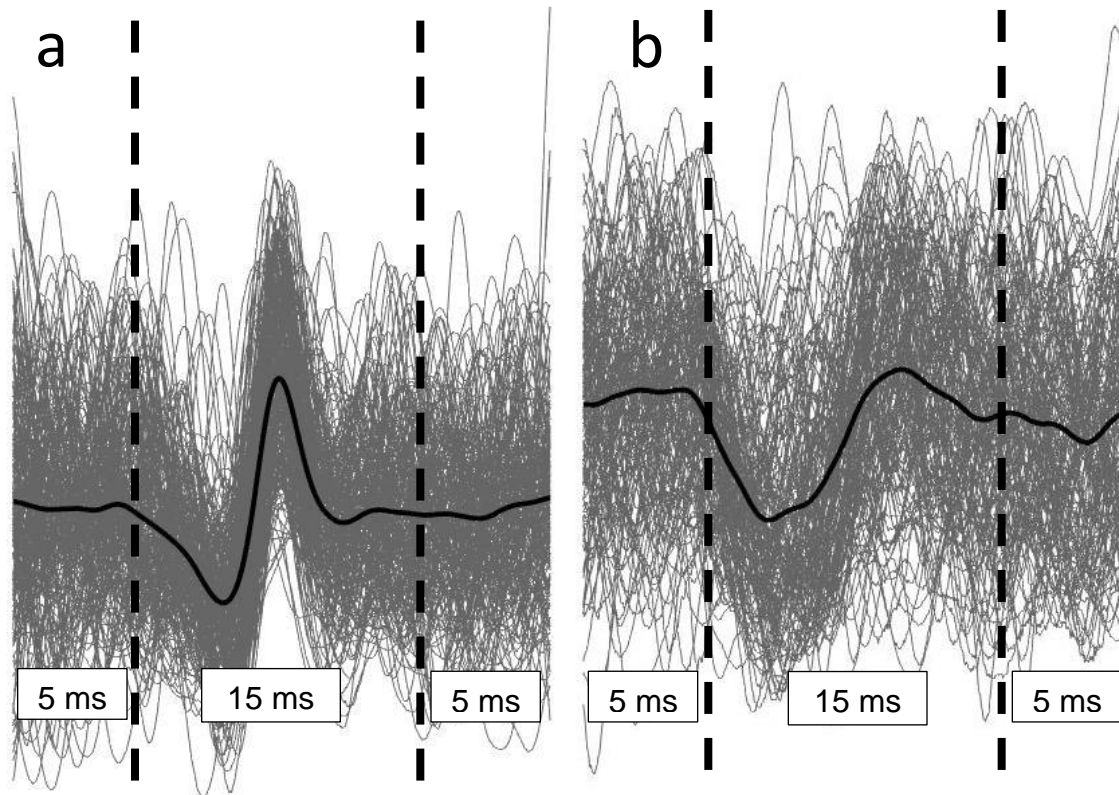


Figure 7. Two samples of motor unit shimmer plots (thin grey lines) with their respective mean templates (black line): (a) clear, unambiguous event against background noise (as denoted by the clear peak and thick band around the mean), (b) an unclear event against background noise (noticeable by the dispersion of the shimmer in the background and unclear template). Both examples have dashed vertical lines to denote where the 15 ms of signal and 5+5 ms of noise is calculated from.

2.4 Motor Unit Behaviour

2.4.1 Henneman's Size Principle

The orderly recruitment of motoneurons from smallest to largest is termed the size principle. The size principle came to fruition as a collection of works that were carried out by Elwood Henneman and his colleagues in the mid-20th century (Mendell, 2005). Originally, this was described as the susceptibility of the motoneurons discharging as a function of their diameter and resistance to current in a hierarchical method (Henneman, 1957). The deactivation of these motoneurons also shows a similar pattern, where the first recruited motoneuron will be the last one to be deactivated. The size of a motoneuron is reflective of the diameter of the axon, however, this can be typically inferred through MUP force-twitch amplitude or MUP peak-to-peak amplitude (Hu et al., 2013b). Hu et al. (2013b) also stated that the MUP size may not be reliable due to the variability in distance of the MUP to the recording site. One group studied MUs identified from the first dorsal interosseous and extensor indicis, and they stated that it is possible to use the conduction velocity of a nerve fibre to estimate the size of the motoneuron (Freund, Budingen, & Dietz, 1975). Overall, the gradation of force is due to the orderly recruitment of motoneurons, thus an increase in excitation and activation of motoneurons will result in a greater output of force, which will be discussed in a further section (Mendell, 2005).

2.4.2 Phenomenon Known as Onion Skin Scheme

One proposed control scheme that modulates the firing rate and recruitment of motor units is termed the “onion skin phenomenon” (De Luca, LeFever, McCue, &

Xenakis, 1982a). It details that the firing rate of MUs will be inversely proportional to the recruitment threshold (De Luca & Contessa, 2012; De Luca, LeFever, McCue, & Xenakis, 1982b). This was identified in publications as early as 1971, where Person and Kudina investigated the discharge pattern and frequency of MUs during voluntary contractions (Person & Kudina, 1972). The basic concept indicates that MUs that are activated earlier will maintain a higher firing rate than MUs that are activated later (De Luca & Contessa, 2015). The term “onion skin” is due to the MUFR patterns resembling the layers of an onion (see Figure 9) (De Luca et al., 2006). Through inspection of Figure 8, the increased level of force requires more recruitment of MUs through further central activation and it is clearly visible that MUs were recruited in an orderly fashion following Henneman’s size principle (see Figure 9). These findings were similar to that of De Luca and Hostage (2010) where subjects performed force tracking tasks to various percentages of MVC while EMG was recorded in the first dorsal interosseous, vastus lateralis and the tibialis anterior. The work affirms previously established findings where participants used their extensor digitorum communis muscle during a steady isometric contractions and the inverse relationship between motor unit recruitment threshold firing rate was found (Monster & Chan, 1977). The potential explanation behind why the high-threshold MUs are firing slower is due to their inherent disadvantage, in which faster firing will induce a faster rate of fatigue, thus they must fire slower in order to continue to fire (De Luca & Hostage, 2010).

While the onion skin phenomenon is commonly reported, there have also been a number of instances where there is a firing rate crossover between earlier and later recruited MUs. This is termed the ‘reverse onion skin’ phenomenon. A study by Hu and

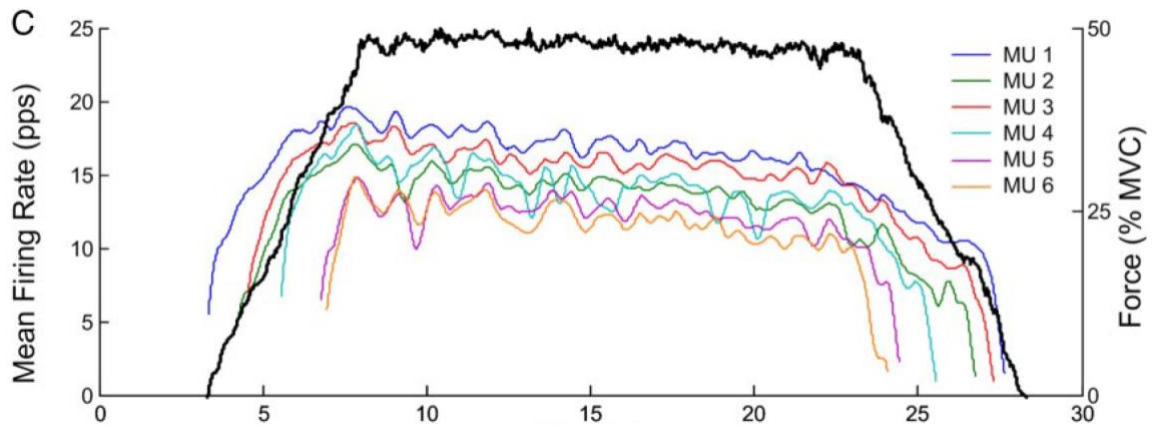


Figure 8. Coloured lines: Mean firing rate of individual motor units identified in the first dorsal interosseous muscle relating to the Y-axis. Black line: force paradigm relating to the right Y-axis. All events are bound by time. De Luca, C. J., Adam, A., Wotiz, R., Gilmore, D. L., Nawab, S. H. (2006). Decomposition of Surface EMG Signals. *Journal of Neurophysiology*.

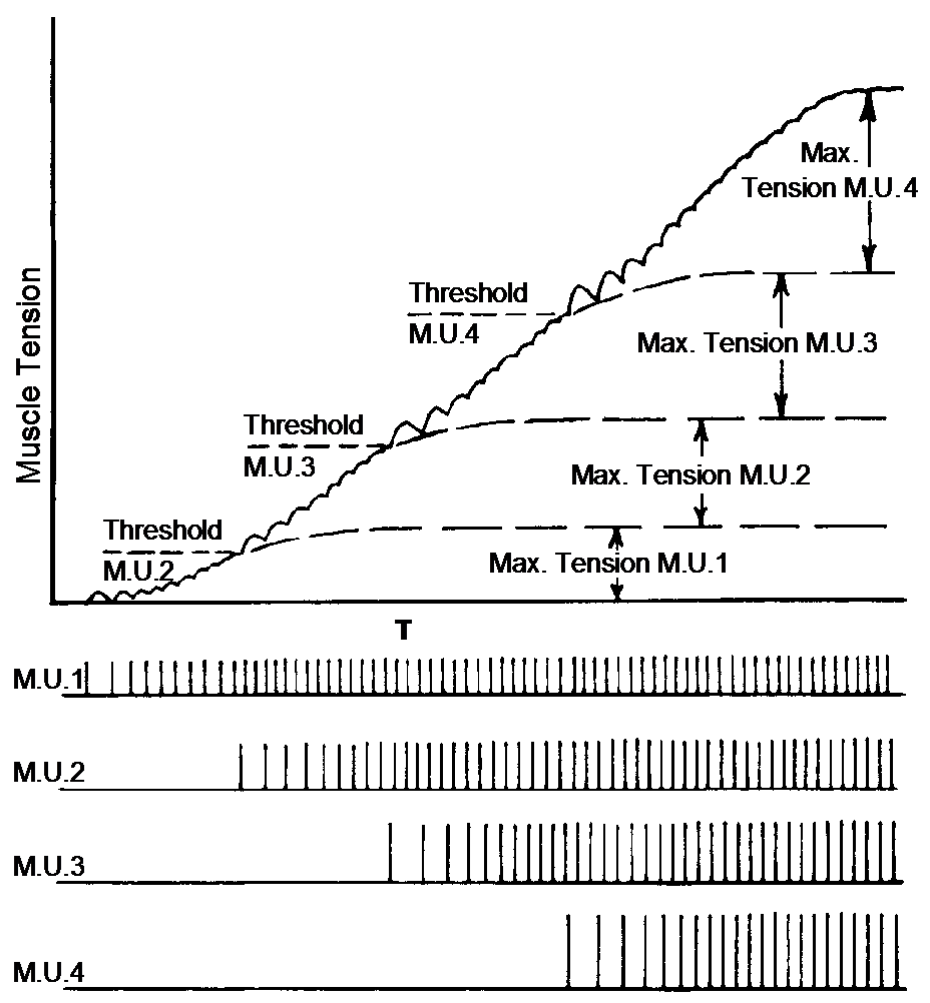


Figure 9. Motor units are recruited in a hierarchical manner with an increase in force output. The lowest threshold motor units are recruited first and the highest threshold motor units are recruited last. The max tension that a motor unit can generate occurs after a short period of time after recruitment. Motor units will summate to generate maximal muscle tension. Winter, D. A. (1990). Biomechanics and motor control of human movement (2nd Ed.). John Wiley & Sons.

colleagues (2014a) was conducted where participants were asked to trace a force paradigm over 3 different step levels, gradually increasing in force until the participant reached 15% MVC. The MU firing data did not reveal any systematic firing rate profile crossings, however there were occasional crossovers, which is a key marker of the reverse onion skin phenomenon. Hu and colleagues (2014a) mentioned that the later recruited MUs who showcase this reverse onion skin profile tend to exhibit a steeper rise in firing rate as the excitation level increases, where it then begins to exceed the firing rates of earlier recruited MUs. Another group analyzed the recruitment threshold and firing properties of motor units in the soleus up to maximal effort (Oya, Riek, & Cresswell, 2009). Oya et al. (2009) found that the initial and peak firing rates for later recruited, higher threshold MUs were significantly higher than the firing rates for the earlier recruited, low threshold MUs, up to 89% MVC. The potential explanation for this occurrence could be due to a persistent inward current mechanism (PIC) by which there is an amplification of synaptic input and could trigger an increase in firing rate, or limit the rate increase (Heckman, Gorassini, & Bennett, 2005). Both of the previously mentioned studies reported some degree of firing rate crossover, where one group tested up to 15% MVC (Hu et al., 2014) and one group tested up to maximal contraction levels (Oya et al., 2009), however De Luca and Hostage (2010) tested across many different muscles and MVC ranges and found that the onion skin profile was dominant in their data. This discrepancy in the data requires further investigation as to the what the underlying mechanisms are and why there are differences across results.

2.5 Muscle Force Regulation

2.5.1 Recruitment Range

As mentioned in the previous section, MUs are recruited in an orderly fashion based on the motoneuron size, thus smallest recruited first and largest recruited last (Henneman, 1957; Mendell, 2005). The force level at which the motor unit is recruited is known as the recruitment threshold (Defreitas et al., 2014). Certain MUs will recruit new MUs up to a certain percentage of MVC while others while have a reliance on the rate coding (modulation through firing rate) of MUs. A study was conducted to investigate the firing rate of MUs during isometric force, where participants performed isometric contractions at 20, 40, 60 and 80% MVC and the mean firing rate of MUs was calculated using indwelling electrodes (Seki & Narusawa, 1996). The investigators found that the firing rate was higher in the smaller muscle (first dorsal interosseous) in comparison to the larger muscle (biceps brachii), which indicates a reliance on MU recruitment for the larger muscle to generate maximum force and a reliance on MU rate coding (modulation of the firing rate) for the smaller muscle to generate maximum force (Seki & Narusawa, 1996). These results were also found previously (Kukulka & Clamann, 1981). A group of investigators further confirmed that the biceps brachii recruitment range was large (from 0.13 to 96.1% MVC) (Christie et al., 2009). Seki and Narusawa (1996) explain that this may be due to the type of muscle fiber because there are Type I in the small muscles for fine motor control and Type II in the larger muscles responsible for gross upper extremity movements. The reliance on rate coding after 50% of maximal contraction effort was also reported in the flexor carpi radialis (Calancie & Bawa, 1985). It was also found that the recruitment range for the tibialis anterior was up to 88% MVC, which indicates a

dependence on the recruitment of new MUs rather than rate coding (Feiereisen, Duchateau, & Hainaut, 1997), this was also reported by Van Cutsem and colleagues (1997).

2.5.2 *Common Drive*

Common drive occurs when there are simultaneous fluctuations in the firing rates of different MUs (Lowery, Stoykov, & Kuiken, 2003; Semmler, Nordstrom, & Wallace, 1997). De Luca and Erim (2002) conducted a study where participants performed ramp contractions at 20-30% MVC with indwelling electrodes within two adjacent forearm extensor muscles, and found a significant amount of correlation between firing rate fluctuations. This may be in part due to the common innervation of muscle fibers which indicates that the central nervous system treats the muscles as a functional unit (De Luca & Erim, 2002; Kamen, Greenstein, & De Luca, 1992). Kamen and colleagues (1992) investigated common drive based on the lateral preference (right hand vs. left hand) in healthy subjects and found that there was a greater amount of common drive in firing rates (at 30% MVC) in the dominant side compared to the non-dominant side. They infer that the results could potentially be due to the organization of peripheral receptors or muscle topography between the dominant and non-dominant limbs. Overall, the common drive illustrates the relationship between the hierarchical recruitment of MUs, the size of the motoneurons and the global output from the central nervous system (De Luca & Erim, 1994).

2.5.3 *Synchronization*

Motor unit synchronization, or short-term synchronization refers to an increase in the tendency for MUs to fire within a few milliseconds of one another (Defreitas et al., 2014; Milner-Brown, Stein, & Lee, 1975). This may be due to the strengthening of reflex pathways shown in trained compared to untrained individuals (Milner-Brown et al., 1975). This may be a neural strategy to increase force production (Semmler, 2002). A group of investigators examined the synchronization of low- and high-threshold MUs at 80% of MVC and found that high-threshold MU pairs demonstrate greater short-term synchronization than lower threshold MU pairs (Defreitas et al., 2014). Furthermore, the amount of synchronization that occurs between different age groups (young vs. old) was not significantly different, even at maximal forces, suggesting that synchronization is not exclusively meant to increase force production (Kamen & Roy, 2000). The synchronization may be due to inherent differences in the membrane properties among different MUs and differences in synaptic strength from other sources (Defreitas et al., 2014).

2.5.4 *Doublets*

When a single MU fires within a short period (2.5 to 20 ms) their paired firings are termed doublets (Simpson, 1969), which are suspected to effectively modulate force by taking advantage of the catch-like properties of muscle. The catch-like property of muscle is the force augmentation that occurs after a burst of two to four pulses takes place (see Figure 10) resulting from increased Ca^{2+} concentration (Garland & Griffin, 1999) and increased stiffness of the series elastic component of the muscle (Binder-

Macleod & Kesar, 2005). Further, the mechanisms underlying the double discharges are dependent on the intrinsic properties of the motoneuron membrane, where a delayed depolarization may occur (Garland & Griffin, 1999). The delayed depolarization is due to the antidromic signals traveling back toward the dendrites again where the membrane is brought closer to threshold, where an additional discharge ensues (Kudina & Churikova, 1990). In a review by Garland and Griffin (1999) it is stated that doublet discharges have been reported in many muscles, including the adductor pollicis, biceps brachii, flexor carpi radialis, trapezius and soleus, to name a few. In regards to the population incidence, It has been observed that occurrence of doublets appears to be greater in younger adults compared to older adults, with insignificant variability between force levels (Christie & Kamen, 2006). Conclusively, doublet discharges may be present as a form of force production or to improve motor performance. Within the present study it is possible that doublets may appear within a decomposition or revealed through spike-triggered averaging.

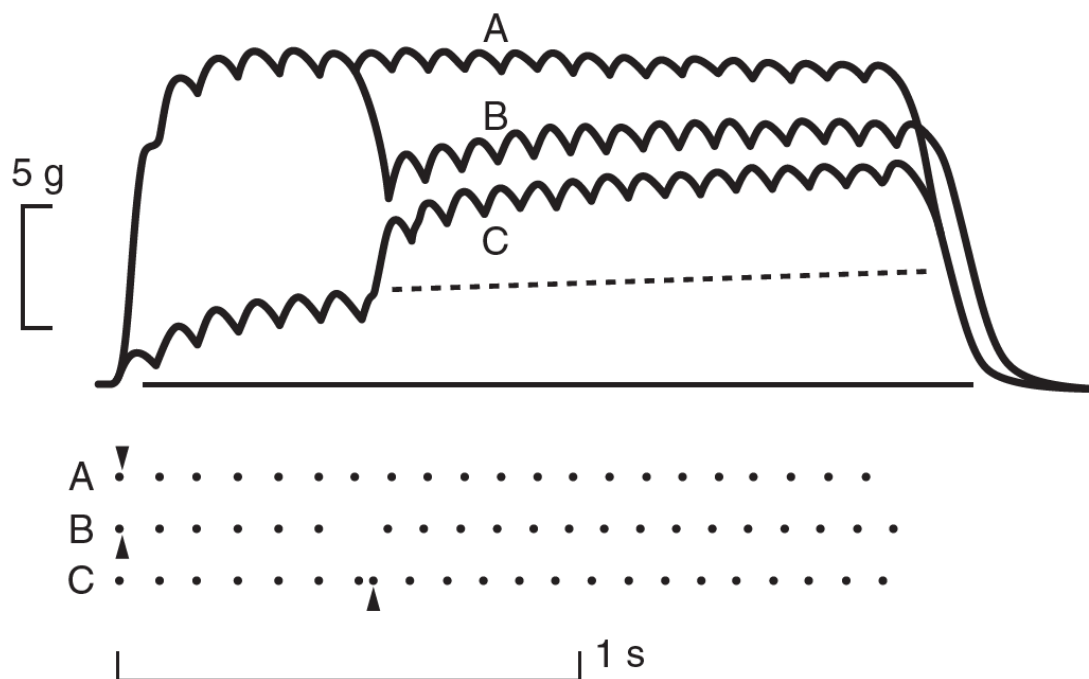


Figure 10. Catch-like properties of muscle as shown through 3 separate situations. In A and B the muscle is stimulated by a doublet pulse immediately. In B, a single drop-out of a pulse reduced the force. In C, an additional firing occurred immediately after another to enhance the force. Kamen G., Gabriel, D.A. (2010). *Essentials of Electromyography. Human Kinetics.*

2.6 Factors That Affect the Surface Electromyographic Signal

There are many factors that impact the origin of the EMG signal, which can range from intrinsic factors to extrinsic factors. Intrinsic factors include the tissues that are between the recording electrode and the muscles (Nordander et al., 2003), the architectural properties of the skeletal muscle (van Eijden & Raadsheer, 1992), muscle fiber conduction velocity (Farina & Merletti, 2004) cross-talk of other muscles (De Luca & Merletti, 1988) and movement artefacts (De Luca, Donald Gilmore, Kuznetsov, & Roy, 2010). Extrinsic factors could be from the changes of muscle temperature (Bigland-Ritchie, Thomas, Rice, Howarth, & Woods, 1992), electrode placement and inter-electrode distance (Rainoldi et al., 2004), skin preparation (Clancy et al., 2002) and fatigue (Bigland-Ritchie & Woods, 1984). The present factors should all be considered before collecting electromyographic data to ensure the integrity and reliability of the work.

2.6.1 *Subcutaneous Tissue*

Surface EMG is inherently limited by the complexity of human anatomy, in which there are layers of skeletal muscle. Deep muscles, such as the multifidus on the spine, require the use of intramuscular EMG electrodes for a reliable recording (Stokes, Henry, & Single, 2003). Intramuscular EMG electrodes may be fine wire or needles that are inserted directly into the muscle belly, which serve the benefit of bypassing the common tissues that are between the surface electrode and the muscle, while also increasing selectivity of the electrode. The EMG signal can be affected by the amount of subcutaneous tissue that is between the recording electrode and the muscle.

Tissue filtering acts as a spatial low-pass filter which distorts the true EMG signal by attenuating the higher frequencies (De la Barrera & Milner, 1994; Kuiken, Lowery, & Stoykov, 2003). In addition, it has been reported that the signal-to-noise ratio is inversely related to the skinfold thickness of the tissue between the recording electrode on the muscle (Zaheer et al., 2012). In a study by De la Barrera and Milner (1994) it was concluded that lower levels of skinfold thickness over the biceps brachii led to greater electrode selectivity. This means that sEMG signals are difficult to compare between subjects and therefore must be normalized to individual participants. In addition to their primary findings, De la Barrera and Milner (1994) found that the median frequency of the power spectrum for the sEMG signal declined with increases in skinfold thickness ($r = -0.92$). Another study was conducted regarding the mean and median power frequency differences between men and women at 20, 40, 60 and 80% MVC, where women generally presented lower mean and median power frequencies (Bilodeau, Arsenault, Gravel, & Bourbonnais, 1992). Pooling participants data while analyzing frequency spectrum characteristics should be done with great care (Bilodeau et al., 1992). More recently, the spectral characteristics of EMG were measured from contractions at 70% MVC in the TA and there was a poor association between median frequency and MU recruitment, likely due to the spatial distribution of MUs (Del Vecchio, Negro, Felici, & Farina, 2017). Skinfold thickness is a necessary measurement to determine if EMG decomposition is possible, since it has been found that greater skinfold thickness values may render decomposition less possible (Hogrel, 2003). Although, the methodology by Hogrel (2003) was not the same as the present study.

2.6.2 *Architectural Properties of Muscle*

As mentioned previously, there are two main types of muscle fibers: slow twitch (Type I) and fast twitch (Type II and Type IIx). The Type I muscle fibers generally have a small diameter and the Type II fiber types are larger (Sherwood et al., 2013). The architectural properties of a muscle, such as the muscle fiber diameter and the muscle length, can affect the myoelectric signal. A linear relationship has been observed between the diameter of a muscle fiber and the conduction velocity in frog fibers (Håkansson, 1956). The linear relationship is attributed to the input resistance properties of the fiber, where an increased diameter would include a greater velocity due to a decreased resistance. The correlation between conduction velocity and fiber diameter has also been observed in vivo in neuromuscular patients (Blijham et al., 2006). Arendt-Nielsen and colleagues (1992) conducted a study where evoked potentials were elicited in participants at 4 different knee angles (5, 45, 90 and 120°, where 5° is near full extension) at 3 contraction levels (0, 25 and 50% MVC). Regardless of contraction level, the conduction velocity declined. This occurrence is due to the lengthening of the muscle fiber, which decreases the diameter of the fiber (Arendt-Nielsen, Gantchev, & Sinkjær, 1992).

Human muscle can be arranged in a variety of orientations, such as parallel or longitudinal (biceps brachii) where fibers extend parallel to the force-generating axis, or uni- and multipennate (vastus lateralis and gluteus, respectively) where fibers are at an angle relative to the force-generating axis (Lieber & Fridén, 2000). The pennation angle is often measured through ultrasound to acquire an accurate measurement (Fukunaga, Kawakami, Kuno, Funato, & Fukashiro, 1997). Through modeling, a group of investigators sought to determine the effects of obliquely arranged muscle fibers of the

gastrocnemius muscle on the surface electromyogram (Mesin, Merletti, & Vieira, 2011). They found that surface electrodes placed over muscles with pennate fibers sample strictly from nearby sources (Mesin et al., 2011). This study was followed up with another in which investigators used high-density sEMG to determine if the MUs were localised in the gastrocnemius (Vieira, Loram, Muceli, Merletti, & Farina, 2011). Their results revealed that the MUs were localised in the gastrocnemius (Vieira et al., 2011), and this may be due to the central nervous system taking advantage of the architectural properties of muscle (Mesin et al., 2011). Understanding the various anatomical arrangements of muscle will aid in identifying appropriate electrode placement (Staudenmann, Roeleveld, Stegeman, & van Dieën, 2010).

2.6.3 *Muscle Fiber Conduction Velocity*

Muscle fiber conduction velocity (MFCV) is a measure of the velocity at which the action potential propagates along the muscle fibers from the motor end plates. The MFCV is an important measurement as it can provide information on neuromuscular disorders (Blijham et al., 2006) and is a major contributor to the power spectrum of the sEMG signal (Arendt-Nielsen & Mills, 1985; Arendt-Nielsen & Zwarts, 1989; Yaar & Niles, 1992). Understanding the velocity at which action potentials propagate along the muscle fiber can offer valuable insight to the initiation of movements (Arendt-Nielsen & Zwarts, 1989). The MFCV is influenced by many factors including muscle temperature (Troni, DeMattei, & Contegiacomo, 1991), muscle length (Arendt-Nielsen et al., 1992), muscle fiber diameter (Blijham et al., 2006; Håkansson, 1956), firing frequency (Morimoto & Masuda, 1984), MU type (Hopf, Herbort, Gnass, Günther, & Lowitzsch, 1974), force of the contraction (Sadoyama & Masuda, 1987; Sbriccoli et al., 2003) and

fatigue (Bigland-Ritchie, Donovan, & Roussos, 1981). During a study that involves the investigation of the neuromuscular system extrinsic variables such as muscle length, muscle temperature and electrode placement should be controlled to ensure the integrity of the data.

The MFCV can affect the EMG signal if the electrode is not placed away from the motor point, which may result in the velocities being interpreted as too high (Arendt-Nielsen & Zwarts, 1989). The motor point is the site of electrical stimulation where the largest muscle contraction is evoked from the smallest stimulus. This is identified through percutaneous repeated electrical stimulation (Bowden & McNulty, 2012). Incorrect estimation of MFCV is also observed with an incorrect electrode orientation. Arendt-Nielsen and Zwarts (1989) recommend placing the electrodes perfectly perpendicular to the muscle fibers to avoid under- or overestimating the velocities. As mentioned previously, the MFCV changes based on the angle of a joint as a result of changing muscle length (Arendt-Nielsen et al., 1992). Inbar and associates (1987) had participants contract their biceps brachii at several different angles (45, 90 and 180°, flexion to extension) and found that median power frequency increased at each joint angle as a function of MFCV. Additionally, the fiber orientation should also be considered, as the MFCV may not be easily estimated from pennate muscle fibers due to the oblique orientation with the electrode recording surface (Farina & Merletti, 2004). This is due to the arrival of the potential at the recording electrode at different distances along the fiber (Mesin et al., 2011).

More recently, Del Vecchio and colleagues (2018) investigated the relationship between MFCV and recruitment threshold of MUs within the tibialis anterior using high-

density sEMG and they found that MFCV was highly correlated with recruitment threshold ($R^2 = 0.7$). Previous work by Sbriccoli and colleagues (2003) investigated the relationship between contraction speed, median frequency and conduction velocity. They reported that the concomitant changes in rate of contraction (MVC/s) were associated with MFCV, in which contractions that were accomplished quickly showed that MFCV was reached at higher MVCs and much faster. Maximal MFCV was reached at 52.3% MVC at 5% MVC/s, and max MFCV was reached at 85% MVC at 20% MVC/s (Sbriccoli et al., 2003). Controlling the speed of contraction when measuring MFCV is imperative based on these findings.

2.6.4 *Cross-talk*

Cross-talk is defined as the recording of action potentials from nearby muscles while the electrode is placed on a specific muscle of interest (De Luca & Merletti, 1988). Classically, it has been measured by using the cross-correlation function which depicts the similarity between two signals, thus revealing commonalities (De Luca & Merletti, 1988; Mogk & Keir, 2003). Extrinsic and intrinsic properties can either increase or decrease the level of cross-talk. The level of cross-talk that is recorded is dependent on the investigator's ability to appropriately place the electrodes over the muscle of interest while being conscious of the inherent anatomical limitations (such as muscles in close proximity). For example, if EMG is being recorded from the flexor carpi radialis when muscles are in close proximity, such as the extensor carpi radialis, the chance of cross-talk in the EMG signal is greater. The detection surface of an electrode may have an electrical field large enough to record activity from both muscles. Winter and colleagues (1994) found that an electrode surface of 5 mm² had a detection depth of 18 mm. Other

investigators noted that electrode size was estimated to have negligible effects on detection depth and state that the signal will be primarily dominated by MUPs located at a depth of 10-12 mm (Fuglevand, Winter, Patla, & Stashuk, 1992). Synergistic muscles will be an exception, as it is not possible to conclude whether the synergist signals have contamination from each another (Winter, Fuglevand, & Archer, 1994), also noted by Mogk & Keir (2003) where they found 50% common signal between electrode pairs over the forearm extensor muscles and 60% common signal between electrode pairs over the forearm flexors.

Controlling for cross-talk is important when reporting the electrical activity of specific muscles. Electrode placement can have a significant effect on the cross-talk in the EMG recording. Winter and colleagues (1994), investigated both a theoretical model and an experimental approach. Both the model and experimental approach were used to investigate the difference in cross-correlation between electrode pairs at various inter-electrode distances. Based on the results, recommendations were made to reduce the amount of cross-talk: use electrodes with smaller surface area and also arrange them in a close bipolar spacing with differential amplification (Winter et al., 1994).

The cross-correlation technique was used under the assumption that there was no extinction of the intracellular action potential at the end-plate and tendon region, which may render cross-correlation techniques as oversimplified (Farina, Merletti, Indino, Nazzaro, & Pozzo, 2002). Conclusively, Farina and colleagues (2002) did settle that minimizing electrode distance for double-differential signals will aid in decreasing cross-talk (Figure 11). A double-differential signal is where three in-line electrodes are differentiated (subtracted from each other) twice to form a double differential (Guerrero,

Spinelli, & Haberman, 2016). Using a 3-bar electrode and/or double-differential amplification is also supported as a method of cross-talk reduction by many (De Luca, Kuznetsov, Gilmore, & Roy, 2012; De Luca & Merletti, 1988; Guerrero et al., 2016). A study was conducted in which EMG was measured from several cat muscles to investigate the cross-talk at various levels of supramaximal stimulation applied at the nerve (Solomonow et al., 1994). They denervated muscles adjacent to the muscle of interest and found that the cross-talk contained in those adjacent was negligible (Solomonow et al., 1994). Solomonow and associates (1994) declared that the cross-talk may be negligible when using EMG for biomechanical studies, this however, is not applicable to all muscle groups (i.e., muscles of the back, gluteus area, etc.).

With relevance to this specific study, it is important to note that the flexor carpi radialis is in close proximity to many other muscles (Mogk & Keir, 2003). Specifically in regards to the Delsys dEMG electrode, where there are 4 differentiated channels acting to counter and reduce the common signal from adjacent muscles and external electronic sources (Nawab et al., 2010).

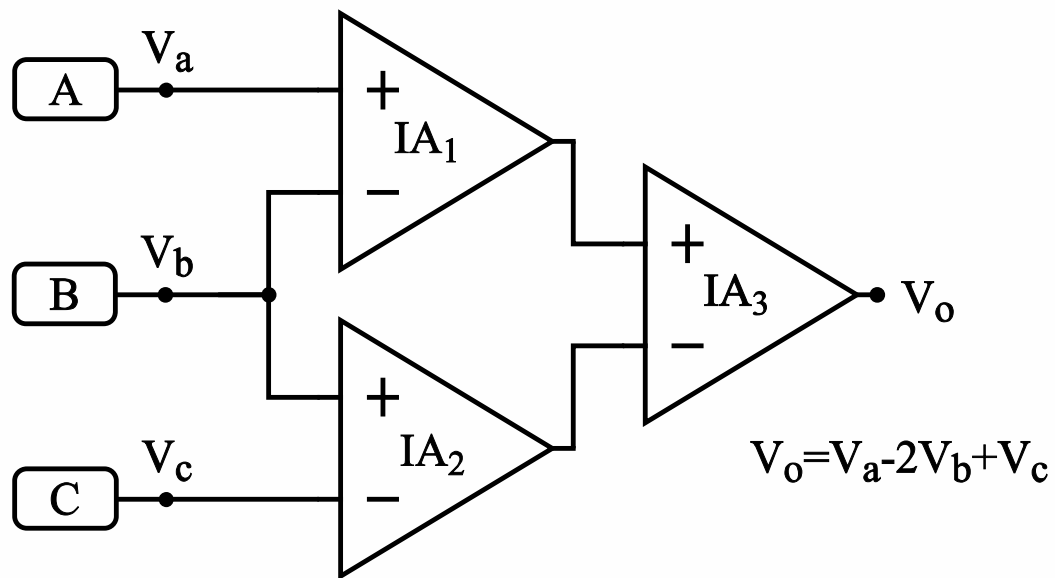


Figure 11. Double-differential amplification, where electrodes are in-line and V_a and V_b are differentiated, then V_b and V_c are differentiated. IA_1 and IA_2 are the single differentiations and IA_3 is the differentiation of IA_1 and IA_2 , therefore IA_3 is a double differential. Guerrero, F. N., Spinelli, E. M., Haberman, M. A. (2016). *IEEE Transactions on Biomedical Circuits and Systems*. Figure 1, page 787.

2.6.5 *Electrode Placement*

The focus of the present thesis is to examine the validity of an automated decomposition system, thus the setup and placement of the electrode must be done in accordance with recommendations on an ideal electrode placement site (Zaheer et al., 2012). Before the electrodes are placed, the skin should be properly prepared to ensure minimal skin-electrode impedance to achieve the best signal amplitude (Clancy et al., 2002). This is easily accomplished by cleansing the skin with alcohol and using a conductive gel between the skin surface and electrode, as recommended by Clancy and colleagues (2002), and mentioned in the SNR section of this document. Anatomical variability must be understood and accounted for, as to avoid areas of excessive subcutaneous tissue (De la Barrera & Milner, 1994), cross-talk from surrounding muscles (Winter et al., 1994) or the innervation zone (Rainoldi et al., 2004).

As mentioned in the previous section, electrode placement is a major contributor to electrode cross-talk (De Luca & Merletti, 1988; Winter et al., 1994), and so it should be done with care. Subcutaneous tissue has been discussed previously, where it is clear that there are negative effects on the EMG signal due to tissue filtering (Bilodeau et al., 1992; De la Barrera & Milner, 1994; Hogrel, 2003; Nordander et al., 2003). The innervation zone, as mentioned previously, is the location where nerve terminations and muscle fibers are connected (Rainoldi et al., 2004). If the electrodes are placed in such a configuration that they straddle the innervation zone, it will result in signal amplitude attenuation (see Figure 12) (Beck et al., 2009; Farina, Merletti, Nazzaro, & Caruso, 2001; Rainoldi et al., 2004). Using a linear electrode array it is possible to easily identify the innervation zone of muscles (Mesin, Merletti, & Rainoldi, 2009). Beck and colleagues

(2009) used a linear electrode array over the vastus lateralis and found that electrodes placed around the innervation zone had low-frequency attenuation and recommend placing electrodes between the innervation zone and the tendon end regions. This has also been recommended by others through experimentation (Rainoldi et al., 2004, 2000) and modelling (Farina et al., 2001). Recently, a study was conducted where a monopolar and bipolar electrode arrangement were used to quantify the reliability of evoked potentials and the reduction of cross-talk (Green, McGuire, & Gabriel, 2015). For EMG on the FCR they found that a bipolar configuration with one electrode placed on the motor point and one directly adjacent in orientation with the fiber direction significantly minimizes cross-talk from the ECR (Green et al., 2015). Lateva and colleagues (2001) reported that the individual phases (onset, spike, terminal wave and slow-afterwave) of the MUP can be used for studying MU properties and inferring muscle fiber architectural characteristics. Due to the nature of the present study, dynamic contractions are not of major importance, but movement during an isometric task must be mitigated to control for the shift of the innervation zone below the electrodes (Rainoldi et al., 2000).

Zaheer and colleagues (2012) stated that the placement of the dEMG sensor has an influence on the total yield of MUPTs that are identified from the decomposition algorithm. The investigators made inferences based on MU yield in several locations on the body (six lower limbs and one upper limb) over muscle bellies that had various amounts of subcutaneous tissue. Based on the findings, Zaheer and colleagues (2012) recommended placing dEMG electrode 1/3 distal from the center of the TA muscle belly due to the MU yield at that sensor site. The innervation zone was investigated in 43 different muscles and the investigators found that there was good uniformity of the

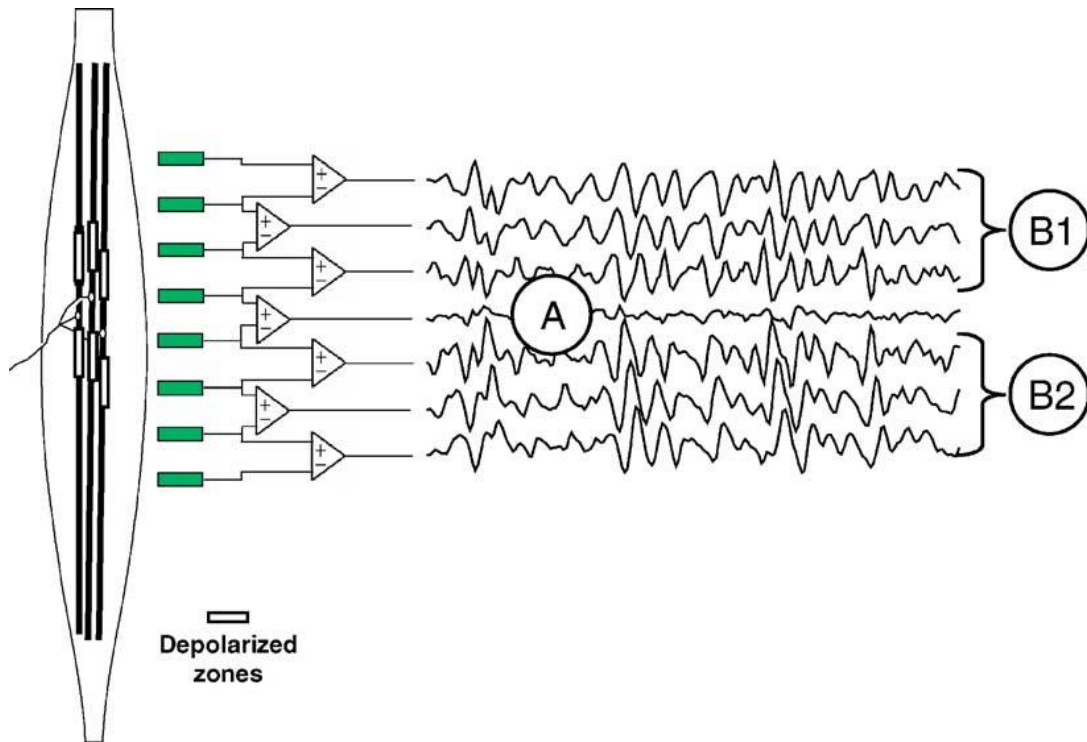


Figure 12. This is an example of an EMG signal that was recorded with a linear electrode array. The electrode array was placed longitudinally with the vastus medialis muscle and it was placed over the innervation zone. There is a clear attenuation of signal amplitude (A), and the phases are reversed for B1 and B2. Rainoldi, A., Melchiorri, G., Caruso, I. (2004). A method for positioning electrodes during surface EMG recordings in lower limb muscles.

innervation zone in the FCR and TA (Beretta Piccoli et al., 2014). This means that across trials the identification of a motor point within these muscles should not be excessively complex or difficult.

2.6.6 *Movement Artifact*

Movement artifact is a source of noise that can occur if the muscle moves under the electrode surface, or if there is movement between the electrode-skin interface (De Luca et al., 2010). De Luca and associates (2010) found that a Butterworth filter with a cutoff frequency of 20 Hz and a slope of 12 dB/oct was recommended to mitigate the noise that resulted from movement artifacts. According to Day (2002), it is ideal to apply a similar filter to the EMG signal, as some movement artifact is comprised of the low frequency components of the EMG power spectrum. Rainoldi and colleagues (2000) noted that the innervation zone below the electrodes shifted approximately 10 mm during dynamic contractions, which may introduce movement artifact into the recorded signal.

2.6.7 *Temperature and EMG*

Temperature in the recording environment should be controlled when recording EMG signals as it has the potential to modulate the results (Bigland-Ritchie et al., 1992; Rutkove, 2000, 2001; Rutkove, Kothari, & Shefner, 1997; Troni et al., 1991).

Temperature can be modulated to invoke changes in the neuromuscular system, whether it be through whole-body or local heating and cooling. Generally, in electrodiagnostic medicine the investigators try to keep temperatures of the upper limb between 34°C and 36°C and the lower limb between 32°C and 34°C. Cooling the muscle effects the neuromuscular system by increasing MUP duration (Bertram, Nishida, Minieka, Janssen,

& Levy, 1995) decreasing Na^+/K^+ pump activity, conduction velocity (Troni et al., 1991), mean power frequency (Winkel & Jørgensen, 1991) and/or muscle contraction force (Rutkove, 2001). Different effects are observed with heating, although the severity of these effects is still of relevance and must be controlled for. It has been reported that with heating up to 42°C (skin temperature) that MUP amplitude and duration decrease while conduction velocity increases (Farina, Arendt-Nielsen, & Graven-Nielsen, 2005; Hodgkin & Katz, 1949; Rutkove et al., 1997b). These changes are likely due to sodium channel function, as understood by Hodgkin and Katz (1949) in a squid model. Furthermore, some of these changes may be due to the mechanical properties of the muscle itself, such as changing of the viscoelastic properties of muscle (Farina, Arendt-Nielsen, & Graven-Nielsen, 2005).

For the purpose of the present study, it is important to note that changes in MU discharge rates occur with temperature changes. Mallette and colleagues (2018) had participants complete isometric contractions in a cold condition (~22° C skin temperature) and thermoneutral condition. The local forearm cooling increased the number of MUs recruited, increased the MUP duration and decreased MUP amplitude (Mallette et al., 2018), findings similar to those reported previously (Rutkove, 2000, 2001). The investigators also reported that MU discharge rates did not change between conditions, which has been previously observed in the first dorsal interosseous following the cooling of 5°C (Bigland-Ritchie et al., 1992). Farina and colleagues (2005) have also reported no difference in the discharge rate of low-threshold MUs at various skin temperatures.

It has been reported that heat has a significant effect on the EMG signal, as reported previously (Racinais, 2013; Rutkove et al., 1997). The RMS EMG amplitude was decreased in both a hot core ($\sim 39^{\circ}\text{C}$) and a hot skin (35.2°C) condition. A decreased RMS amplitude may be explained by the shortening of the time that the voltage-gated sodium (Na^{+}) channels remain open when temperature increases (Hodgkin & Katz, 1949; Racinais, 2013). Considerations for temperature should be noted when conducting a study, as temperature may be a large influencer on the outcome of the collection of the EMG signal.

2.6.8 *Muscular Fatigue*

Muscular fatigue can be described as the inability of a muscle to sustain a required or expected force (Bigland-Ritchie et al., 1981; Bigland-Ritchie & Woods, 1984). This can be due to metabolic changes in the periphery associated with a high rate of energy turnover due to muscle cross-bridge events or a lack of descending neural drive (Sacco, McIntyre, & Jones, 1994). When a build-up of metabolites occurs, such as the accumulation of hydrogen (H^{+}) or lactate, the rate of adenosine triphosphate (ATP) supply declines. The gathering of such metabolites as well as potassium (K^{+}) in the extracellular spaces leads to a decreased effectiveness of calcium (Ca^{2+}) and thus there is a reduction in excitation-contraction coupling (Bigland-Ritchie & Woods, 1984). More recently, other factors have been said to the cause, such as an accumulation of inorganic phosphate (P_i) (Westerblad, Allen, & Lännergren, 2002). The accumulation of P_i results from the breakdown of creatine phosphate. The P_i may act directly on the myofibrils by binding to an active site and reducing the force generating capacity or by binding to Ca^{2+} directly in the sarcoplasmic reticulum (Westerblad et al., 2002). With fatigue, motor units

must then have higher activation rates to maintain the same level of force through means of rate coding (Fuglevand, Macefield, & Bigland-Ritchie, 1999). The effects of fatiguing contractions can be seen through the depression of the EMG amplitude that is recorded (Dimitrova & Dimitrov, 2003; Enoka, 2012). Fatigue also appears as a shift to the lower frequencies in the frequency spectrum due to the increase of low-frequency components (24 to 48 Hz) and the decrease in the high-frequency components (136 to 400 Hz) (Bigland-Ritchie et al., 1981; Komi & Tesch, 1979). This shift has been more dominant with individuals who had greater amounts of fast-twitch fibers (Komi & Tesch, 1979). The shift in the spectrum to the lower-frequency components with a concomitant decline in force generating capacities after fatigue may suggest that there is an impairment of the excitation-contraction coupling, since EMG responses were still recorded even though tension was not significantly generated (Fuglevand et al., 1999).

The MFCV, median power frequency (MDF) and mean power frequency (MPF) is said to be affected by fatigue. In a study by Arendt-Nielsen and Mills (1985) participants contracted at various levels ranging from 10% to 90% MVC. The investigators noted that a linear relationship existed between the MPF and MFCV, however for 10-20% MVC the MPF and MFCV increased, while contractions of 30% MVC or higher led to both variables decreasing (Arendt-Nielsen & Mills, 1985). These results were later replicated within a healthy and a clinical cohort (neuropathy, myasthenia, myotonia, myopathy) population. Participants sustained a maximum continuous contraction for as long as possible. The researchers found that MFCV decreased linearly with fatigue. The MPF decreased with fatigue as well (Yaar & Niles, 1992). Sbriccoli and colleagues (2003) measured the influence of the speed of a

contraction on several variables, including conduction velocity and MDF. They found that with higher speed of contraction to maximal effort led to a steeper decline in the MDF (Sbriccoli et al., 2003). The MDF and MPF both declined after sustained contractions of the TA at 20 and 80% MVC (Merletti et al., 1990). The reduction in MFCV, and MDF was also observed in the brachioradialis in a study where participants held sustained contractions of the elbow flexors (Lowery, Nolan, & O'Malley, 2002). Recently, using the dEMG system, investigators had participants fatigue their vastus lateralis muscle. The participants exhibited an increase in motor unit firing rates, recruitment of new motor units and decrease in motor unit recruitment thresholds. The investigators reported that the control scheme remained unchanged (Contessa, De Luca, & Kline, 2016).

2.7 Electromyographic Decomposition

For years many investigators have sought to develop technology to extract the rudimentary information of single MUs from the complex sEMG signal (Drost, Stegeman, van Engelen, & Zwarts, 2006; Lefever & De Luca, 1982; Merletti, Holobar, & Farina, 2008; Nawab et al., 2010). Decomposition of the sEMG signal is the process of separating the constituent MUPs that form the interference pattern (Stashuk, 2001). This has been accomplished using semi-automated (McGill, Lateva, & Marateb, 2005) and fully-automated technology (Gazzoni, Farina, & Merletti, 2004; Merletti et al., 2008; Nawab et al., 2010). Decomposition software has been used with both sEMG (De Luca et al., 2006; Drost et al., 2006; Gazzoni et al., 2004; Merletti et al., 2008; Nawab et al., 2010) and indwelling EMG signals (McGill, Cummins, & Dorfman, 1985; Nawab, Wotiz, & De Luca, 2008; Stashuk & de Bruin, 1988; Stashuk & Qu, 1996). When

evaluating the validity of the decomposition technology, it is important to ensure that the MU firing times are true to ensure that one MU can be discriminated from another (Qu & Stashuk, 1993; Stashuk & Qu, 1996). The focus of this thesis is to only use MU data that is considered valid by removing data in which we do not have high confidence. The following section introduces and details the specific processes that several investigators have developed for their own methods of decomposition.

2.7.1 *Delsys Decomposition EMG System*

The Delsys dEMG system is currently commercially available. The decomposition is fully automated and requires minimal input from the user. The process requires a 5-pin electrode that creates 4 differential EMG channels and then the signal is automatically decomposed with the Precision Decomposition III (PD III) algorithm (De Luca et al., 2006; Nawab et al., 2010) (Figure 13). The PD III algorithm uses template matching to assign MUPs to their respective MU based on their shape and firing statistics. The PD III algorithm includes an artificial intelligence procedure known as the PD-IPUS (Integrated Processing and Understanding of Signals) stage and the PD-IGAT (Iterative Generate and Test) stage (Figure 14). Figure 15 shows a sample of data acquired using the dEMG system.

The PD-IPUS stage is used for template creation, template matching and updating. The PD-IPUS framework is meant to handle signals, like electromyograms, that are zero-mean random (stochastic) and non-deterministic (may exhibit different behaviour although the input is the same). This is accomplished by using a maximum *a posteriori* (MAP) receiver. The MAP receiver ensures that the matching of templates is

accomplished by using information of the identified templates for further matching, such that only information from the signal itself is being used, and nothing known beforehand. The PD-IGAT stage is specifically designed to identify which MUPTs have a presence in any of the superpositions that occur within the sEMG signal. Superpositions occur when two or more MUPs occur at a similar instance in time and distort one another as observed in the recorded EMG signal (Etawil & Stashuk, 1996). Templates are combined based on MUPs that are of greater likelihood and the search for the superposition is stopped if the template combination that models the sEMG superposition can be subtracted from the sEMG signal and reduce the net energy by at least 50%. If there are competing answers, the combination of MUPs that most accurately represents the local firing time is selected.

Nawab and colleagues (2010) were able to successfully decompose sEMG signals into their constituent MUPTs using their automatic algorithm, this included five different muscles and various levels of force ranging up to 100% MVC. Their results yield on average for all MUPTs a high accuracy of 92.5%, and reaching 97% at certain times, using the decompose-synthesize-decompose-compare validation approach (Nawab et al., 2010).

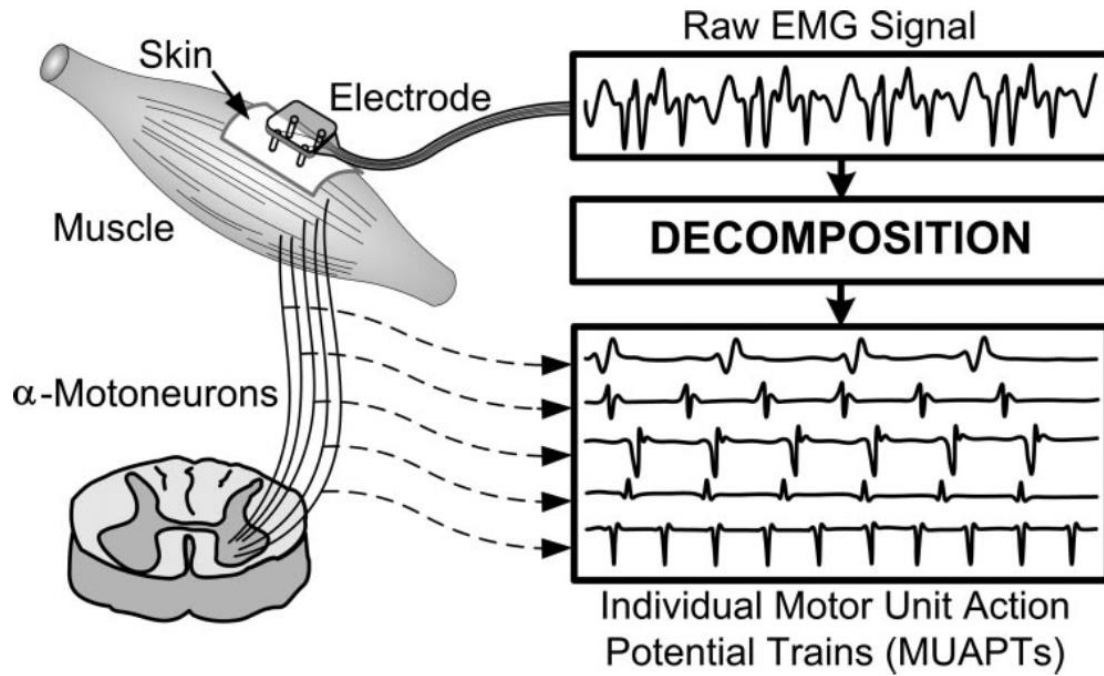


Figure 13. Visual depiction of the surface EMG decomposition algorithm. De Luca, C. J., Adam, A., Wotiz, R., Gilmore, L. D., Nawab, S. H. (2006). Decomposition of surface EMG signals. *Journal of Neurophysiology*.

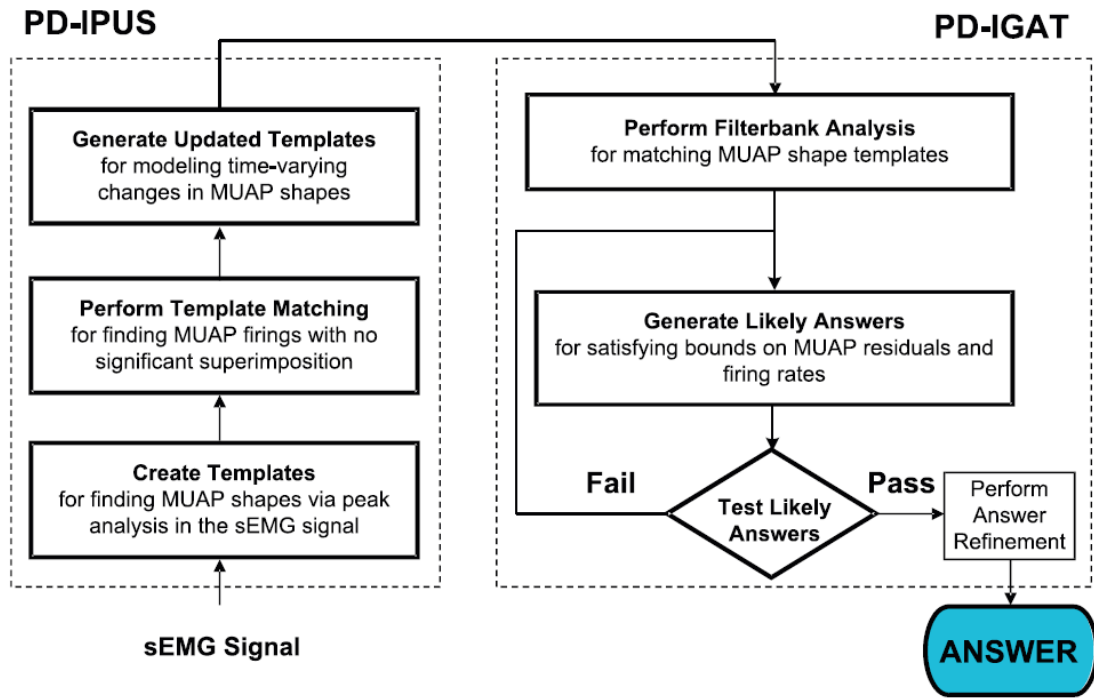


Figure 14. Diagram of the PD-IPUS and PD-IGAT stages of MU decomposition. The PD-IPUS is used for template creation, template matching and updating templates. The PD-IGAT is used to discriminate MUPs that have led to a superposition in the signal. Nawab, S. H., Chang, S., De Luca, C. J. (2010). High-yield decomposition of surface EMG signals. *Clinical Neurophysiology*.

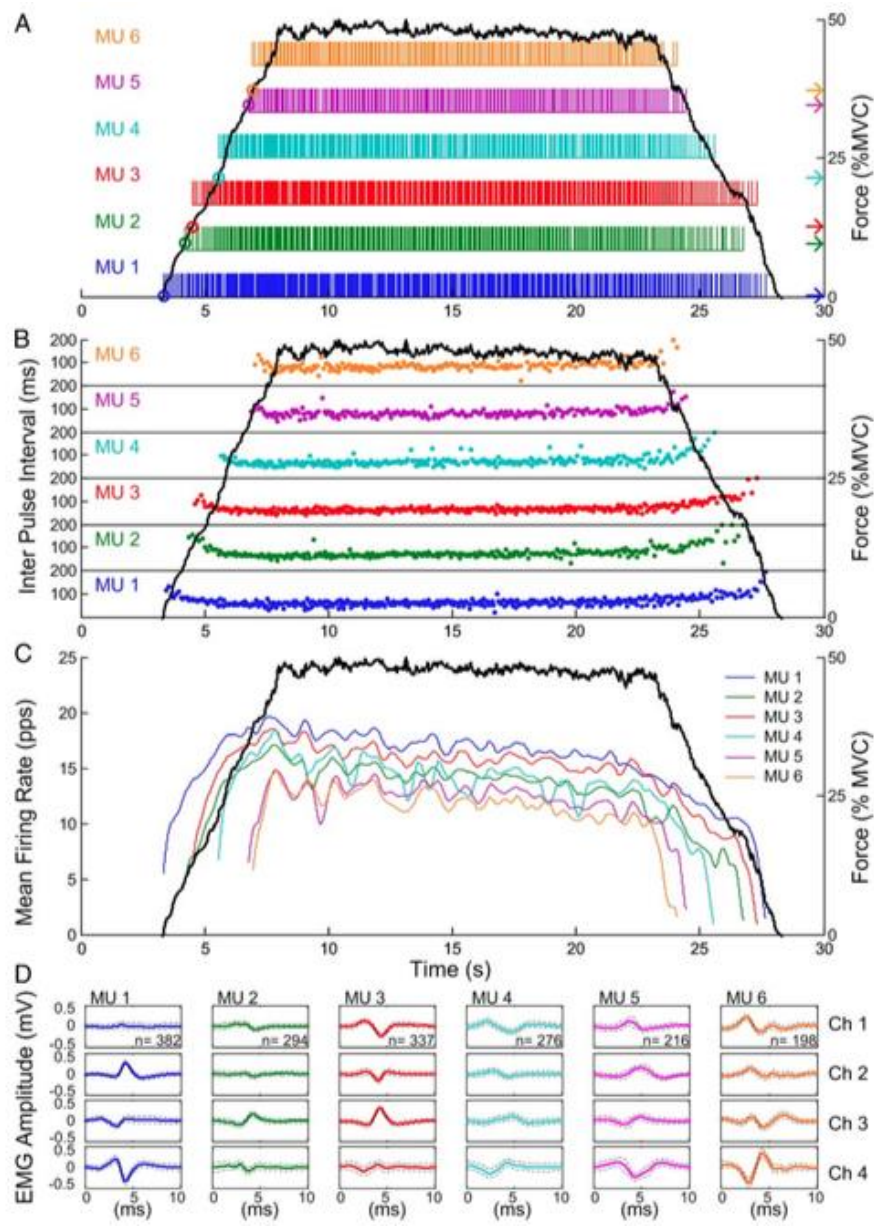


Figure 15. Sample of motor unit firing statistics as observed from the dEMG system. From top to bottom: MUDR of each identified MU respectively; inter-pulse interval for each identified MU; the mean firing rate for each identified; templates of the MUs identified from the decomposition. De Luca, C. J., Adam, A., Wotiz, R., Gilmore, L. D., Nawab, S. H. (2006). Decomposition of surface EMG signals. *Journal of Neurophysiology*.

2.7.2 High-density sEMG Decomposition

High-density sEMG (HD-sEMG) has been used frequently in the last 20 years. It requires the use of multiple, closely spaced electrodes in a grid formation (multi-channel surface EMG), which provides the investigator with temporal and spatial information about the distribution of the electrical activity from the muscle (Figure 16) (Farina, Holobar, Merletti, & Enoka, 2010; Merletti, Botter, Troiano, Merlo, & Minetto, 2009; Merletti et al., 2008; Zwarts & Stegeman, 2003). Investigators have used electrode grid arrays to decompose the sEMG signal with success (Drost et al., 2006; Holobar, Farina, Gazzoni, Merletti, & Zazula, 2009; Merletti et al., 2008, 2008) (Figure 17). Decomposition is accomplished using blind source separation (BSS), which is a method of separating a set of mixed signals without the use of any information given *a priori* (Holobar & Zazula, 2007). The benefit of using the BSS method is that the decomposition is not sensitive to the superpositions of MU action potentials (Merletti et al., 2008).

The detailed mathematics and engineering constituting the source separation procedure is found in Holobar and Zazula (2007). In simple terms, first the EMG signal is combined, then an instant in time where there is high MU activity is selected, the MU discharge pattern is then blindly reconstructed with no *a priori* information, and single MU discharge patterns are filtered out. This is repeated until the entirety of the signal has been decomposed. This algorithm has been refined to only accept MUs that exhibit SNRs (as reported by the investigators as “PNR”, for pulse-to-noise ratio) that are greater than

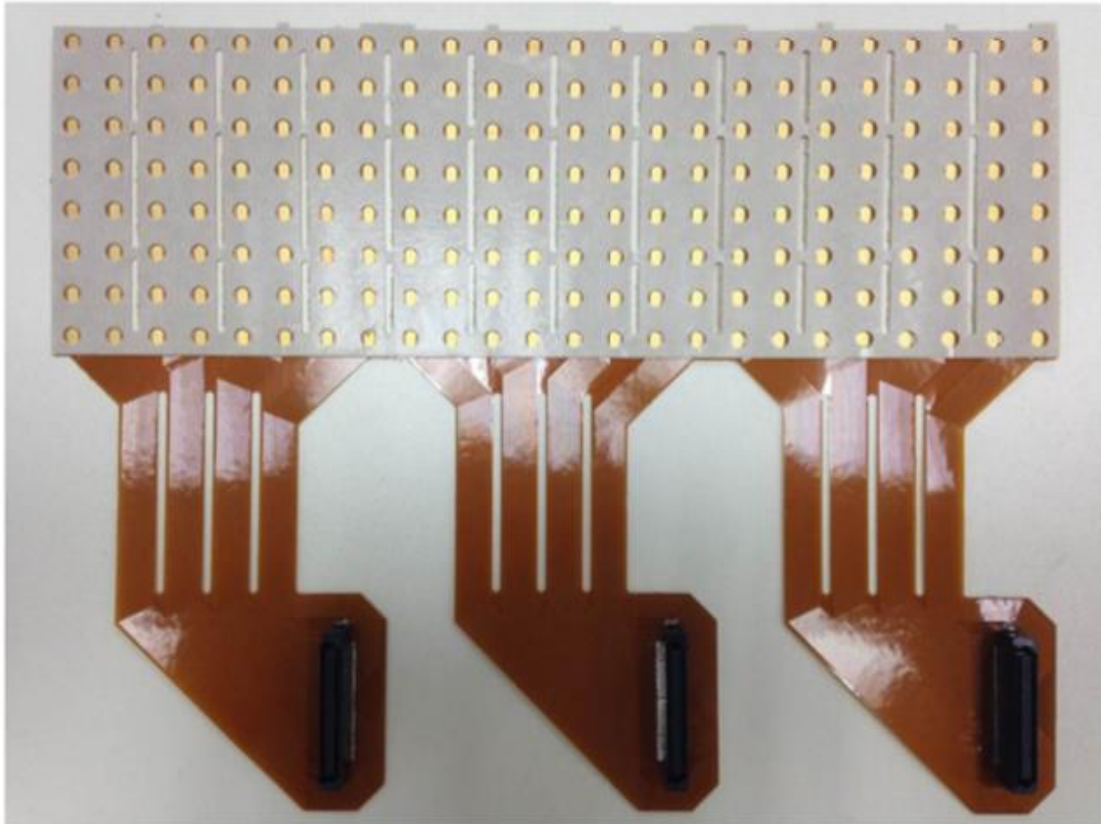


Figure 16. A 192-electrode high-density sEMG grid with an inter-electrode distance of 10 mm. Pan, L., Zhang, D., Jiang, N., Sheng, X., Zhu, X. (2015). Improving robustness against electrode shift of high density EMG for myoelectric control through common spatial patterns. *Journal of NeuroEngineering and Rehabilitation*.

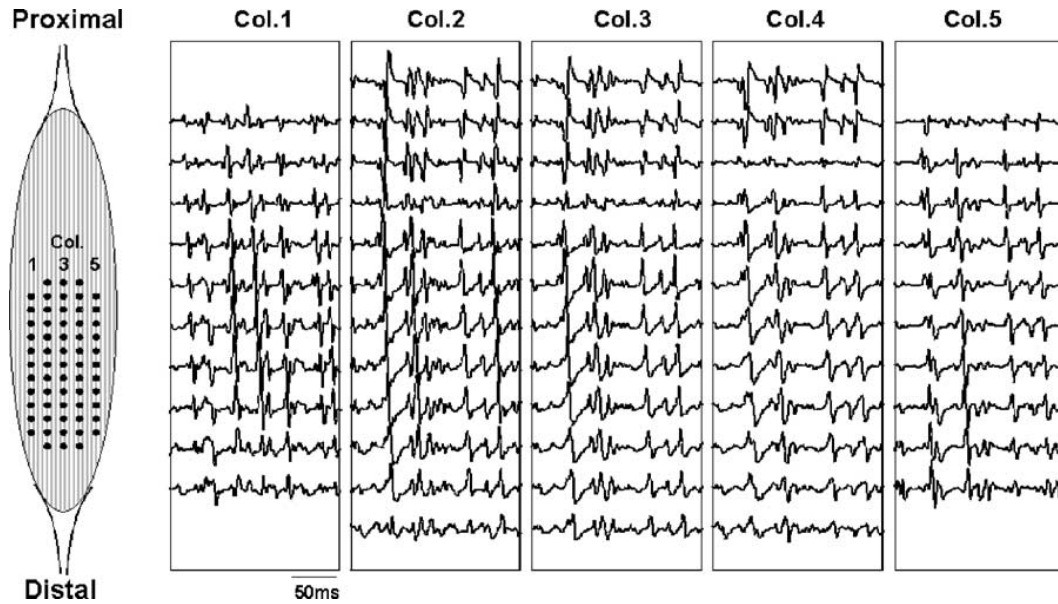


Figure 17. Surface EMG signals that was recorded from the biceps brachii using a 61-electrode grid array. Each individual waveform within each column represents a double-differentially amplified signal. Gazzoni, M., Farina, D., Merletti, R. (2004). A new method for the extraction and classification of single motor unit action potentials from surface EMG signals. *Journal of Neuroscience Methods*.

30 dB (Holobar, Minetto, & Farina, 2014). This allows for a more reliable decomposition, even at contractions of 70% MVC.

2.7.3 *Decomposition-based Quantitative EMG*

Clustering techniques were introduced by Stashuk and Qu (1996b) for EMG decomposition, where similarity and dissimilarity measures are used to partition groups of MUPs into categories (Stashuk, 1999b, 2001). This process was accomplished with unsupervised classification, meaning that the investigator does not feed the algorithm any information *a priori*, and all assignment criteria are developed based on the data itself. The similarity and dissimilarity criteria are determined by comparing the waveforms based on attributes that are measurable between each MUP. In the context of signal processing, this may indicate that the attributes of interest are times of occurrence, MUP amplitude or MUP shape, for example. The Euclidean distance is the most frequently used similarity measure, which depicts the straight-line distance between two defined points, therefore a closer distance suggests a greater similarity and it can be calculated on the basis of specific variables such as amplitude or inter-discharge interval.

The following is reported from Stashuk and Qu (1996b). The algorithm that was used by Stashuk and Qu (1996b) was based on k-means clustering in which a number k is chosen based on some immediate criteria if using supervised learning (such as MUP shape), or k is arbitrarily selected when using an unsupervised learning model. Then, other data points are assigned to k based on their Euclidean (straight-line) distance from that point. The cluster centers are recalculated and iterated until all possible assignments are made and the intra-cluster variance is completely minimized (Galluccio, Michel, Comon, & Hero, 2012; Stashuk & Qu, 1996). The steps were slightly modified to include

the addition of shape- and temporal-based clustering (STBC) information, as the performance of the k-means clustering is influenced by the initial selection of the primary clustering value. The updated STBC version includes a user-selected cluster initialization and a learning phase. As taken directly from the publication:

1. Cluster initialization: choose the initial number of cluster and the cluster centers using the information from the firing patterns.
2. Learning phase: use K-means clustering, cluster splitting based on firing pattern information, selection of core cluster members and ignore clusters with too few members.
3. Individual-cluster threshold classification: use a threshold based on individual clusters to assign candidate MUPs. This is data-driven and no distribution of MUPs is assumed.
4. Cluster splitting: split single clusters into pairs of clusters based on firing-pattern information.
5. Cluster merging: merge pairs of clusters into single clusters based on shape and firing-pattern information.

The algorithm was successful and able to decompose an indwelling EMG signal correctly, with assignment accuracy of the STBC algorithm between 95.3 and 100%. This assignment accuracy was based specifically on the ratio of number of correctly assigned MUPs to the total number of MUPs assigned. Stashuk and Qu (1996b) also manually decomposed the indwelling EMG signals to compare the results directly to the automated

decomposition, which demonstrated further success (see Figure 18 and Figure 19). One major limitation of clustering is that selecting *a priori* information to be used as a fixed similarity across all clusters is not feasible for complex signals, such that the MUP clusters may vary substantially between one another (Stashuk & Qu, 1996b). The authors also created an error-filtered estimation (EFE) algorithm that estimates the mean and standard deviation of inter-pulse intervals (IPIs) and removes erroneous firings that do not belong to the MUPT (Stashuk & Qu, 1996a). This has been done with MUPTs that contain as much as 60% error in firings and only requires 10 or more correct firings.

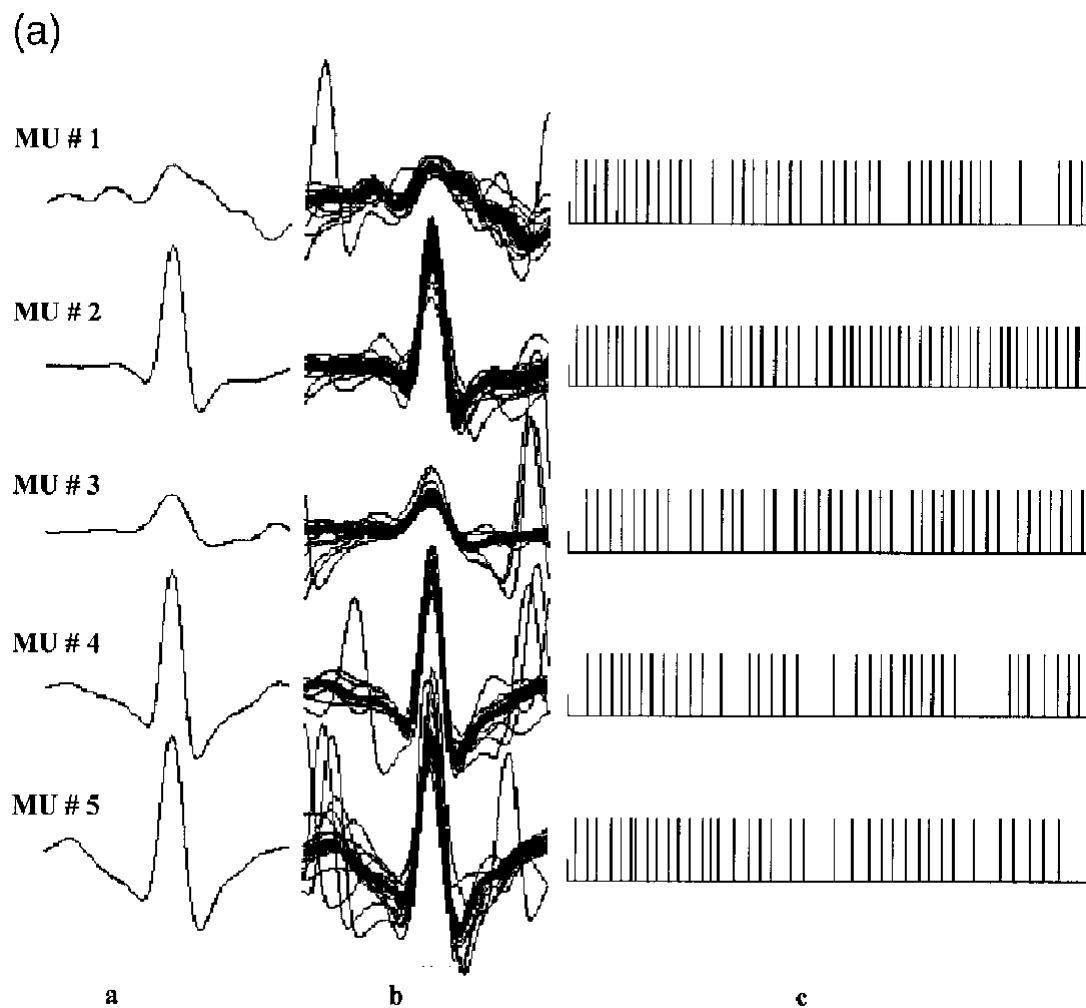


Figure 18. (a) Manually decomposed EMG signals with the (a) MUP template, (b) the MUP shimmer plot and (c) the firing times for the respective firings. Stashuk, D. W. (2001). EMG signal decomposition: how can it be accomplished and used? *Journal of Electromyography and Kinesiology*.

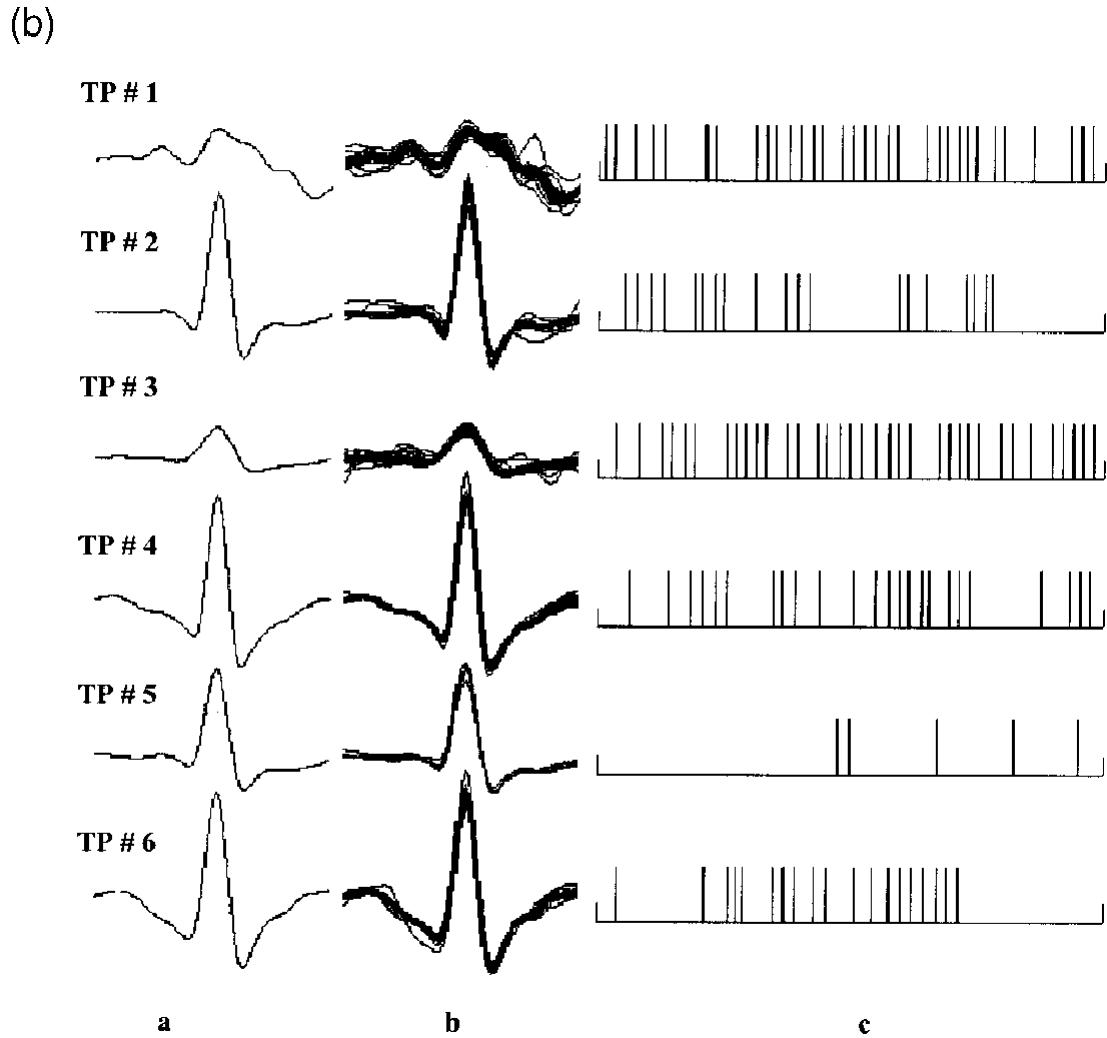


Figure 19. (b) Clustering algorithm results, with the (a) MUP template, (b) the MUP shimmer plot and (c) the firing times for the respective firings. Stashuk, D. W. (2001). EMG signal decomposition: how can it be accomplished and used? *Journal of Electromyography and Kinesiology*.

2.8 Validation Techniques

2.8.1 Reconstruct & Test Method

De Luca and LeFever (1982) were interested in EMG signal decomposition through the use of a fully automatic, mathematical algorithm. Before this idea was conceived, there was a great deal of visual identification by a human operator for MU detection which took a long time for completion. De Luca and LeFever (1982) developed an algorithm that required minimal human operation but could yield accurate results. Four main sequential steps were detailed: locate the MUP in the waveform of the myoelectric signal; identify if it can be grouped with previously detected MUs and if not, assign the MUP to a new MU template; use the MUP that was identified to update the template; remove the MUP from the myoelectric signal and restart from the first step. The signal was continuously decomposed until all MUPs above a certain amplitude threshold are removed. Throughout the process, the template is continuously updated allowing the algorithm to function even when the MUAP is subjected to variation. This methodology is foundational for what was later termed *Precision Decomposition*, as explained in a previous section (De Luca et al., 2006; Nawab et al., 2010).

The reconstruct and test approach (also known as the decompose-synthesize-decompose-compare [DSDC]) validation method involves automated decomposition of the sEMG signal, from which the decomposed signal is then resynthesized and white Gaussian noise, with a variance that is equal to the residual signal, is added to the resynthesized signal (see Figure 20). The goal of this validation protocol is to overcome the limitations of the two-source test (De Luca & Hostage, 2010). The resynthesized

signal is then compared with the original decomposition and any discrepancies between the two decompositions are considered to be errors. The strength of this validation method is that it compares all of the decomposed MUPTs, not just a small subset, that would be validated through the two-source method (De Luca et al., 2015). Limitations to this validation model are further explored in a later section.

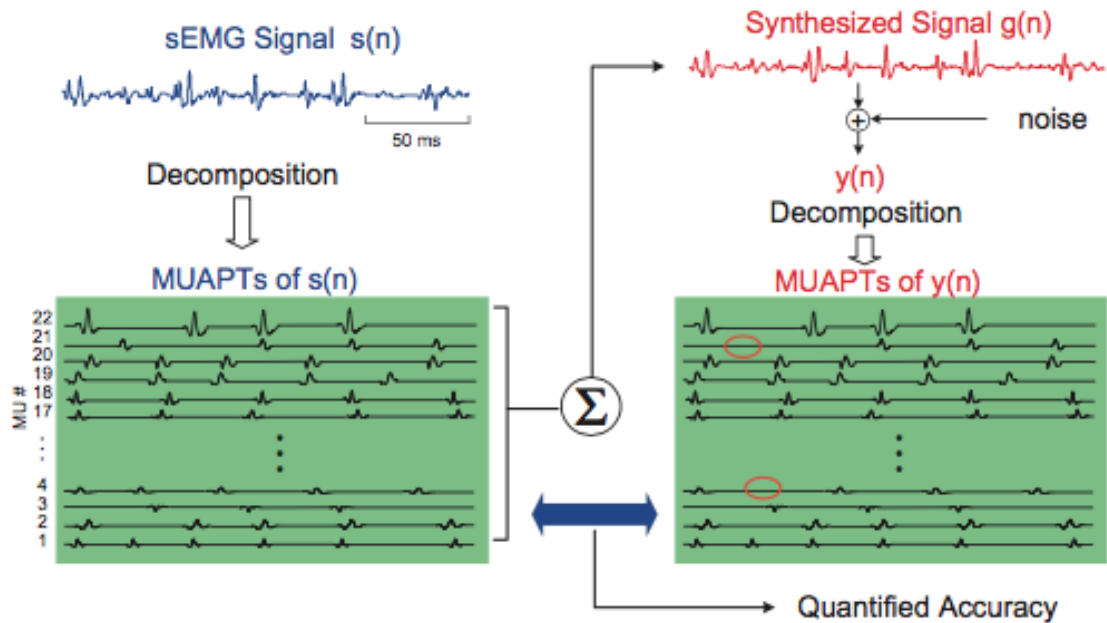


Figure 20. Decompose-synthesize-decompose-compare visual outline. The sEMG signal is decomposed into its constituent MUAPTs. The decomposed MUAPTs are then resynthesized and Gaussian noise equal to the residual from the first decomposition is redistributed across the signal. The resynthesized signal is then decomposed again and is compared to the original decomposition. Nawab, S. H., Chang, S., De Luca, C. J. (2010). High-yield decomposition of surface EMG signals. *Clinical Neurophysiology*.

2.8.2 *Two-Source Method of Validation*

Early validation methods of EMG signal decomposition accuracy were initiated by Mambrito and De Luca (1984), in which the decomposition algorithm developed by De Luca and LeFever (1982) was applied to two recorded intramuscular EMG signals taken from the same muscle (tibialis anterior) at a distance of 1 cm apart. The researchers found that the two sources showed 100% agreement for the common MUPs from their 1415 detections (Mambrito & De Luca, 1984). The same group of researchers used an identical technique to validate their sEMG decomposition data, by placing a surface sensor array over the skin surface of the tibialis anterior with a quadrifilar needle sensor inserted directly below the surface sensor, at 1 cm depth (De Luca et al., 2006). This technique was then successfully adapted to be used with a pair of sEMG sensors that were spaced closely and simultaneously recorded the contraction (Nawab et al., 2010).

Some have suggested that the most effective way to validate the decomposition accuracy is through the two-source method (Farina & Enoka, 2011; Farina et al., 2010). If the two-source method is being used with an indwelling electrode and a surface electrode, the issue of invasiveness arises. De Luca and Nawab (2011) stated that there are two deficiencies that exist when using the two-source method; firings are from a small subset of common MUPTs that are detected by both sensors and it does not offer any insight on the remainder of the MUs detected in the sEMG signal, and if intramuscular EMG is used then a different algorithm is required to decompose the signal compared to the sEMG source. The two-source method has appeared to be a reliable source of validation for determining the accuracy of a decomposition algorithm, although the deficiencies and

limitations of the method should be considered moving forward (De Luca et al., 2006; Farina et al., 2010; Hu et al., 2014; Nawab et al., 2010).

2.8.3 *Spike Triggered Averaging*

Spike triggered averaging (STA) is a method of waveform averaging in which segments of a signal are time-aligned based on a triggering event (such as a firing from a MUP), then an epoch centered around the event is used as a window to average all of the detected events based on the respective triggers (Hu et al., 2013b; Hu, Rymer, & Suresh, 2013c). As an example: the dEMG algorithm from Delsys provides the operator with all of the identified MUP firing instances, which can be used as the trigger for collecting the MUP within a specific epoch. The epoch is determined by the operator (25 ms in the present thesis) and is then used to average all MUPs that are associated with the MU firings. The product is an averaged signal of the MUPs based on the firing times from a single MU.

Spike triggered averaging introduces some problems including superpositioning of different action potentials from other motor units and spurious firings from other sources (Hu et al., 2013c). Hu and colleagues (2014b) sought to determine the validity of a skin surface EMG decomposition algorithm due to the scarcity of routine assessment procedures for the validity of automated decomposition software. The group used inter-spike intervals (ISIs) to examine the firing statistics of the identified MUs from the sEMG signal (Hu et al., 2014b). It is possible to validate the accuracy of the dEMG through inter-spike intervals (ISIs). This method involved a two-step process and included the use of intramuscular EMG. The first step involved spike triggered averaging

and the second step involved the alignment of the intramuscular EMG and sEMG raw signals. Histograms for ISIs were created for both the sEMG and intramuscular EMG data and then overlaid upon one another to elucidate the similarities and differences between the signals.

Cross-validation between the ISIs for intramuscular EMG and sEMG signals provided confirmation of the presence of a MU discharge. Correlation coefficients were calculated for the coefficient of variation for the ISIs based on the accuracy percent from the cross-validation for the ISIs, and a moderate negative correlation was revealed based on that relationship ($r = -0.65$, $p < 0.001$). Analysis of the ISI statistic led to uncovering valuable information regarding the accuracy of sEMG decomposition and where errors may be found during decomposition (Hu et al., 2014b).

2.8.4 *The Gap Statistic*

Using the output of any sort of clustering algorithm, such as the previously mentioned k-means clustering, it is possible to estimate the number of clusters that exist in a set of data (Tibshirani, Walther, & Hastie, 2001). A gap statistic is used to select features that effectively represent MUPs within a specific MUPT (Parsaei & Stashuk, 2011). The algorithm explained by Parsaei and Stashuk (Parsaei & Stashuk, 2011) describes two main parts of a similar gap-based validity approach, the adaptive gap-based MUPT validation. First, the algorithm estimates the gap values between the MUPs that are assigned to a given cluster (MUPT), and second, the samples with significant gap values are used to represent the MUPs within the cluster. Investigators compared several validation methods after decomposing simulated and real EMG data. The results suggest

that the adaptive gap-based MUPT method was the most effective, as it was faster and among the top four of the evaluated validation methods (Parsaei & Stashuk, 2011). It yielded the highest accuracy for valid trains (93.8%), a moderately high accuracy for detecting invalid trains (73.9%) and the best total accuracy (91.5%), while also being the fastest computation.

2.8.5 *Debate on the Accuracy and Validation of the dEMG System.*

Since the advent of the dEMG system (De Luca et al., 2006; Nawab et al., 2010) there has been ongoing debate regarding the validation methodology of that sEMG decomposition (De Luca & Nawab, 2011; Farina & Enoka, 2011; De Luca et al., 2015; Farina et al., 2015). The debate consisted of a series of letters to the editor in regard to claims originally made by De Luca et al. (2006) on their sEMG decomposition technology. Farina and Enoka (2011) led the discussion by elucidating issues with the decomposition methods and validation. Recall from a previous section that the decompose-synthesize-decompose-compare (DSDC) (also known as the reconstruct-and-test approach) validation method was used to assess the accuracy of the sEMG decomposition. Farina and Enoka (2011) argued that there were several concerns with the validation methods, the following section contain four that were of most importance for De Luca and Nawab (2011) to rebut.

Farina and Enoka proposed that De Luca and Hostage (2010) decomposed a set of synthetic signals that were generated by themselves, of which the discharge times were known for all MUs. De Luca and Nawab (2011) stated that the reconstructed signals from Nawab et al. (2010) and De Luca and Hostage (2010) are synthetic sEMG signals that

contain known MUAP shapes and firing times from the decomposition. The issue with the rebuttal from De Luca and Nawab (2011) is that their results are dependent on a signal that was acquired by them, so the known times are a result of their own decomposition. Decomposing a synthetic signal from another research group may strengthen their argument of validity since the decomposition must reveal the same MUAP shapes and firing rates to a high accuracy. De Luca and Nawab (2011) argue that there are 3 flaws with the use of a synthetic signal: (1) it is a generic test that may not accurately model an sEMG signal; (2) the firing rates are assigned by choice and (3) it would not consider the changing shape of a MUAP that occur in the sEMG signal as a result of movement (electrode or participant), fatigue or disease.

The next claim was in regard to the bias in the first decomposition created by the disagreement between the first decomposition and the decomposition of the reconstructed signal (Farina & Enoka, 2011). There appears to be bias because the decomposition of the reconstructed signal did not contain firings that were exclusively detected in that decomposition compared to the first decomposition. De Luca and Nawab (2011) claim that the argument was based on “false conjecture” and iterated that the figure was not meant to identify false positives and false negatives, but instead was meant to be used as a reference to acknowledge the similarity of the decompositions. They also state that several MUs in the figure exemplify false negatives and false positives but are not clearly stated as such. The false positive and false negative criterion are used in the accuracy assessment that are used in Nawab et al. (2010) and De Luca and Hostage (2010) (see Figure 21).

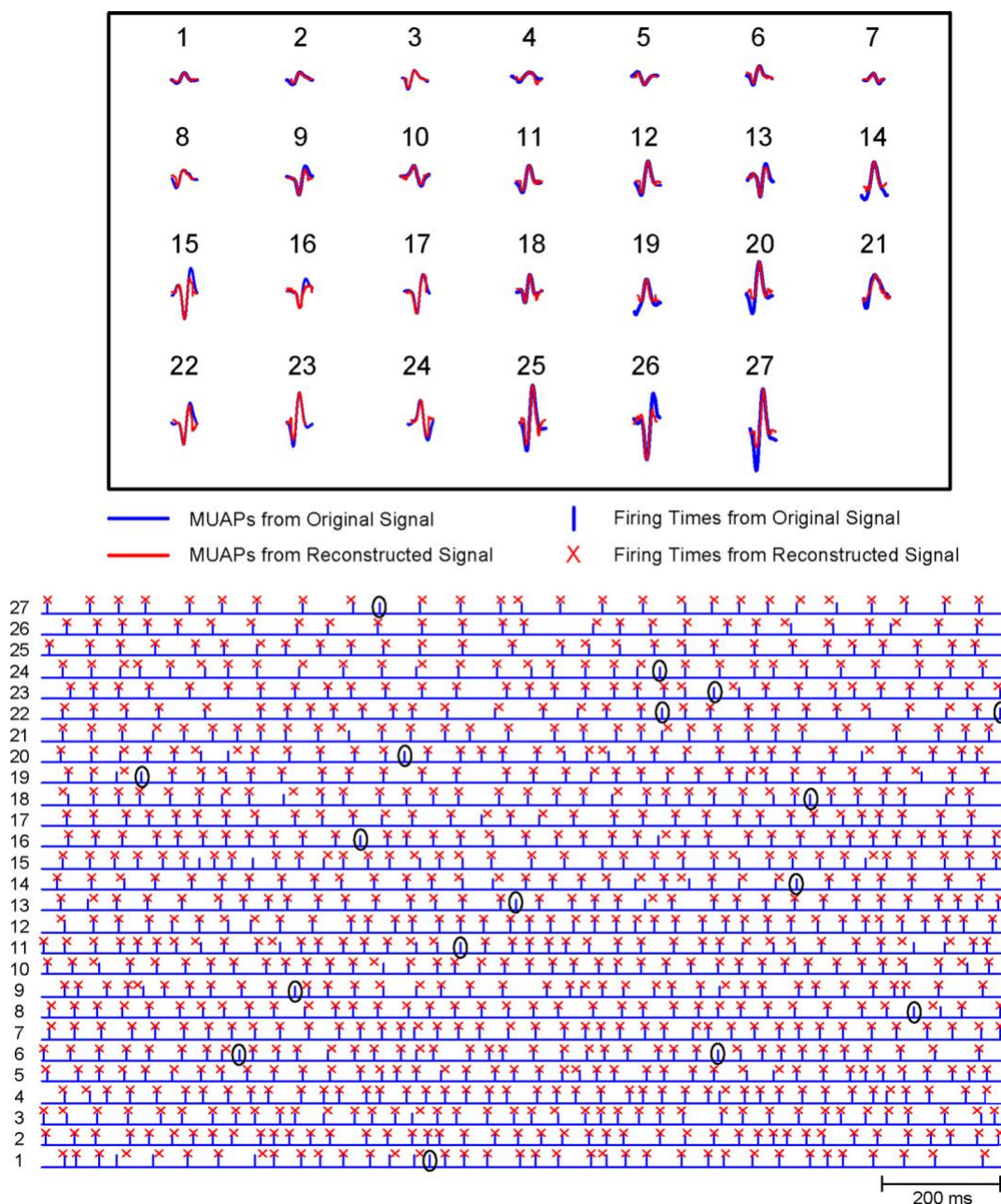


Figure 21. Comparison of the MUs obtained through decomposition of the original sEMG signal and the reconstructed signal. *Top:* the individual MUs that were identified in both decompositions. *Bottom:* a short epoch of the firings from the detected MUs, errors were marked with an oval. De Luca, C. J., Hostage, E. C. (2010). Relationship between firing rate and recruitment threshold of motoneurons in voluntary isometric contractions.

The low power in the residual signal would indicate that the Gaussian noise that is being imposed on the reconstructed signal is going to force the reconstructed signal to look identical and thus their decompositions may be similar. In this case, the decomposition may appear to be accurate (Farina & Enoka, 2011). De Luca and Nawab (2011) explained that not all residual signals have low power, and the claim was based on a generality of a single example.

In a later clarification, it is mentioned that the four-channel (5-pin) electrode is designed to record overlapping MUAPs from many MUs in the sEMG signal (De Luca et al., 2015). Thus, the sEMG signal that is generated includes MUAPs that are likely to have superposition. De Luca and associates (2015) state that an algorithm that can incorrectly decompose the sEMG signal into non-overlapping segments is not appropriate to be used for DSDC validation.

Farina and Enoka (2011) claimed that the decomposition method had not been validated with anything except the DSDC approach, however, this is not the case. De Luca et al. (2006) used the two-source test that was earlier introduced by Mambrito and De Luca (1984). In the study of interest there was a comparison of intramuscular EMG to sEMG recordings from 13 contractions of the FDI with an average accuracy of $94.3 \pm 1.9\%$. Furthermore, Nawab et al. (2010) compared the decomposition of two sEMG signals and found an accuracy of 92%. The two-source test contains some deficiencies as mentioned in a previous section regarding the two-source methodology.

In the last exchange of letters, Farina and colleagues (Farina et al., 2015) stated that the critical issue in the field of EMG decomposition is ultimately the validity of the

decomposition. They then clarified that the DSDC validation procedure is not adequate since it is not measuring the accuracy of the decomposition. The DSDC validation method does not reflect the quality of the MUAPs that are decomposed, rather it assesses if the decomposition can be accomplished again with a similar reconstructed signal. Farina et al. (2015) continue to highlight the pressing issue of overcoming the source separation problem, in which residual noise decreases with an increase in noise sources. They did not shift in their stance that the DSDC validation method remains to be problematic and that the two-source test is still the best validation method (Farina et al., 2015).

The goal of this thesis is to facilitate the validation of discharge times that are obtained through automated decomposition of the sEMG signal by means of removing extraneous firings that do not correspond with selected predetermined parameters. The proposed task is easy to implement and requires minimal computation time from the operator.

CHAPTER 3: Methods

3.1 Participants

The force and sEMG data are from 20 participants (10 males and 10 females). Participants with neurological or musculoskeletal disorders or injuries of the upper limbs as well those who were outside the age range of 18-35, were excluded from the study. This study was cleared by Brock University Research Ethics Board (REB: #16-313 and REB: #18-042 Appendix 2).

3.2 Experimental Task

The data collection took place inside a Faraday cage. Participants watched a computer screen in front of them that provided visual feedback of the force being exerted on the load cell. Three MVCs were performed by the participant for 3 s to determine what 20% and 60% MVC was for the following trials. Adequate inter-trial rest (2 minutes) was implemented to minimize any fatigue effects as done previously in the laboratory (Gabriel, Lester, Lenhardt, & Cambridge, 2007). The force was provided as direct feedback through a computer monitor to facilitate the holding of the contraction. Participants were asked to trace a ramp on the screen that represented 20% MVC force based on the most stable MVC effort. The 20% MVC force trace was used as a signal quality check for the dEMG electrode to ensure high-quality recordings as indicated by a high SNR, and low skin and line interference. Participants were then required to complete two additional ramp contractions to 60% MVC. The participant had to trace a force-time pattern in which the rising contraction increased by 10% MVC/s for 6 seconds, then was maintained at 60% MVC for 15 seconds and decreased by 10% MVC/s for 6 seconds.

3.3 Apparatus and Instrumentation

Subjects were asked to participate in a task familiarization session on a separate day prior to beginning the experimental protocol. Participants were seated so they were comfortable and able to insert their hand into the custom jig, with the forearm in supination (Figure 22), their arm was required to rest comfortably. The setup of the custom-made device included an Interface MB-100 load cell (Interface, Scottsdale, AZ), which allowed for the measurement of wrist flexion force. The forearm was rested on the wooden surface to reduce the amount of contribution from elbow flexion and shoulder flexion.

The motor point, which is the area of the muscle where a contraction can be elicited by the most minimal intensity stimulation (Bowden & McNulty, 2012), was located through low-level, repeated percutaneous electrical stimulation over the FCR at 1.5 pulses/s. The motor point was marked using indelible ink to use as reference for downstream placement of the dEMG electrode. To ensure proper electrode placement, the palmaris longus was also identified with this method as to avoid an improper electrode placement. Preparatory work for the electrode included shaving the skin surface over the FCR, cleaning the skin surface with alcohol, using a light abrasive cream (NuPrep, Weaver and Co., Aurora, CO) to remove dead skin from the skin surface and then using alcohol to clean it once more.

The 5-pin dEMG electrode was placed approximately 2 cm distally from the identified motor point and secured with tape. The dEMG electrode has an interelectrode

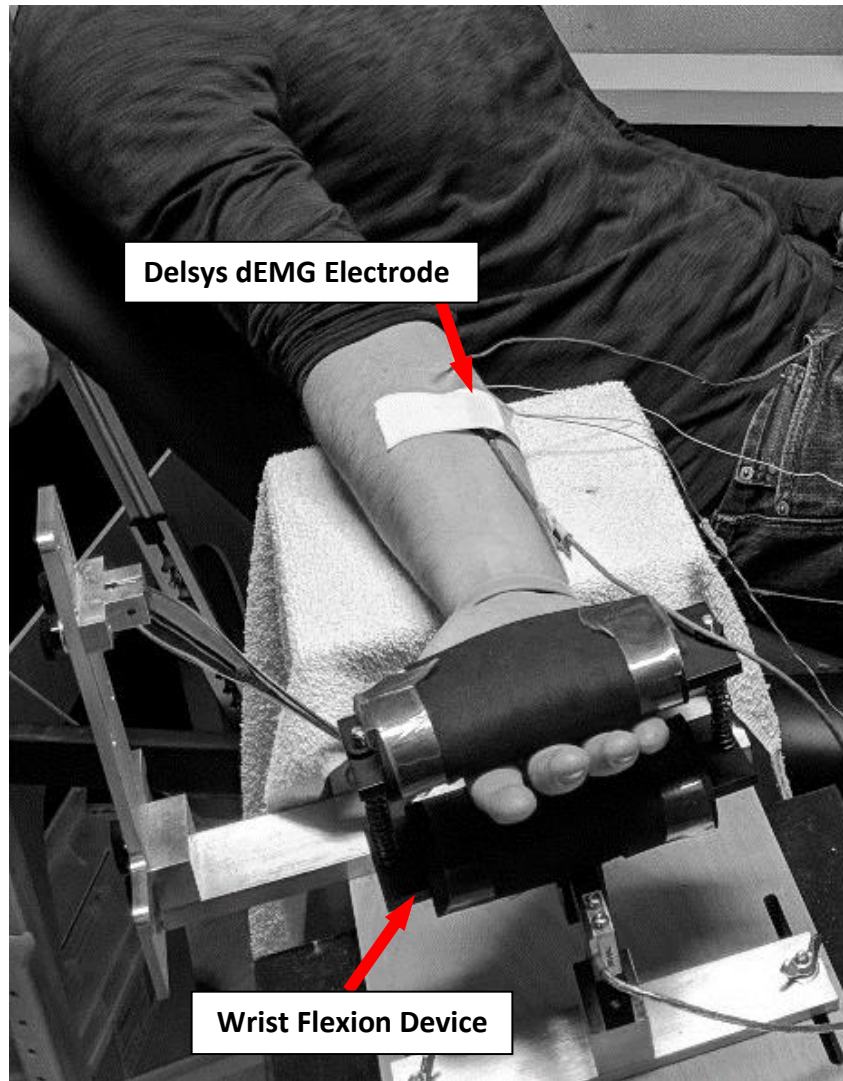


Figure 22. Participant seated comfortably their hand comfortably placed in the jig. The dEMG sensor is secured to the skin surface over the FCR with tape. The force paradigm is viewable on the monitor with direct feedback of the participant's applied force.

distance of 5 mm resulting in four channels of differential EMG. The ground electrode was placed over the olecranon process of the ulna. The EMG signal and force signals were collected using the Delsys Bagnoli-16 (Delsys, Natick, MA). Force was sampled at 20,000 Hz. The EMG signals were amplified 1000 times and the signal was filtered between 20 and 450 Hz and digitized at 20,000 Hz.

3.4 Data Reduction

Files were stored on a lab computer and all data was reduced offline. The sEMG files that are associated with each trial for all limbs on each test day were processed through the dEMG automated decomposition (dEMG, version 4.1.1.0, Delsys, Natick, MA). The firing times that were acquired from the decomposition were used to isolate the MUPs from each identified MU. Each MUP occupied a 25 ms epoch centered at the discharge time, and templates were calculated for each MUPT (Bezerianos, Laskaris, Fotopoulos, & Papathanasopoulos, 1995). Templates were calculated for each of the four channels from the dEMG sensor.

The variability in MUP shapes contributing to a template was assessed by calculating the variance ratio (VR) on the MUPT. The calculation was completed on the central 15 ms of the epoch, which was considered the signal portion of the MUP. The signal-to-noise (SNR) of each 25 ms epoch was also calculated. Similar to the VR, the root-mean-square (RMS) amplitude of the central 15 ms was the signal. The average RMS amplitude of the two outer 5 ms portions of the epoch was the noise. Figure 23 shows the shimmer plots of two different representative MUPTs, one where no denoising was necessary (top panel), and another that would be subjected to the denoising routine (bottom panel). The mean VR and SNR across all four channels is presented in the top

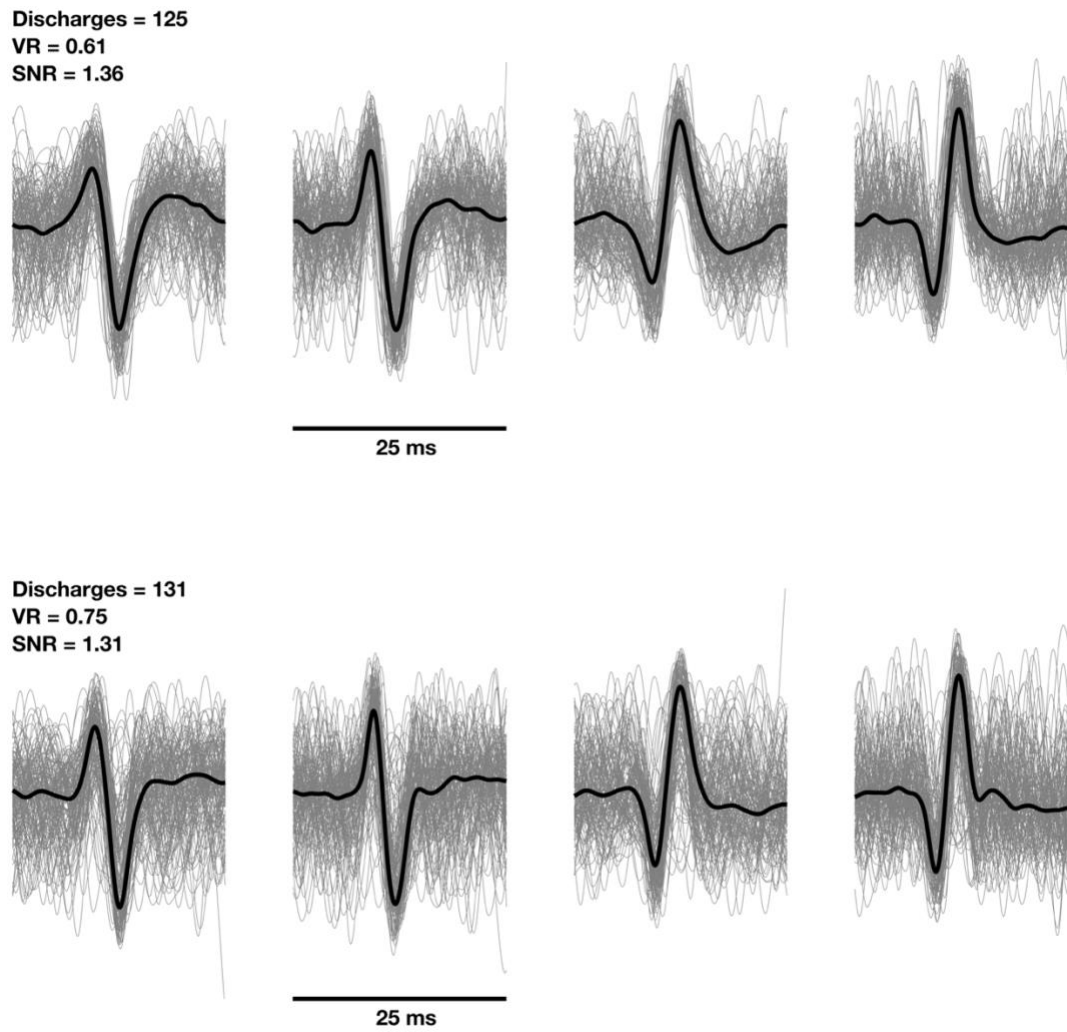


Figure 23. The shimmer plots. The gray waveforms are the individual motor unit (MU) potentials with the motor unit potential train. The thick black line is the MU template for each channel. The total number of discharges is presented in the top right corner of channel 1. The variance ratio (VR) and signal-to-noise-ratio (SNR) are also presented in the top left corner, and they represent the mean across channels.

right of the first channel. Note that the error-free MUPT has a lower VR and higher SNR, and it is characteristically free of waveforms that obscure the peaks and valleys of the template. All the discharge times for the MUPT in the top panel would be considered valid (Parsaei & Stashuk, 2009). The denoising routine then aims to remove the waveforms that obscure the peaks and valleys of the MU template.

3.5 Editing of Motor Unit Potential Trains

Automated editing of the MUPTs was performed through a graphical user interface (GUI) that was custom written in MATLAB (MathWorks Inc., Natick, MA). The GUI was to allow visual inspection of the denoising process. Two sets of parameters for inclusion of MUPs within a MUPT were compared, corresponding to relaxed versus strict criteria. Relaxed criteria were the initial point at which discharge times would be removed with minimal loss as a percentage of the total number. Strict criteria resulted in a greater percentage of loss in the total number of discharge times with the upper limit of 50%, to remain well-within the accuracy of the EFE algorithm. There were five parameters:

1. The correlation between the MUP and the MUP template had to be greater than $r=0.0$ (relaxed) or $r=0.3$ (strict) (Davila & Mobin, 1992);
2. The relaxed criteria had no initial SNR requirement for MUPs, but a minimal value of 0.3 was required for the strict criteria (Florestal, Mathieu, & Malanda, 2006);

3. The MUP peak had to occur within the 95% (relaxed) or 68% (strict) confidence interval of the location of that peak of the MUP template (Dorfman, Howard, & McGill, 1989; Stålberg, Ekstedt, & Broman, 1971b);
4. Based on the work of Zennaro (2002), criteria 4 and 5 were designed to isolate those MUPs that cluster around the main peak. If the main MUP template peak is positive, the MUP peak should not fall below the isoelectric line (relaxed), or below 0.3 times the peak value (strict) of MUP template. The polarity of these criteria changes for a main peak that is negative;
5. If the main MUP template peak is negative, the MUP peak should not exceed 5 times the peak value (relaxed) of MUP template, or below 3 times the peak value (strict) of MUP template. The polarity of these criteria changes for a main peak that is negative.

Representative examples of the same MUPTs denoised by both the relaxed and strict criteria are depicted in Figure 24 and Figure 25, respectively. Figure 24 shows that the difference in IDIs calculated on denoised data without (50.74 ± 11.50 ms) and with (55.09 ± 12.02) the EFE algorithm. The later compares with the 55.75 ± 12.46 ms for the original discharge times. There was a 19.26% loss in discharge times, an 8.9% reduction in the VR, and a less than 0.5% increase in SNR. Figure 25 shows that strict criteria resulted in an increased loss of discharge times to 24.94%, while the VR remained nearly the same but the SNR increased by almost 2%. The parameters of the denoising algorithm were specific enough to allow MUPTs to pass through unaltered if they were error-free. However, the parameters could be ‘tuned’ to separate MUPTs in the case of

superposition. Figure 26 depicts two different MUs, but only one fits the underlying shimmer plot. Note the shadow peak in the top panels at approximately 7 ms, which is also present in the MU template in the residuals. Additional tuning is possible if greater separation is desired.

3.6 Statistics

The percent loss in discharge times was limited to 50%, but the remaining total number could be less than required for a stable estimate and removed. Moreover, the same MUPT could be affected differently between relaxed versus strict criteria. For example, the same MU that would pass through the relaxed denoising criteria unaltered would have MU discharge times removed under the strict criteria. Thus, the changes would only be present in the strict condition. It is also the case, that a MU might be present in the relaxed denoising condition, but the number of discharges would fall below the minimum required (at least 50% of a MUPT) for calculation of the IDI using the EFE algorithm; it would be removed and not present in the strict condition. In total, there were 375 MUs common across all three conditions. The criterion measures were the: VR, SNR, the peak-to-peak (P-P) amplitude of the MU template, the P-P duration, and the IDI. When necessary, data transformations were applied to ensure normality and homogeneity of variances, as evaluated using probability plots and Levene's test, respectively (Bartlett, 1936; Berry, 1987; Hosken, Buss, & Hodgson, 2018).

A single-factor, repeated measures analysis of variance (ANOVA) was used to evaluate the criterion measures before and after denoising using both relaxed and strict criteria for MUP inclusion with the MUPT. Significant differences were further explored using planned comparisons (Kirk, 2012). The relationship between the IDIs calculated on

the original MU discharge times versus those calculated using the EFE algorithm for the relaxed and strict criteria, were evaluated using linear regression analysis (Kleinbaum, Kupper, Nizam, & Rosenberg, 2013). There were 550 MUs in common between the original and relaxed conditions, and there was 538 MUs in common between the original and strict conditions. The number of MUs for regression analysis is greater because commonality is only required for two versus three conditions.

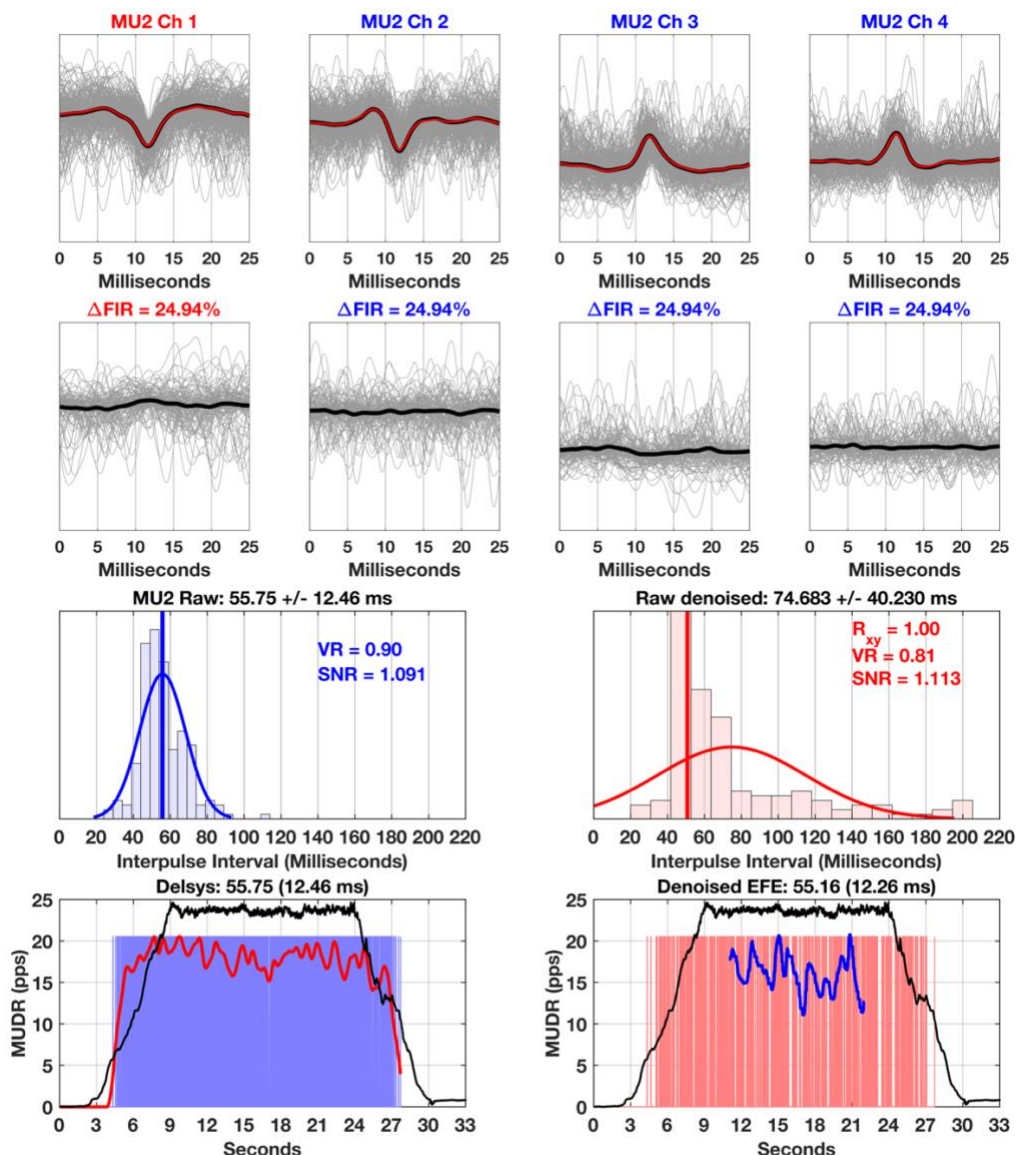


Figure 24. Representative example of denoising a motor unit potential train (MUPT) using relaxed criteria. The top panels are the shimmer plots, one for each channel. The shimmer plots include the MU templates calculated before (black) and after (red) denoising. The waveforms removed from each channel are plotted immediately below it, indicating the percent decrease in discharge times (ΔFIR). Beneath the residuals plots are the frequency-distribution curves of the inter-discharge intervals (IDIs) before (left) and after (right) denoising. The variance ratio (VR), the signal-to-noise ratio (SNR), and the cross-correlation coefficient (R_{xy}) for the MU template before and after denoising. The bottom graphs plot the isometric wrist flexion force-time curves and instantaneous motor unit discharge rate (MUDR) before (left) and after (right) denoising. After denoising, the mean and standard deviation of the IDIs was calculated using the Error Filtered Estimation algorithm.

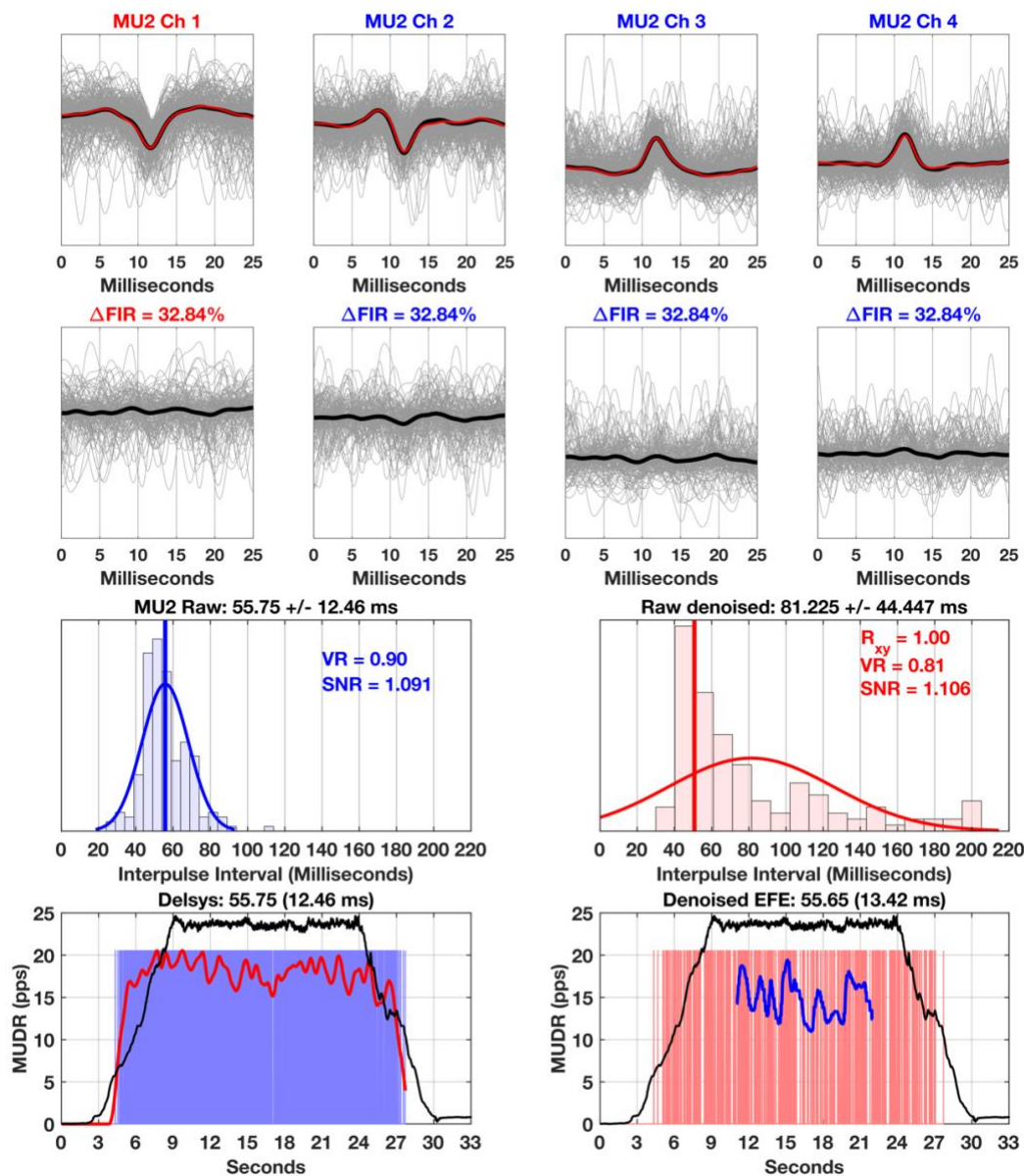


Figure 25. Representative example of denoising a motor unit potential train (MUPT) using strict criteria. The top panels are the shimmer plots, one for each channel. The shimmer plots include the MU templates calculated before (black) and after (red) denoising. The waveforms removed from each channel are plotted immediately below it, indicating the percent decrease in discharge times (Δ FIR). Beneath the residuals plots are the frequency-distribution curves of the inter-discharge intervals (IDIs) before (left) and after (right) denoising. The variance ratio (VR), the signal-to-noise ratio (SNR), and the cross-correlation coefficient (R_{xy}) for the MU template before and after denoising. The bottom graphs plot the isometric wrist flexion force-time curves and instantaneous motor unit discharge rate (MUDR) before (left) and after (right) denoising. After denoising, the mean and standard deviation of the IDIs was calculated using the Error Filtered Estimation algorithm.

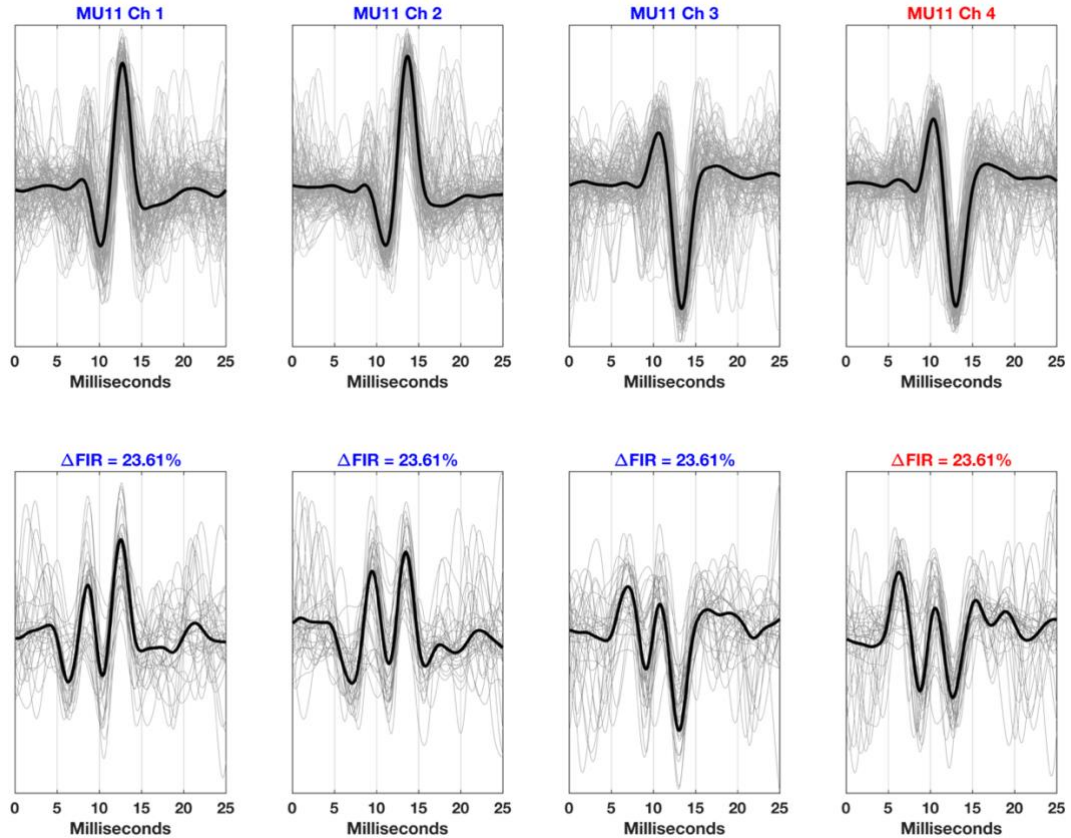


Figure 26. Representative example of superposition of two motor unit potential trains (MUPTs) using strict criteria. The top panels are the shimmer plots, one for each channel. The shimmer plots include one MU templates calculated after denoising (black). The waveforms removed from each channel are plotted immediate below it, indicating the percent decrease in discharge times (Δ FIR). A portion of the MUPs from a second MUPTs appears in the residuals, sufficient to generate a second MU template. Note the shadow peak in the top panels at approximately 7 ms, which is also present in the MU template in the residuals. Additional tuning is possible if greater separation is desired.

CHAPTER 4: Results

The means and standard deviations for the criterion measures are presented in Table 1. The variance ratio (VR) exhibited a significant decrease of 24.88% across the three conditions ($F_{(2, 748)}=1209.13$, $p<0.01$). The majority of the decrease (20.26%) occurred with the relaxed condition. Increasing the parameters to the strict criteria then resulted in a 5.8% reduction, compared to the relaxed criteria ($F_{(1, 748)}=74.00$, $p<0.01$). Similarly, the signal-to-noise ratio (SNR) exhibited a significant increase of 6.0% across the three conditions ($F_{(2, 748)}=343.02$, $p<0.01$). Half of the increase (3.12%) was due to the relaxed condition. Increasing the parameters to the strict criteria then resulted in a 2.98% increase, compared to the relaxed criteria ($F_{(1, 748)}=167.39$, $p<0.01$). As might be expected, there was significant increase in the loss of discharges times from $19.20 \pm 9.98\%$ for the relaxed criteria to $25.34 \pm 11.41\%$ for the strict criteria ($t_{(374)}=-29.19$, $p<0.01$).

It was expected that denoising would have an impact on the peak-to-peak (P-P) amplitude of the MU template. The one-way ANOVA revealed a significant difference between the three conditions ($F_{(2, 748)}=14.09$, $p<0.01$). The reduction was a 1.49% reduction in P-P amplitude between the original and relaxed criteria, however, the P-P amplitude exhibited a 1.22% increase between the relaxed and strict criteria ($F_{(1, 748)}=10.79$, $p<0.05$). Despite the rise, both denoising criteria resulted in an overall lower P-P amplitude compared to the original condition ($F_{(1, 748)}=17.39$, $p<0.01$). The duration between MUP peaks (P-P duration) followed a less consistent pattern of change. The one-way ANOVA revealed a significant difference between the three conditions ($F_{(2, 748)}=5.68$, $p<0.01$). There was a 0.89% reduction in P-P duration between the original and

relaxed criteria. However, the P-P duration increased 1.92% between the relaxed and strict criteria ($F_{(1, 748)}=11.32, p<0.05$). There was no overall pattern of change in the P-P duration determined from original versus denoised MU discharge times for the relaxed and strict criteria ($F_{(1, 748)}=0.03, p=0.857$).

Regression analysis was first performed on the original MU discharge times without denoising to evaluate the efficacy of the EFE algorithm in calculating the IDIs in the absence of removed data (see Figure 27). The results were a significant correlation of $r=0.99$ ($p<0.05$). The standard error of estimate (SEE) was only 2.32 ms (3.20%). The correlation between the original and denoised MU discharge times for the relaxed and strict criteria remained equally high r 's= 0.99 ($p<0.05$). There was an increase in the SEE for both the relaxed (2.68 ms, 3.69%) and strict (3.73 ms, 5.14%) criteria. Bonferroni-corrected paired t -tests, revealed no significant difference in the SEE of IDIs for the original and denoised MUPTs using the relaxed criteria ($t_{(539)}=-1.72, p>0.05$), or between the relaxed and strict criteria ($t_{(526)}=-1.931, p>0.05$).

Table 1. Means (M) and standard deviations (S) for the motor unit template peak-to-peak (P-P) amplitude, the duration between the P-P amplitudes, variance ratio (VR), and the signal-to-noise ratio (SNR) for the original and denoise MU discharge times.

	No Denoising	Relaxed Criteria	Strict Criteria
	M ± SD	M ± SD	M ± SD
VR	0.7696 ± 0.1339	0.6137 ± 0.1092	0.5781 ± 0.1124
SNR	1.1945 ± 0.1599	1.2330 ± 0.1883	1.2708 ± 0.2098
P-P Amplitude (mV)	0.3688 ± 0.2799	0.3633 ± 0.2781	0.3678 ± 0.2816
P-P Duration (ms)	5.5965 ± 1.7650	5.5465 ± 1.6939	5.6552 ± 1.8256

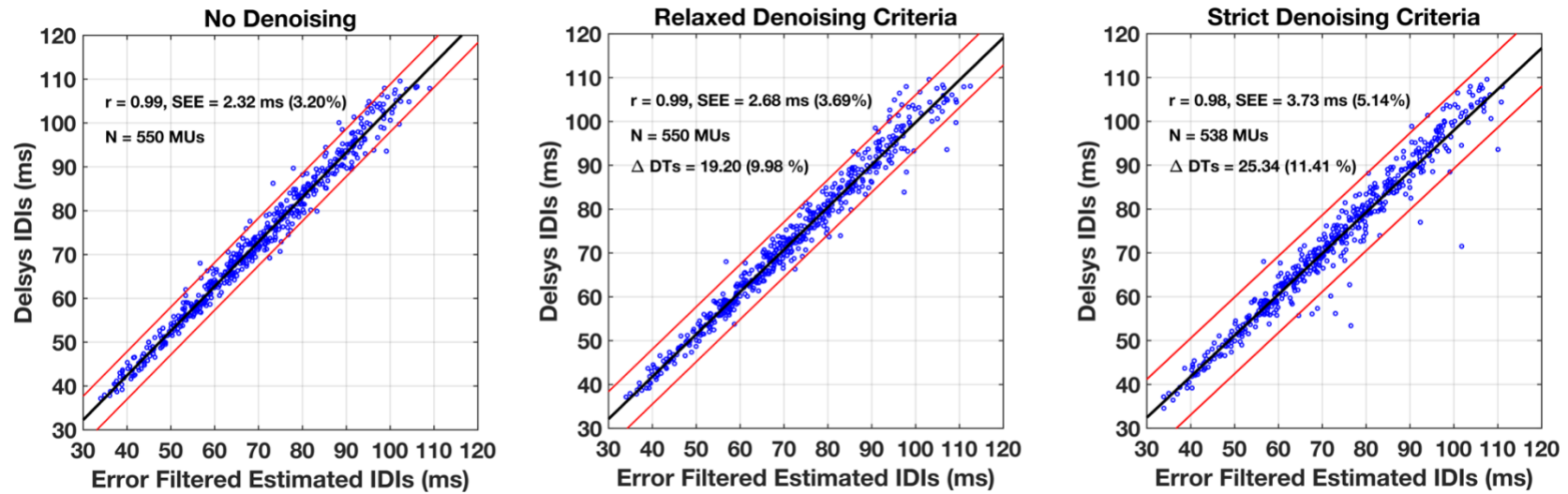


Figure 27. Regression analysis of IDIs calculated on the original motor unit discharge times versus those obtained using the Error Filtered Estimation (EFE) algorithm on the denoised data using the relaxed and strict criteria. The difference in the number of sampled motor units was due the removal of discharge times relative to the requirement for an absolute minimum. While the percent decrease was constrained to 50%, the minimum absolute number was 30% of discharge times within a motor unit potential train.

CHAPTER 5: Discussion

In this paper we demonstrated that an automated routine for editing MUPTs based on the shape of the contributing MUPs, resulted in a significant decrease in the VR and an increase in SNR. The MUPs that were removed were associated with discharge times that were assumed to be erroneous. Removal of erroneous discharge times had a significant impact on MUP template quantification. Since direct calculation of the IDI on MUPTs with removed discharge times is problematic, we also demonstrated that the EFE algorithm could estimate the IDI with near perfect correlation with the original data.

Research groups using the dEMG system have set the accuracy rating of the dEMG reconstruct-and-test (internal MU decomposition validation) to 85-95% (Beck, DeFreitas, & Stock, 2011; Defreitas et al., 2014; Stock, Beck, & Defreitas, 2012). Additionally, Hu and colleagues (2014b) conducted a correlational analysis between the coefficient of variation (CV) of peak-to-peak (P-P) amplitude and dEMG internal decomposition accuracy and observed a significant negative relationship, suggesting that lower accuracy ratings from the dEMG system are associated with higher CVs. The negative relationship justifies the use of a higher rating for the dEMG decomposition results. For the present study, a >90% accuracy rating was required for all decomposed MUs. For a more detailed explanation of the reconstruct-and-test approach, also known as the deconstruct-synthesize-deconstruct-compare test, the interested reader should reference Nawab and colleagues (2010).

McManus and colleagues (2017) recently used statistical techniques to remove MUs from the analysis. First, the CV was calculated for the P-P amplitude of the MUPT templates and then the maximum linear correlation coefficient was calculated between

the spike-triggered average (STA) template and the dEMG template. These measures were used to select MUs that were deemed 'reliable'. If a MU did not exhibit an average correlation coefficient of >0.7 and a CV for P-P amplitude of <0.3 , it was removed prior to analysis. In an earlier study, McManus and colleagues (2015; McManus, Hu, Rymer, Suresh, & Lowery, 2016) used a similar approach, however, MUs were required to have an average correlation coefficient of >0.8 and a CV for P-P amplitude of <0.2 . With such stringent criteria, McManus and colleagues (2016) were only able to analyze $27.7 \pm 14\%$ of MUs. In contrast, the proposed routine results in a minimal loss of MUPTs, which is absolutely critical when evaluating patients where the initial number of MUPTs is greatly reduced (Boe, Stashuk, & Doherty, 2007; Hu, Suresh, Rymer, & Suresh, 2015, 2016; McNeil, Doherty, Stashuk, & Rice, 2005).

It is common practice for investigators to discard MUPTs based on discharge statistics when working with either surface or indwelling EMG (Holobar et al., 2014; McManus et al., 2015, 2017; Muceli et al., 2015; Negro, Muceli, Castronovo, Holobar, & Farina, 2016). For example, MUPTs with a CV >0.3 are often removed from analysis. Holobar and colleagues (2010; 2014) implemented a similar strategy as McManus and associates (2017) in which MUs that exhibited a CV of >0.3 were excluded from their analysis, as they were deemed to have had irregular discharge patterns. Motor unit potential trains with unusually long (200–400 ms) or short (<20 ms) IDIs are also commonly removed to ensure a stable estimate of the mean and standard deviation (Christie et al., 2009; Holobar et al., 2010). The dEMG algorithm requires IDIs that are 350 ms or less (Nawab et al., 2010).

The MUP P-P amplitude and duration between the two major peaks of the MUPs were quantified in the present study. There was a significant overall decrease in P-P amplitude between the original data and that obtained through denoising, and there was a significant albeit slight increase between the two denoising conditions. An initial decrease between the original data and both denoising criteria might be expected due to the removal of high amplitude noise around the peak. The relaxed criteria would remove the high amplitude noise by requiring the waveform peak to occur within the 95% confidence interval of the peak for the MUP template. The same is true for the maximum peak limits. Pilot work revealed that the peak parameter affected 85% of the MUPTs. With the majority of high amplitude noise removed, increasing the parameters for the strict criteria had a more pronounced effect on the lower amplitude noise which would increase the overall mean P-P amplitude. Indirect support is given by the observation that the majority of the decrease in the VR occurred with the relaxed criteria, but the percent increase in SNR was nearly equal across criteria.

The changes in MUP P-P amplitude were small but statistically significant, which was influenced by the large MU sample size (N=375). However, the observed changes of 1.3% are of practical importance in reducing the variability of P-P amplitude within the context of pre-experimental planning, sample size estimation, detecting significant differences following an intervention or disease tracking (Christie, Kamen, Boucher, Inglis, & Gabriel, 2010; Pope, Hester, Benik, & DeFreitas, 2016; Shefner, Jillapalli, & Bradshaw, 1999). For example, Shefner and colleague (2007) studied a technique for motor unit number estimate in amyotrophic lateral sclerosis patients. They measured the P-P amplitude of the surface MUP across 12 months and reported a stable difference of

114.7 μV to 122.3 μV . This difference in P-P amplitude over the 12-month period amounted to 8.33%, but the potential difference of 1.3% due to denoising is a non-trivial portion of this range. Martinez-Valdes and colleagues (2017) tracked MUs across weeks using a high-density sEMG system and observed good to excellent (0.73–0.93) intraclass correlation coefficients (ICCs) for MUP P-P amplitude across sessions at 30-50% MVC, but the means and standard deviations were not reported. Nevertheless, both the reliability and identification of the same MUP across test sessions could be enhanced by denoising.

The present study quantified the duration between the major positive and negative peaks of the MUP, rather than the traditional duration, primarily for the unambiguity of this particular metric. Automated determination of MUP duration is a difficult problem as the determination of the onset and termination of the MUP is still affected by noise (Rodríguez et al., 2007; Rodríguez-Carreño, Gila-Useros, & Malanda-Trigueros, 2012), with manual detection still the gold-standard (Boe et al., 2010; Boe, Dalton, Harwood, Doherty, & Rice, 2009). We then based our duration measure on the work of Brown and colleagues (Brown & Yates, 1982; Carleton & Brown, 1979; Kadrie & Brown, 1978) who used the duration between positive and negative peaks of surface potentials obtained with electrical stimulation of the peripheral nerve. The duration between the positive and negative peaks has been shown to be highly sensitive to the health status of the neuromuscular system and physiological conditions that affect muscle fiber conduction velocity (Rodriguez-Falces, Navallas, Malanda, & Rodriguez-Martin, 2014). The P-P duration changed in a similar manner as P-P amplitude. That is, there was an overall significant *F*-ratio. The relaxed criteria had only a slight impact on the P-P

duration with the majority of change occurring between the relaxed and strict criteria. The increase in P-P amplitude between the relaxed and strict criteria was associated with a concomitant increase (1.92%) P-P duration. While the percent change might be considered trivial if the changes were due to a physiological intervention, the difference would have practical meaning in terms of greater precision and reducing error variability (Rodríguez et al., 2007; Rodríguez-Carreño et al., 2012; Shefner et al., 1999).

One technique for the validating indwelling MUPTs is based on MUP shapes contributing to the MUP template (Parsaei & Stashuk, 2009, 2011). An ensemble of MUPs grouped tightly together provides the investigator a greater degree of confidence in the validity of the discharge times associated with the MUPT. The current study extends this approach to editing MUPTs obtained by surface EMG decomposition. One editing approach is to remove MUPs that fall outside the 95% confidence interval of the template (Zennaro et al., 2002), which is a form of *a posteriori* template matching. MUP quantification and multivariate classification is another successful scheme (Parsaei & Stashuk, 2009, 2011). The present study also emphasized MUP shape by removing waveforms that were uncorrelated with the MUP template, and other noise criteria related to peak location, peak amplitude, and the overall SNR. The efficacy of this approach was assessed, in part, by decreases in the variability (variance ratio, VR) of the MUP ensemble associated with MUPT.

The nearly 25% total reduction in VR represents significant decrease in the variability in MUP ensemble shape to 0.578 ± 0.1124 , which is lower than that depicted in the top panel of Figure 23. This is the first application of the VR to surface detected MUPs, but the level of reproducibility of MUP shape may be considered very good when

compared to the evoked compound muscle action potential (CMAP), which has a much higher SNR. Because the CMAP is an evoked maximal potential, it has been shown to have a high degree of reproducibility with a VR of 0.244 ± 0.169 . However, in comparison with the CMAP, the surface detected MUP can also exhibit a highly reproducible shape and lower SNR (Boe, Stashuk, & Doherty, 2004). As a result, the ensemble will resemble a ‘thick’ band of waveforms (Figure 23). This difference in amplitude at each point in time results in a higher VR, despite how reproducible the shape is. For this reason, changes in the SNR are an important part of the denoising routine.

Use of the EFE algorithm has long been established for use in manual editing of the indwelling MUPTs (Stashuk & Qu, 1996a). The current study extends its use for editing of MUPTs obtained through decomposition of the surface EMG signal. Its performance as a robust estimator is highlighted by the lack of significant difference in the SEE of IDIs when applied to the original MUPTs versus those denoised by the relaxed criteria, where the number of discharges was reduced by $19.2 \pm 9.98\%$. The same was true for the difference between the relaxed and strict criteria, where the number of discharges was reduced further to $25.35 \pm 11.41\%$. The SEE of IDIs for the strict condition (5.4%) was nearly half the predicted 11% when detected errors are less than 60% of the MUPT and CV in IDIs is less than 20% (Stashuk & Qu, 1996a). While the reduction in discharge times was limited to 50%, the strict condition included MUPTs with reductions that approached that limit. The EFE algorithm has been shown to estimate the true mean without bias for MUPTs containing errors up to 70%, and with as few as ten discharges. To facilitate the automated process, the current work used a

conservative approach, limiting the reduction in discharge times to 50% and the minimum number of discharges had to be 30. Although, these limits allow greater error detection by ‘tuning’ the five parameters during manual editing, if desired.

5.1 Conclusion

Automated editing of MUPTs based on shape resulted in a significant reduction in shape variability (VR) and in the SNR, which also had an impact on the measures extracted from the MUP template. Changes in the P-P amplitude and the duration were dependent on the level of denoising. Greater precision in MUP template quantification may be obtained by using the strict denoising criteria, and the mean IDI may be estimated using the EFE algorithm, with no significant difference from the relaxed criteria. If MUP template quantification is not required, the relaxed criteria may be preferred.

5.2 Future Work

Decomposition of both the surface and indwelling EMG signals combines both MUP shape and discharges statistics. To identify the same MU across test session, Cescon and Gazzoni (2010) used a Euclidean distance cut-off of 0.3 for MUP shape. While not reported in this thesis, the Euclidean distance in MUP shape between MUPTs was calculated for all four channels. Denoising had no impact on the Euclidean distance, where approximately 55% of the MUPTs in a single trial had a Euclidean distance of less than or equal to 0.3. This finding emphasizes the original observations of Buchtal (1957) obtained on indwelling multielectrode recordings of MU territories. Potentials from different MUs can appear identical in shape and are differentiated only by their discharge characteristics. For this reason, MUPT discharge statistics are also part of decomposition

algorithms (Nawab et al., 2010; Parsaei & Stashuk, 2012). Once a MUPT has been denoised, future work should evaluate the efficacy of spike train metrics (Satuvuori & Kreuz, 2018; Victor & Purpura, 1996) as an adjunct to the Euclidean distance to differentiate MUPTs, and ensure that only uniquely identified MU are used for analysis.

References

- Andreassen, S., & Rosenfalck, A. (1978). Recording from a single motor unit during strong effort. *IEEE Transactions on Biomedical Engineering*, (6), 501–508.
- Arendt-Nielsen, L., Gantchev, N., & Sinkjær, T. (1992). The influence of muscle length on muscle fibre conduction velocity and development of muscle fatigue. *Electroencephalography and Clinical Neurophysiology/Evoked Potentials Section*, 85(3), 166–172. [https://doi.org/10.1016/0168-5597\(92\)90128-X](https://doi.org/10.1016/0168-5597(92)90128-X)
- Arendt-Nielsen, L., & Mills, K. R. (1985). The relationship between mean power frequency of the EMG spectrum and muscle fibre conduction velocity. *Electroencephalography and Clinical Neurophysiology*, 60(2), 130–134. [https://doi.org/10.1016/0013-4694\(85\)90019-7](https://doi.org/10.1016/0013-4694(85)90019-7)
- Arendt-Nielsen, L., & Zwarts, M. (1989). Measurement of Muscle Fiber Conduction Velocity in Humans: Techniques and Applications. *Journal of Clinical Neurophysiology*, 6(2).
- Basmajian, J. V., & De Luca, C. J. (1985). *Muscles alive*. Williams & Wilkins.
- Beck, T. W., DeFreitas, J. M., & Stock, M. S. (2011). The Effects of a Resistance Training Program on Average Motor Unit Firing Rates. *Clinical Kinesiology (Online Edition)*, 65(1), 1–8.
- Beck, T. W., Housh, T. J., Cramer, J. T., Stout, J. R., Ryan, E. D., Herda, T. J., ... Defreitas, J. M. (2009). Electrode placement over the innervation zone affects the low-, not the high-frequency portion of the EMG frequency spectrum. *Journal of Electromyography and Kinesiology*, 19(4), 660–666. <https://doi.org/10.1016/j.jelekin.2008.04.001>

- Beretta Piccoli, M., Rainoldi, A., Heitz, C., Wüthrich, M., Boccia, G., Tomasoni, E., ...
Barbero, M. (2014). Innervation zone locations in 43 superficial muscles: Toward a standardization of electrode positioning: Innervation Zone Location and sEMG. *Muscle & Nerve*, 49(3), 413–421. <https://doi.org/10.1002/mus.23934>
- Bertram, M. F., Nishida, T., Minieka, M. M., Janssen, I., & Levy, C. E. (1995). Effects of temperature on motor unit action potentials during isometric contraction. *Muscle & Nerve*, 18(12), 1443–1446. <https://doi.org/10.1002/mus.880181215>
- Bezerianos, A., Laskaris, N., Fotopoulos, S., & Papathanasopoulos, P. (1995). Data dependent weighted averages for recording of evoked potential signals. *Electroencephalography and Clinical Neurophysiology/Evoked Potentials Section*, 96(5), 468–471. [https://doi.org/10.1016/0168-5597\(95\)00070-9](https://doi.org/10.1016/0168-5597(95)00070-9)
- Bigland-Ritchie, B., Donovan, E. F., & Roussos, C. S. (1981). Conduction velocity and EMG power spectrum changes in fatigue of sustained maximal efforts. *Journal of Applied Physiology*, 51(5), 1300–1305.
<https://doi.org/10.1152/jappl.1981.51.5.1300>
- Bigland-Ritchie, B., Thomas, C. K., Rice, C. L., Howarth, J. V., & Woods, J. J. (1992). Muscle temperature, contractile speed, and motoneuron firing rates during human voluntary contractions. *Journal of Applied Physiology*, 73(6), 2457–2461.
<https://doi.org/10.1152/jappl.1992.73.6.2457>
- Bigland-Ritchie, B., & Woods, J. J. (1984). Changes in muscle contractile properties and neural control during human muscular fatigue. *Muscle & Nerve*, 7(9), 691–699.
<https://doi.org/10.1002/mus.880070902>

- Bilodeau, M., Arsenault, A. B., Gravel, D., & Bourbonnais, D. (1992). Influence of gender on the EMG power spectrum during an increasing force level. *Journal of Electromyography and Kinesiology: Official Journal of the International Society of Electrophysiological Kinesiology*, 2(3), 121–129. [https://doi.org/10.1016/1050-6411\(92\)90009-8](https://doi.org/10.1016/1050-6411(92)90009-8)
- Binder-Macleod, S., & Kesar, T. (2005). Catchlike property of skeletal muscle: Recent findings and clinical implications. *Muscle & Nerve*, 31(6), 681–693. <https://doi.org/10.1002/mus.20290>
- Blijham, P. J., ter Laak, H. J., Schelhaas, H. J., van Engelen, B. G. M., Stegeman, D. F., & Zwarts, M. J. (2006). Relation between muscle fiber conduction velocity and fiber size in neuromuscular disorders. *Journal of Applied Physiology*, 100(6), 1837–1841. <https://doi.org/10.1152/jappphysiol.01009.2005>
- Boe, S. G., Antonowicz, N. M., Leung, V. W., Shea, S. M., Zimmerman, T. C., & Doherty, T. J. (2010). High inter-rater reliability in analyzing results of decomposition-based quantitative electromyography in subjects with or without neuromuscular disorder. *Journal of Neuroscience Methods*, 192(1), 138–145. <https://doi.org/10.1016/j.jneumeth.2010.07.024>
- Boe, S. G., Dalton, B. H., Harwood, B., Doherty, T. J., & Rice, C. L. (2009). Inter-rater reliability of motor unit number estimates and quantitative motor unit analysis in the tibialis anterior muscle. *Clinical Neurophysiology*, 120(5), 947–952. <https://doi.org/10.1016/j.clinph.2009.02.168>
- Boe, S. G., Stashuk, D. W., Brown, W. F., & Doherty, T. J. (2005). Decomposition-based quantitative electromyography: Effect of force on motor unit potentials and motor

unit number estimates. *Muscle & Nerve*, 31(3), 365–373.

<https://doi.org/10.1002/mus.20266>

Boe, S. G., Stashuk, D. W., & Doherty, T. J. (2004). Motor unit number estimation by decomposition-enhanced spike-triggered averaging: Control data, test-retest reliability, and contractile level effects. *Muscle & Nerve*, 29(5), 693–699.

<https://doi.org/10.1002/mus.20031>

Boe, S. G., Stashuk, D. W., & Doherty, T. J. (2007). Motor unit number estimates and quantitative motor unit analysis in healthy subjects and patients with amyotrophic lateral sclerosis. *Muscle & Nerve*, 36(1), 62–70.

<https://doi.org/10.1002/mus.20784>

Bowden, J. L., & McNulty, P. A. (2012). Mapping the motor point in the human tibialis anterior muscle. *Clinical Neurophysiology*, 123(2), 386–392.

<https://doi.org/10.1016/j.clinph.2011.06.016>

Boyd, D. C., Lawrence, P. D., & Bratty, P. J. A. (1979). The Effect of Electromyographic Jitter on Single Motor Unit EMG Potentials. *IEEE Transactions on Biomedical Engineering*, 8.

Brown, W. R. A., & Yates, S. (1982). Percutaneous localization of conduction abnormalities in human entrapment neuropathies. *The Canadian Journal of Neurological Sciences. Le Journal Canadien Des Sciences Neurologiques*, 9(4), 391–400.

Buchthal, F., Guld, C., & Rosenfalck, P. (1957). Multielectrode Study of the Territory of a Motor Unit. *Acta Physiologica Scandinavica*, 39(1), 83–104.

<https://doi.org/10.1111/j.1748-1716.1957.tb01411.x>

- Calancie, B., & Bawa, P. (1985). Voluntary and reflexive recruitment of flexor carpi radialis motor units in humans. *Journal of Neurophysiology*, 53(5), 1194–1200. <https://doi.org/10.1152/jn.1985.53.5.1194>
- Calder, K. M., Hall, L.-A., Lester, S. M., Inglis, J. G., & Gabriel, D. A. (2005). Reliability of the biceps brachii M-wave. *Journal of NeuroEngineering and Rehabilitation*, 8.
- Campos, C., Malanda, A., Gila, L., Segura, V., Lasanta, I., & Artieda, J. (2000). Quantification of jiggle in real electromyographic signals. *Muscle & Nerve*, 23(7), 1022–1034. [https://doi.org/10.1002/1097-4598\(200007\)23:7<1022::AID-MUS4>3.0.CO;2-3](https://doi.org/10.1002/1097-4598(200007)23:7<1022::AID-MUS4>3.0.CO;2-3)
- Carleton, S. A., & Brown, W. F. (1979). Changes in motor unit populations in motor neurone disease. *Journal of Neurology, Neurosurgery & Psychiatry*, 42(1), 42–51. <https://doi.org/10.1136/jnnp.42.1.42>
- Castronovo, A. M., Mrachacz-Kersting, N., Stevenson, A. J. T., Holobar, A., Enoka, R. M., & Farina, D. (2018). Decrease in force steadiness with aging is associated with increased power of the common but not independent input to motor neurons. *Journal of Neurophysiology*. <https://doi.org/10.1152/jn.00093.2018>
- Cescon, C., & Gazzoni, M. (2010). Short term bed-rest reduces conduction velocity of individual motor units in leg muscles. *Journal of Electromyography and Kinesiology: Official Journal of the International Society of Electrophysiological Kinesiology*, 20(5), 860–867. <https://doi.org/10.1016/j.jelekin.2010.03.008>

- Christie, A., Inglis, J. G., Kamen, G., & Gabriel, D. A. (2009). Relationships between surface EMG variables and motor unit firing rates. *European Journal of Applied Physiology, 107*(2), 177–185. <https://doi.org/10.1007/s00421-009-1113-7>
- Christie, A., & Kamen, G. (2006). Doublet Discharges in Motoneurons of Young and Older Adults. *Journal of Neurophysiology, 95*(5), 2787–2795. <https://doi.org/10.1152/jn.00685.2005>
- Christie, A., Kamen, G., Boucher, J. P., Inglis, J. G., & Gabriel, D. A. (2010). A Comparison of Statistical Models for Calculating Reliability of the Hoffmann Reflex. *Measurement in Physical Education and Exercise Science, 14*(3), 164–175. <https://doi.org/10.1080/1091367X.2010.495549>
- Clancy, E. A., Morin, E. L., & Merletti, R. (2002). Sampling, noise-reduction and amplitude estimation issues in surface electromyography. *Journal of Electromyography and Kinesiology, 12*(1), 1–16. [https://doi.org/10.1016/S1050-6411\(01\)00033-5](https://doi.org/10.1016/S1050-6411(01)00033-5)
- Clark, D. A. (1931). Muscle counts of motor units: A study in innervation ratios. *American Journal of Physiology-Legacy Content, 96*(2), 296–304. <https://doi.org/10.1152/ajplegacy.1931.96.2.296>
- Contessa, P., De Luca, C. J., & Kline, J. C. (2016). The compensatory interaction between motor unit firing behavior and muscle force during fatigue. *Journal of Neurophysiology, 116*(4), 1579–1585. <https://doi.org/10.1152/jn.00347.2016>
- Contessa, P., Letizi, J., De Luca, G., & Kline, J. C. (2018). Contribution from motor unit firing adaptations and muscle coactivation during fatigue. *Journal of Neurophysiology, 119*(6), 2186–2193. <https://doi.org/10.1152/jn.00766.2017>

- Conwit, R. A., Tracy, B., Jamison, C., McHugh, M., Stashuk, D., Brown, W. F., & Metter, E. J. (1997). Decomposition-enhanced spike-triggered averaging: Contraction level effects. *Muscle & Nerve*, *20*(8), 976–982.
- Daube, J. R., & Rubin, D. I. (2009). Needle electromyography. *Muscle & Nerve*, *39*(2), 244–270. <https://doi.org/10.1002/mus.21180>
- Davila, C. E., & Mobin, M. S. (1992). Weighted averaging of evoked potentials. *IEEE Transactions on Biomedical Engineering*, *39*(4), 338–345.
- Day, S. (2002). Important factors in surface EMG measurement. *Bortec Biomedical*, *16*.
- De la Barrera, E. J., & Milner, T. E. (1994). The effects of skinfold thickness on the selectivity of surface EMG. *Electroencephalography and Clinical Neurophysiology/Evoked Potentials Section*, *93*(2), 91–99. [https://doi.org/10.1016/0168-5597\(94\)90071-X](https://doi.org/10.1016/0168-5597(94)90071-X)
- De Luca, C. J. (1979). Physiology and Mathematics of Myoelectric Signals. *IEEE Transactions on Biomedical Engineering*, *26*(6).
- De Luca, C. J. (1997). The use of surface electromyography in biomechanics. *Journal of Applied Biomechanics*, *13*(2), 135–163.
- De Luca, C. J., Adam, A., Wotiz, R., Gilmore, L. D., & Nawab, S. H. (2006). Decomposition of Surface EMG Signals. *Journal of Neurophysiology*, *96*(3), 1646–1657. <https://doi.org/10.1152/jn.00009.2006>
- De Luca, C. J., & Contessa, P. (2012). Hierarchical control of motor units in voluntary contractions. *Journal of Neurophysiology*, *107*(1), 178–195. <https://doi.org/10.1152/jn.00961.2010>

- De Luca, C. J., & Contessa, P. (2015). Biomechanical benefits of the onion-skin motor unit control scheme. *Journal of Biomechanics*, *48*(2), 195–203.
<https://doi.org/10.1016/j.jbiomech.2014.12.003>
- De Luca, C. J., Donald Gilmore, L., Kuznetsov, M., & Roy, S. H. (2010). Filtering the surface EMG signal: Movement artifact and baseline noise contamination. *Journal of Biomechanics*, *43*(8), 1573–1579.
<https://doi.org/10.1016/j.jbiomech.2010.01.027>
- De Luca, C. J., & Erim, Z. (1994). Common drive of motor units in regulation of muscle force. *Trends in Neurosciences*, *17*(7), 299–305.
- De Luca, C. J., & Erim, Z. (2002). Common Drive in Motor Units of a Synergistic Muscle Pair. *Journal of Neurophysiology*, *87*(4), 2200–2204.
<https://doi.org/10.1152/jn.00793.2001>
- De Luca, C. J., & Hostage, E. C. (2010). Relationship Between Firing Rate and Recruitment Threshold of Motoneurons in Voluntary Isometric Contractions. *Journal of Neurophysiology*, *104*(2), 1034–1046.
<https://doi.org/10.1152/jn.01018.2009>
- De Luca, C. J., Kuznetsov, M., Gilmore, L. D., & Roy, S. H. (2012). Inter-electrode spacing of surface EMG sensors: Reduction of crosstalk contamination during voluntary contractions. *Journal of Biomechanics*, *45*(3), 555–561.
<https://doi.org/10.1016/j.jbiomech.2011.11.010>
- De Luca, C. J., LeFever, R. S., McCue, M. P., & Xenakis, A. P. (1982a). Behaviour of human motor units in different muscles during linearly varying contractions. *The*

Journal of Physiology, 329(1), 113–128.

<https://doi.org/10.1113/jphysiol.1982.sp014293>

De Luca, C. J., LeFever, R. S., McCue, M. P., & Xenakis, A. P. (1982b). Control scheme governing concurrently active human motor units during voluntary contractions.

The Journal of Physiology, 329(1), 129–142.

<https://doi.org/10.1113/jphysiol.1982.sp014294>

De Luca, C. J., & Merletti, R. (1988). Surface myoelectric signal cross-talk among muscles of the leg. *Electroencephalography and Clinical Neurophysiology*, 69(6), 568–575. [https://doi.org/10.1016/0013-4694\(88\)90169-1](https://doi.org/10.1016/0013-4694(88)90169-1)

De Luca, C. J., & Nawab, S. H. (2011). Reply to Farina and Enoka: The Reconstruct-and-Test Approach Is the Most Appropriate Validation for Surface EMG Signal Decomposition to Date. *Journal of Neurophysiology*, 105(2), 983–984.

<https://doi.org/10.1152/jn.01060.2010>

De Luca, C. J., Nawab, S. H., & Kline, J. C. (2015). Clarification of methods used to validate surface EMG decomposition algorithms as described by Farina et al. (2014). *Journal of Applied Physiology*, 118(8), 1084–1084.

<https://doi.org/10.1152/jappphysiol.00061.2015>

Defreitas, J. M., Beck, T. W., Ye, X., & Stock, M. S. (2014). Synchronization of low- and high-threshold motor units: Synchronization of Low- and High-Threshold Motor Units. *Muscle & Nerve*, 49(4), 575–583. <https://doi.org/10.1002/mus.23978>

Del Vecchio, A., Negro, F., Felici, F., & Farina, D. (2017). Associations between motor unit action potential parameters and surface EMG features. *Journal of Applied Physiology*, 123(4), 835–843. <https://doi.org/10.1152/jappphysiol.00482.2017>

- Del Vecchio, A., Negro, F., Felici, F., & Farina, D. (2018). Distribution of muscle fibre conduction velocity for representative samples of motor units in the full recruitment range of the tibialis anterior muscle. *Acta Physiologica*, *222*(2), e12930. <https://doi.org/10.1111/apha.12930>
- Dimitrova, N. A., & Dimitrov, G. V. (2003). Interpretation of EMG changes with fatigue: Facts, pitfalls, and fallacies. *Journal of Electromyography and Kinesiology*, *13*(1), 13–36. [https://doi.org/10.1016/S1050-6411\(02\)00083-4](https://doi.org/10.1016/S1050-6411(02)00083-4)
- Dorfman, L. J., Howard, J. E., & McGill, K. C. (1989). Motor unit firing rates and firing rate variability in the detection of neuromuscular disorders. *Electroencephalography and Clinical Neurophysiology*, *73*(3), 215–224. [https://doi.org/10.1016/0013-4694\(89\)90122-3](https://doi.org/10.1016/0013-4694(89)90122-3)
- Drost, G., Stegeman, D. F., van Engelen, B. G. M., & Zwarts, M. J. (2006). Clinical applications of high-density surface EMG: A systematic review. *Journal of Electromyography and Kinesiology*, *16*(6), 586–602. <https://doi.org/10.1016/j.jelekin.2006.09.005>
- Enoka, R. M. (2012). Muscle fatigue—From motor units to clinical symptoms. *Journal of Biomechanics*, *45*(3), 427–433. <https://doi.org/10.1016/j.jbiomech.2011.11.047>
- Enoka, R. M. (2019). Physiological validation of the decomposition of surface EMG signals. *Journal of Electromyography and Kinesiology*, *46*, 70–83. <https://doi.org/10.1016/j.jelekin.2019.03.010>
- Enoka, R. M., & Duchateau, J. (2015). Inappropriate interpretation of surface EMG signals and muscle fiber characteristics impedes understanding of the control of

- neuromuscular function. *Journal of Applied Physiology*, *119*(12), 1516–1518.
<https://doi.org/10.1152/jappphysiol.00280.2015>
- Enoka, R. M., & Fuglevand, A. J. (2001). Motor unit physiology: Some unresolved issues. *Muscle & Nerve*. Retrieved from https://journals-scholarsportal-info.proxy1.lib.uwo.ca/pdf/0148639x/v24i0001/4_mupsui.xml
- Etawil, H., & Stashuk, D. W. (1996). Resolving superimposed motor unit action potentials. *Medical and Biological Engineering and Computing*, *34*(1), 33–40.
- Farina, D., Arendt-Nielsen, L., & Graven-Nielsen, T. (2005). Effect of temperature on spike-triggered average torque and electrophysiological properties of low-threshold motor units. *Journal of Applied Physiology*, *99*(1), 197–203.
- Farina, D., & Enoka, R. M. (2011). Surface EMG Decomposition Requires an Appropriate Validation. *Journal of Neurophysiology*, *105*(2), 981–982.
<https://doi.org/10.1152/jn.00855.2010>
- Farina, D., & Holobar, A. (2016). Characterization of Human Motor Units From Surface EMG Decomposition. *Proceedings of the IEEE*, *104*(2), 353–373.
<https://doi.org/10.1109/JPROC.2015.2498665>
- Farina, D., Holobar, A., Merletti, R., & Enoka, R. M. (2010). Decoding the neural drive to muscles from the surface electromyogram. *Clinical Neurophysiology*, *121*(10), 1616–1623. <https://doi.org/10.1016/j.clinph.2009.10.040>
- Farina, D., & Merletti, R. (2004). Methods for estimating muscle fibre conduction velocity from surface electromyographic signals. *Medical & Biological Engineering & Computing*, *42*(4), 432–445. <https://doi.org/10.1007/BF02350984>

- Farina, D., Merletti, R., & Enoka, R. M. (2015). Reply to De Luca, Nawab, and Kline: The proposed method to validate surface EMG signal decomposition remains problematic. *Journal of Applied Physiology*, *118*(8), 1085–1085. <https://doi.org/10.1152/jappphysiol.00107.2015>
- Farina, D., Merletti, R., Indino, B., Nazzaro, M., & Pozzo, M. (2002). Surface EMG crosstalk between knee extensor muscles: Experimental and model results. *Muscle & Nerve*, *26*(5), 681–695. <https://doi.org/10.1002/mus.10256>
- Farina, D., Merletti, R., Nazzaro, M., & Caruso, I. (2001). Effect of joint angle on EMG variables in leg and thigh muscles. *IEEE Engineering in Medicine and Biology Magazine*, *20*(6), 62–71. <https://doi.org/10.1109/51.982277>
- Feiereisen, P., Duchateau, J., & Hainaut, K. (1997). Motor unit recruitment order during voluntary and electrically induced contractions in the tibialis anterior: *Experimental Brain Research*, *114*(1), 117–123. <https://doi.org/10.1007/PL00005610>
- Florestal, J. R., Mathieu, P. A., & Malanda, A. (2006). Automated decomposition of intramuscular electromyographic signals. *IEEE Transactions on Biomedical Engineering*, *53*(5), 832–839. <https://doi.org/10.1109/TBME.2005.863893>
- Freund, H. J., Budingen, H. J., & Dietz, V. (1975). Activity of single motor units from human forearm muscles during voluntary isometric contractions. *Journal of Neurophysiology*, *38*(4), 933–946. <https://doi.org/10.1152/jn.1975.38.4.933>
- Fuglevand, A. J., Macefield, V. G., & Bigland-Ritchie, B. (1999). Force-Frequency and Fatigue Properties of Motor Units in Muscles That Control Digits of the Human

Hand. *Journal of Neurophysiology*, 81(4), 1718–1729.

<https://doi.org/10.1152/jn.1999.81.4.1718>

Fuglevand, A. J., Winter, D. A., Patla, A. E., & Stashuk, D. W. (1992). Detection of motor unit action potentials with surface electrodes: Influence of electrode size and spacing. *Biological Cybernetics*, 67(2), 143–153.

<https://doi.org/10.1007/BF00201021>

Fukunaga, T., Kawakami, Y., Kuno, S., Funato, K., & Fukashiro, S. (1997). Muscle architecture and function in humans. *Journal of Biomechanics*, 30(5), 457–463.

[https://doi.org/10.1016/S0021-9290\(96\)00171-6](https://doi.org/10.1016/S0021-9290(96)00171-6)

Gabriel, D. A., Lester, S. M., Lenhardt, S. A., & Cambridge, E. D. J. (2007). Analysis of surface EMG spike shape across different levels of isometric force. *Journal of Neuroscience Methods*, 159(1), 146–152.

<https://doi.org/10.1016/j.jneumeth.2006.07.004>

Galluccio, L., Michel, O., Comon, P., & Hero, A. O. (2012). Graph based k-means clustering. *Signal Processing*, 92(9), 1970–1984.

<https://doi.org/10.1016/j.sigpro.2011.12.009>

Garland, S. J., & Griffin, L. (1999). Motor unit double discharges: Statistical anomaly or functional entity? *Canadian Journal of Applied Physiology*, 24(2), 113–130.

Gath, I., & Stålberg, E. (1981). In situ measurement of the innervation ratio of motor units in human muscles. *Experimental Brain Research*, 43, 377–382.

Gazzoni, M., Farina, D., & Merletti, R. (2004). A new method for the extraction and classification of single motor unit action potentials from surface EMG signals.

Journal of Neuroscience Methods, 136(2), 165–177.

<https://doi.org/10.1016/j.jneumeth.2004.01.002>

- Green, L. A., McGuire, J., & Gabriel, D. A. (2015). Flexor carpi radialis surface electromyography electrode placement for evoked and voluntary measures. *Muscle & Nerve*, 52(5), 818–825. <https://doi.org/10.1002/mus.24631>
- Griep, P. A. M., Boon, K. L., & Stegeman, D. F. (1978). A study of the motor unit action potential by means of computer simulation. *Biological Cybernetics*, 30(4), 221–230.
- Guerrero, F. N., Spinelli, E. M., & Haberman, M. A. (2016). Analysis and Simple Circuit Design of Double Differential EMG Active Electrode. *IEEE Transactions on Biomedical Circuits and Systems*, 10(3), 787–795. <https://doi.org/10.1109/TBCAS.2015.2492944>
- Håkansson, C. H. (1956). Conduction Velocity and Amplitude of the Action Potential as Related to Circumference in the Isolated Fibre of Frog Muscle. *Acta Physiologica Scandinavica*, 37(1), 14–34. <https://doi.org/10.1111/j.1748-1716.1956.tb01338.x>
- Heckman, C. J., Gorassini, M. A., & Bennett, D. J. (2005). Persistent inward currents in motoneuron dendrites: Implications for motor output. *Muscle & Nerve*, 31(2), 135–156. <https://doi.org/10.1002/mus.20261>
- Henneman, E. (1957). Relation between Size of Neurons and Their Susceptibility to Discharge. *Science*, 126(3287), 1345–1347. <https://doi.org/10.1126/science.126.3287.1345>
- Hershler, C., & Milner, M. (1978). An Optimality Criterion for Processing Electromyographic (EMG) Signals Relating to Human Locomotion. *IEEE*

Transactions on Biomedical Engineering, BME-25(5), 413–420.

<https://doi.org/10.1109/TBME.1978.326338>

Hodgkin, A. L., & Katz, B. (1949). The effect of temperature on the electrical activity of the giant axon of the squid. *The Journal of Physiology*, *109*(1–2), 240–249.

<https://doi.org/10.1113/jphysiol.1949.sp004388>

Hogrel, J.-Y. (2003). Use of surface EMG for studying motor unit recruitment during isometric linear force ramp. *Journal of Electromyography and Kinesiology: Official Journal of the International Society of Electrophysiological Kinesiology*, *13*(5), 417–423.

Holobar, A., & Farina, D. (2014). Blind source identification from the multichannel surface electromyogram. *Physiological Measurement*, *35*(7), R143–R165.

<https://doi.org/10.1088/0967-3334/35/7/R143>

Holobar, A., Farina, D., Gazzoni, M., Merletti, R., & Zazula, D. (2009). Estimating motor unit discharge patterns from high-density surface electromyogram. *Clinical Neurophysiology*, *120*(3), 551–562. <https://doi.org/10.1016/j.clinph.2008.10.160>

Holobar, A., Minetto, M. A., Botter, A., Negro, F., & Farina, D. (2010). Experimental Analysis of Accuracy in the Identification of Motor Unit Spike Trains From High-Density Surface EMG. *IEEE Transactions on Neural Systems and Rehabilitation Engineering*, *18*(3), 221–229. <https://doi.org/10.1109/TNSRE.2010.2041593>

Holobar, A., Minetto, M. A., & Farina, D. (2014). Accurate identification of motor unit discharge patterns from high-density surface EMG and validation with a novel signal-based performance metric. *Journal of Neural Engineering*, *11*(1), 016008.

<https://doi.org/10.1088/1741-2560/11/1/016008>

- Holobar, A., & Zazula, D. (2007). Multichannel blind source separation using convolution kernel compensation. *IEEE Transactions on Signal Processing*, (9), 4487.
- Hopf, H. C., Herbort, R.-L., Gnass, M., Günther, H., & Lowitzsch, K. (1974). Fast and slow contraction times associated with fast and slow spike conduction of skeletal muscle fibres in normal subjects and in spastic hemiparesis. *Zeitschrift Für Neurologie*, 206(3), 193–202. <https://doi.org/10.1007/BF00316533>
- Hu, X., Rymer, W. Z., & Suresh, N. L. (2013a). Assessment of validity of a high-yield surface electromyogram decomposition. *Journal of Neuroengineering and Rehabilitation*, 10, 99. <https://doi.org/10.1186/1743-0003-10-99>
- Hu, X., Rymer, W. Z., & Suresh, N. L. (2013b). Motor unit pool organization examined via spike-triggered averaging of the surface electromyogram. *Journal of Neurophysiology*, 110(5), 1205–1220. <https://doi.org/10.1152/jn.00301.2012>
- Hu, X., Rymer, W. Z., & Suresh, N. L. (2013c). Reliability of spike triggered averaging of the surface electromyogram for motor unit action potential estimation: Reliability Assessment of STA of sEMG. *Muscle & Nerve*, 48(4), 557–570. <https://doi.org/10.1002/mus.23819>
- Hu, X., Rymer, W. Z., & Suresh, N. L. (2014a). Control of motor unit firing during step-like increases in voluntary force. *Frontiers in Human Neuroscience*, 8. <https://doi.org/10.3389/fnhum.2014.00721>
- Hu, X., Suresh, A. K., Rymer, W. Z., & Suresh, N. L. (2015). Assessing altered motor unit recruitment patterns in paretic muscles of stroke survivors using surface

electromyography. *Journal of Neural Engineering*, 12(6), 066001.

<https://doi.org/10.1088/1741-2560/12/6/066001>

Hu, X., Suresh, A. K., Rymer, W. Z., & Suresh, N. L. (2016). Altered motor unit discharge patterns in paretic muscles of stroke survivors assessed using surface electromyography. *Journal of Neural Engineering*, 13(4), 046025.

<https://doi.org/10.1088/1741-2560/13/4/046025>

Hu, X., Suresh, N. L., Jeon, B., Shin, H., & Rymer, W. Z. (2014b). *Statistics of Inter-spike Intervals as a Routine Measure of Accuracy in Automatic Decomposition of Surface Electromyogram*. <https://doi.org/10.1109/EMBC.2014.6944387>

Imanishi, N. M. D., Nakajima, H. M. D., & Aiso, S. M. D. (2000). Anatomic Study of the Venous Drainage Architecture of the Forearm Skin and Subcutaneous Tissue. *Plastic & Reconstructive Surgery*, 106(6), 1287–1294.

Inbar, G. F., Allin, J., & Kranz, H. (1987). Surface EMG spectral changes with muscle length. *Medical & Biological Engineering & Computing*, 25(6), 683–689.

<https://doi.org/10.1007/BF02447340>

Kadaba, M. P., Wootten, M. E., Gainey, J., & Cochran, G. V. B. (1985). Repeatability of phasic muscle activity: Performance of surface and intramuscular wire electrodes in gait analysis. *Journal of Orthopaedic Research*, 3(3), 350–359.

<https://doi.org/10.1002/jor.1100030312>

Kadrie, H. A., & Brown, W. F. (1978). Neuromuscular transmission in myasthenic single motor units. *Journal of Neurology, Neurosurgery & Psychiatry*, 41(3), 205–214.

<https://doi.org/10.1136/jnnp.41.3.205>

- Kamen, G., & Gabriel, D. A. (2010). *Essentials of electromyography*. Champaign, IL : Human Kinetics, c2010. (Main Library - 5th Floor RC 77.5 K36 2010).
- Kamen, G., Greenstein, S. S., & De Luca, C. J. (1992). Lateral dominance and motor unit firing behavior. *Brain Research*, *576*(1), 165–167. [https://doi.org/10.1016/0006-8993\(92\)90625-J](https://doi.org/10.1016/0006-8993(92)90625-J)
- Kamen, G., & Roy, A. (2000). Motor unit synchronization in young and elderly adults. *European Journal of Applied Physiology*, *81*(5), 403–410. <https://doi.org/10.1007/s004210050061>
- Keenan, K. G., Farina, D., Maluf, K. S., Merletti, R., & Enoka, R. M. (2005). Influence of amplitude cancellation on the simulated surface electromyogram. *Journal of Applied Physiology*, *98*(1), 120–131.
- Komi, P. V., & Tesch, P. (1979). EMG frequency spectrum, muscle structure, and fatigue during dynamic contractions in man. *European Journal of Applied Physiology and Occupational Physiology*, *42*(1), 41–50.
- Kudina, L. P., & Churikova, L. I. (1990). Testing excitability of human motoneurons capable of firing double discharges. *Electroencephalography and Clinical Neurophysiology*, *75*(4), 334–341. [https://doi.org/10.1016/0013-4694\(90\)90111-V](https://doi.org/10.1016/0013-4694(90)90111-V)
- Kuiken, T. A., Lowery, M. M., & Stoykov, N. S. (2003). The effect of subcutaneous fat on myoelectric signal amplitude and cross-talk. *Prosthetics and Orthotics International*, *27*, 48–54.
- Kukulka, C. G., & Clamann, H. P. (1981). Comparison of the recruitment and discharge properties of motor units in human brachial biceps and adductor pollicis during isometric contractions. *Brain Research*, *219*(1), 45–55.

- Lateva, Z. C., & McGill, K. C. (2001). Estimating motor-unit architectural properties by analyzing motor-unit action potential morphology. *Clinical Neurophysiology*, 9.
- Lefever, R. S., & De Luca, C. J. (1982). A Procedure for Decomposing the Myoelectric Signal Into Its Constituent Action Potentials - Part I: Technique, Theory, and Implementation. *IEEE Transactions on Biomedical Engineering*, BME-29(3), 149.
- Lieber, R. L., Fazeli, B. M., & Botte, M. J. (1990). Architecture of selected wrist flexor and extensor muscles. *The Journal of Hand Surgery*, 15(2), 244–250.
- Lieber, R. L., & Fridén, J. (2000). Functional and clinical significance of skeletal muscle architecture. *Muscle & Nerve*, 23(11), 1647–1666. [https://doi.org/10.1002/1097-4598\(200011\)23:11<1647::AID-MUS1>3.0.CO;2-M](https://doi.org/10.1002/1097-4598(200011)23:11<1647::AID-MUS1>3.0.CO;2-M)
- Liu, A.-T., Liu, B.-L., Lu, L.-X., Chen, G., Yu, D.-Z., Zhu, L., ... Jiang, H. (2014). Architectural properties of the neuromuscular compartments in selected forearm skeletal muscles. *Journal of Anatomy*, 225(1), 12–18. <https://doi.org/10.1111/joa.12193>
- Loeb, G. E., & Gans, C. (1986). *Electromyography for experimentalists*. University of Chicago Press.
- Lowery, M. M., Stoykov, N. S., & Kuiken, T. A. (2003). A simulation study to examine the use of cross-correlation as an estimate of surface EMG cross talk. *Journal of Applied Physiology*, 94(4), 1324–1334. <https://doi.org/10.1152/jappphysiol.00698.2002>
- Lowery, M., Nolan, P., & O'Malley, M. (2002). Electromyogram median frequency, spectral compression and muscle fibre conduction velocity during sustained sub-

maximal contraction of the brachioradialis muscle. *Journal of Electromyography and Kinesiology: Official Journal of the International Society of Electrophysiological Kinesiology*, 12(2), 111–118.

Luttgens, K., & Wells, K. F. (1982). *Kinesiology: Scientific basis of human motion*.

Saunders College Pub.

Mallette, M. M., Green, L. A., Gabriel, D. A., & Cheung, S. S. (2018). The effects of local forearm muscle cooling on motor unit properties. *European Journal of Applied Physiology*, 118(2), 401–410. <https://doi.org/10.1007/s00421-017-3782-y>

Mambrito, B., & De Luca, C. J. (1984). A technique for the detection, decomposition and analysis of the EMG signal. *Electroencephalography and Clinical Neurophysiology*, 58(2), 175–188. [https://doi.org/10.1016/0013-4694\(84\)90031-2](https://doi.org/10.1016/0013-4694(84)90031-2)

Martinez-Valdes, E., Negro, F., Laine, C. M., Falla, D., Mayer, F., & Farina, D. (2017).

Tracking motor units longitudinally across experimental sessions with high-density surface electromyography: Motor unit tracking with high-density EMG.

The Journal of Physiology, 595(5), 1479–1496. <https://doi.org/10.1113/JP273662>

McGill, K. C., Cummins, K. L., & Dorfman, L. J. (1985). Automatic Decomposition of

the Clinical Electromyogram. *IEEE Transactions on Biomedical Engineering*,

BME-32(7), 470–477. <https://doi.org/10.1109/TBME.1985.325562>

McGill, K. C., Lateva, Z. C., & Marateb, H. R. (2005). EMGLAB: An interactive EMG

decomposition program. *Journal of Neuroscience Methods*, 149(2), 121–133.

<https://doi.org/10.1016/j.jneumeth.2005.05.015>

McManus, L., Hu, X., Rymer, W. Z., Lowery, M. M., & Suresh, N. L. (2015). Changes in

motor unit behavior following isometric fatigue of the first dorsal interosseous

muscle. *Journal of Neurophysiology*, *113*(9), 3186–3196.

<https://doi.org/10.1152/jn.00146.2015>

McManus, L., Hu, X., Rymer, W. Z., Suresh, N. L., & Lowery, M. M. (2016). Muscle fatigue increases beta-band coherence between the firing times of simultaneously active motor units in the first dorsal interosseous muscle. *Journal of Neurophysiology*, *115*(6), 2830–2839. <https://doi.org/10.1152/jn.00097.2016>

McManus, L., Hu, X., Rymer, W. Z., Suresh, N. L., & Lowery, M. M. (2017). Motor Unit Activity during Fatiguing Isometric Muscle Contraction in Hemispheric Stroke Survivors. *Frontiers in Human Neuroscience*, *11*.

<https://doi.org/10.3389/fnhum.2017.00569>

McNeil, C. J., Doherty, T. J., Stashuk, D. W., & Rice, C. L. (2005). Motor unit number estimates in the tibialis anterior muscle of young, old, and very old men. *Muscle & Nerve*, *31*(4), 461–467. <https://doi.org/10.1002/mus.20276>

Mendell, L. M. (2005). The size principle: A rule describing the recruitment of motoneurons. *Journal of Neurophysiology*, *93*(6), 3024–3026.

<https://doi.org/10.1152/classicessays.00025.2005>

Merletti, R., Botter, A., Troiano, A., Merlo, E., & Minetto, M. A. (2009). Technology and instrumentation for detection and conditioning of the surface electromyographic signal: State of the art. *Clinical Biomechanics*, *24*(2), 122–134.

<https://doi.org/10.1016/j.clinbiomech.2008.08.006>

Merletti, R., Holobar, A., & Farina, D. (2008). Analysis of motor units with high-density surface electromyography. *Journal of Electromyography and Kinesiology*, *18*(6), 879–890. <https://doi.org/10.1016/j.jelekin.2008.09.002>

- Merletti, R., Knaflitz, M., & De Luca, C. J. (1990). Myoelectric manifestations of fatigue in voluntary and electrically elicited contractions. *Journal of Applied Physiology*, *69*(5), 1810–1820. <https://doi.org/10.1152/jappl.1990.69.5.1810>
- Mesin, L., Merletti, R., & Rainoldi, A. (2009). Surface EMG: The issue of electrode location. *Journal of Electromyography and Kinesiology*, *19*(5), 719–726.
- Mesin, L., Merletti, R., & Vieira, T. M. (2011). Insights gained into the interpretation of surface electromyograms from the gastrocnemius muscles: A simulation study. *Journal of Biomechanics*, *44*(6), 1096–1103.
- Milner-Brown, H. S., Stein, R. B., & Lee, R. G. (1975). Synchronization of human motor units: Possible roles of exercise and supraspinal reflexes. *Electroencephalography and Clinical Neurophysiology*, *38*(3), 245–254.
- Mizuno, M., Secher, N. H., & Quistorff, B. (1994). ³¹P-NMR spectroscopy, rsEMG, and histochemical fiber types of human wrist flexor muscles. *Journal of Applied Physiology (Bethesda, Md.: 1985)*, *76*(2), 531–538.
- Mogk, J. P. M., & Keir, P. J. (2003). Crosstalk in surface electromyography of the proximal forearm during gripping tasks. *Journal of Electromyography and Kinesiology*, *13*(1), 63–71. [https://doi.org/10.1016/S1050-6411\(02\)00071-8](https://doi.org/10.1016/S1050-6411(02)00071-8)
- Monster, A. W., & Chan, H. (1977). Isometric force production by motor units of extensor digitorum communis muscle in man. *Journal of Neurophysiology*, *40*(6), 1432–1443. <https://doi.org/10.1152/jn.1977.40.6.1432>
- Morimoto, S., & Masuda, M. (1984). Dependence of conduction velocity on spike interval during voluntary muscular contraction in human motor units. *European*

Journal of Applied Physiology and Occupational Physiology, 53(3), 191–195.

<https://doi.org/10.1007/BF00776588>

Muceli, S., Poppendieck, W., Negro, F., Yoshida, K., Hoffmann, K. P., Butler, J. E., ...

Farina, D. (2015). Accurate and representative decoding of the neural drive to muscles in humans with multi-channel intramuscular thin-film electrodes: Multi-channel intramuscular EMG electrode. *The Journal of Physiology*, 593(17), 3789–3804. <https://doi.org/10.1113/JP270902>

Nawab, S. H., Chang, S.-S., & De Luca, C. J. (2010). High-yield decomposition of surface EMG signals. *Clinical Neurophysiology*, 121(10), 1602–1615.


<https://doi.org/10.1016/j.clinph.2009.11.092>

Nawab, S. H., Wotiz, R. P., & De Luca, C. J. (2008). Decomposition of indwelling EMG signals. *Journal of Applied Physiology*, 105(2), 700–710.

<https://doi.org/10.1152/jappphysiol.00170.2007>

Negro, F., Muceli, S., Castronovo, A. M., Holobar, A., & Farina, D. (2016). Multi-channel intramuscular and surface EMG decomposition by convolutive blind source separation. *Journal of Neural Engineering*, 13(2), 026027.

<https://doi.org/10.1088/1741-2560/13/2/026027>

Nordander, C., Willner, J., Hansson, G.-, Larsson, B., Unge, J., Granquist, L., & Skerfving, S. (2003). Influence of the subcutaneous fat layer, as measured by ultrasound, skinfold calipers and BMI, on the EMG amplitude. *European Journal of Applied Physiology*, 89(6), 514–519. [https://doi.org/10.1007/s00421-003-0819-](https://doi.org/10.1007/s00421-003-0819-1)

- Oya, T., Riek, S., & Cresswell, A. G. (2009). Recruitment and rate coding organisation for soleus motor units across entire range of voluntary isometric plantar flexions: Recruitment and rate coding strategies for soleus motor units. *The Journal of Physiology*, 587(19), 4737–4748. <https://doi.org/10.1113/jphysiol.2009.175695>
- Pan, L., Zhang, D., Jiang, N., Sheng, X., & Zhu, X. (2015). Improving robustness against electrode shift of high density EMG for myoelectric control through common spatial patterns. *Journal of NeuroEngineering and Rehabilitation*, 12(1), 110. <https://doi.org/10.1186/s12984-015-0102-9>
- Parsaei, H., & Stashuk, D. W. (2009, September). *MUP shape-based validation of a motor unit potential train*. 2551–2554. <https://doi.org/10.1109/IEMBS.2009.5334758>
- Parsaei, H., & Stashuk, D. W. (2011). Adaptive motor unit potential train validation using MUP shape information. *Medical Engineering & Physics*, 33(5), 581–589. <https://doi.org/10.1016/j.medengphy.2010.12.012>
- Parsaei, H., & Stashuk, D. W. (2012). *Motor Unit Potential Train Validation and Its Application in EMG Signal Decomposition*. <https://doi.org/10.5772/37561>
- Perry, J., Easterday, C. S., & Antonelli, D. J. (1981). Surface versus intramuscular electrodes for electromyography of superficial and deep muscles. *Phys Ther*, 61(1), 7–15.
- Person, R. S., & Kudina, L. P. (1972). Discharge frequency and discharge pattern of human motor units during voluntary contraction of muscle. *Electroencephalography and Clinical Neurophysiology*, 32(5), 471–483.

- Piasecki, M., Ireland, A., Piasecki, J., Stashuk, D. W., McPhee, J. S., & Jones, D. A. (2018). The reliability of methods to estimate the number and size of human motor units and their use with large limb muscles. *European Journal of Applied Physiology*, *118*(4), 767–775. <https://doi.org/10.1007/s00421-018-3811-5>
- Podnar, S. (2004). Usefulness of an increase in size of motor unit potential sample. *Clinical Neurophysiology*, *115*(7), 1683–1688. <https://doi.org/10.1016/j.clinph.2004.02.016>
- Pope, Z. K., Hester, G. M., Benik, F. M., & DeFreitas, J. M. (2016). Action potential amplitude as a noninvasive indicator of motor unit-specific hypertrophy. *J Neurophysiol*, *7*.
- Qu, Y., & Stashuk, D. W. (1993). Clustering of motor unit action potentials using shape and temporal information. *Proceedings of the 15th Annual International Conference of the IEEE Engineering in Medicine and Biology Society*, 1209–1210. <https://doi.org/10.1109/IEMBS.1993.979098>
- Racinais, S. (2013). Hot ambient conditions shift the Force / EMG relationship. *SpringerPlus*, *2*(1), 317. <https://doi.org/10.1186/2193-1801-2-317>
- Rainoldi, A., Melchiorri, G., & Caruso, I. (2004). A method for positioning electrodes during surface EMG recordings in lower limb muscles. *Journal of Neuroscience Methods*, *134*(1), 37–43. <https://doi.org/10.1016/j.jneumeth.2003.10.014>
- Rainoldi, A., Nazzaro, M., Merletti, R., Farina, D., Caruso, I., & Gaudenti, S. (2000). Geometrical factors in surface EMG of the vastus medialis and lateralis muscles. *Journal of Electromyography and Kinesiology*, *10*(5), 327–336. [https://doi.org/10.1016/S1050-6411\(00\)00024-9](https://doi.org/10.1016/S1050-6411(00)00024-9)

- Rodríguez, I., Gila, L., Malanda, A., Gurtubay, I. G., Mallor, F., Gómez, S., ...
Rodríguez, J. (2007). Motor Unit Action Potential Duration, I: Variability of Manual and Automatic Measurements: *Journal of Clinical Neurophysiology*, 24(1), 52–58. <https://doi.org/10.1097/01.wnp.0000236606.53923.0d>
- Rodríguez-Carreño, I., Gila-Useros, L., & Malanda-Trigueros, A. (2012). Motor unit action potential duration: Measurement and significance. In *Advances in Clinical Neurophysiology*. InTech.
- Rodriguez-Falces, J. (2017). A new method for the localization of the innervation zone based on monopolar surface-detected potentials. *Journal of Electromyography and Kinesiology*, 35, 47–60. <https://doi.org/10.1016/j.jelekin.2017.05.004>
- Rodriguez-Falces, J., Navallas, J., Malanda, A., & Rodriguez-Martin, O. (2014). Comparison of the duration and power spectral changes of monopolar and bipolar M waves caused by alterations in muscle fibre conduction velocity. *Journal of Electromyography and Kinesiology*, 24(4), 452–464. <https://doi.org/10.1016/j.jelekin.2014.04.002>
- Roy, S. H., De Luca, C. J., & Schneider, J. (1986). Effects of electrode location on myoelectric conduction velocity and median frequency estimates. *Journal of Applied Physiology*, 61(4), 1510–1517. <https://doi.org/10.1152/jappl.1986.61.4.1510>
- Rutkove, S. B. (2000). Pseudofacilitation: A temperature-sensitive phenomenon. *Muscle & Nerve*, 23(1), 115–118.
- Rutkove, S. B. (2001). Effects of temperature on neuromuscular electrophysiology. *Muscle & Nerve*, 24(7), 867–882.

- Rutkove, S. B., Kothari, M. J., & Shefner, J. M. (1997). Nerve, muscle, and neuromuscular junction electrophysiology at high temperature. *Muscle & Nerve*, 20(4), 431–436.
- Sacco, P., McIntyre, D. B., & Jones, D. A. (1994). Effects of length and stimulation frequency on fatigue of the human tibialis anterior muscle. *Journal of Applied Physiology*, 77(3), 1148–1154. <https://doi.org/10.1152/jappl.1994.77.3.1148>
- Sadoyama, T., & Masuda, T. (1987). Changes of the average muscle fiber conduction velocity during a varying force contraction. *Electroencephalography and Clinical Neurophysiology*, 67(5), 495–497. [https://doi.org/10.1016/0013-4694\(87\)90014-9](https://doi.org/10.1016/0013-4694(87)90014-9)
- Satuvuori, E., & Kreuz, T. (2018). Which spike train distance is most suitable for distinguishing rate and temporal coding? *Journal of Neuroscience Methods*, 299, 22–33. <https://doi.org/10.1016/j.jneumeth.2018.02.009>
- Sbriccoli, P., Bazzucchi, I., Rosponi, A., Bernardi, M., De Vito, G., & Felici, F. (2003). Amplitude and spectral characteristics of biceps Brachii sEMG depend upon speed of isometric force generation. *Journal of Electromyography and Kinesiology*, 13(2), 139–147. [https://doi.org/10.1016/S1050-6411\(02\)00098-6](https://doi.org/10.1016/S1050-6411(02)00098-6)
- Segal, R. L., Wolf, S. L., DeCamp, M. J., Chopp, M. T., & English, A. W. (1991). Anatomical Partitioning of Three Multiarticular Human Muscles. *Cells Tissues Organs*, 142(3), 261–266. <https://doi.org/10.1159/000147199>
- Seki, K., & Narusawa, M. (1996). Firing rate modulation of human motor units in different muscles during isometric contraction with various forces. *Brain Research*, 719(1–2), 1–7.

- Semmler, J. G. (2002). Motor unit synchronization and neuromuscular performance. *Exercise and Sport Sciences Reviews, 30*(1), 8–14.
- Semmler, J. G., Nordstrom, M. A., & Wallace, C. J. (1997). Relationship between motor unit short-term synchronization and common drive in human first dorsal interosseous muscle. *Brain Research, 767*, 314–320.
- Shefner, J. M., Cudkowicz, M. E., Zhang, H., Schoenfeld, D., & Jilapalli, D. (2007). Revised statistical motor unit number estimation in the Celecoxib/ALS trial. *Muscle & Nerve, 35*(2), 228–234. <https://doi.org/10.1002/mus.20671>
- Shefner, J. M., Jilapalli, D., & Bradshaw, D. Y. (1999). Reducing intersubject variability in motor unit number estimation. *Muscle & Nerve, 22*(10), 1457–1460.
- Sherwood, L., Kell, R. T., & Ward, C. A. (2013). *Human physiology*. Nelson Education.
- Simpson, J. A. (1969). Terminology of electromyography. *Electroencephalography and Clinical Neurophysiology, 26*(2), 224–226. [https://doi.org/10.1016/0013-4694\(69\)90217-X](https://doi.org/10.1016/0013-4694(69)90217-X)
- Solomonow, M., Baratta, R., Bernardi, M., Zhou, B., Lu, Y., Zhu, M., & Acierno, S. (1994). Surface and wire EMG crosstalk in neighbouring muscles. *Journal of Electromyography and Kinesiology, 4*(3), 131–142.
- Song, D. H., Chung, M. E., Han, Z.-A., Kim, S. Y., Park, H. K., & Seo, Y. J. (2014). Anatomic Localization of Motor Points of Wrist Flexors. *American Journal of Physical Medicine & Rehabilitation, 93*(4), 282–286.
- Stålberg, E., Ekstedt, J., & Broman, A. (1971a). The electromyographic jitter in normal human muscles. *Electroencephalography and Clinical Neurophysiology, 31*(5), 429–438. [https://doi.org/10.1016/0013-4694\(71\)90164-7](https://doi.org/10.1016/0013-4694(71)90164-7)

- Stålberg, E., Ekstedt, J., & Broman, A. (1971b). The electromyographic jitter in normal human muscles. *Electroencephalography and Clinical Neurophysiology*, *31*(5), 429–438. [https://doi.org/10.1016/0013-4694\(71\)90164-7](https://doi.org/10.1016/0013-4694(71)90164-7)
- Stålberg, E. V., & Sonoo, M. (1994). Assessment of variability in the shape of the motor unit action potential, the “jiggle,” at consecutive discharges. *Muscle & Nerve*, *17*(10), 1135–1144. <https://doi.org/10.1002/mus.880171003>
- Stashuk, D., & de Bruin, H. (1988). Automatic decomposition of selective needle-detected myoelectric signals. *IEEE Transactions on Bio-Medical Engineering*, *35*(1), 1–10. <https://doi.org/10.1109/10.1330>
- Stashuk, D., & Qu, Y. (1996a). Robust method for estimating motor unit firing-pattern statistics. *Medical and Biological Engineering and Computing*, *34*(1), 50–57. <https://doi.org/10.1007/BF02637022>
- Stashuk, D. W. (1999a). Decomposition and quantitative analysis of clinical electromyographic signals. *Medical Engineering & Physics*, *21*(6–7), 389–404.
- Stashuk, D. W. (1999b). Decomposition and quantitative analysis of clinical electromyographic signals. *Medical Engineering & Physics*, *21*(6–7), 389–404. [https://doi.org/10.1016/S1350-4533\(99\)00064-8](https://doi.org/10.1016/S1350-4533(99)00064-8)
- Stashuk, D. W. (2001). EMG signal decomposition: How can it be accomplished and used? *Journal of Electromyography and Kinesiology*, *11*(3), 151–173.
- Stashuk, D. W., & Qu, Y. (1996b). Adaptive motor unit action potential clustering using shape and temporal information. *Medical and Biological Engineering and Computing*, *34*(1), 41–49.

- Staudenmann, D., Roeleveld, K., Stegeman, D. F., & van Dieën, J. H. (2010). Methodological aspects of SEMG recordings for force estimation – A tutorial and review. *Journal of Electromyography and Kinesiology*, *20*(3), 375–387. <https://doi.org/10.1016/j.jelekin.2009.08.005>
- Stock, M. S., Beck, T. W., & Defreitas, J. M. (2012). Effects of fatigue on motor unit firing rate versus recruitment threshold relationships. *Muscle & Nerve*, *45*(1), 100–109. <https://doi.org/10.1002/mus.22266>
- Stokes, I. A. F., Henry, S. M., & Single, R. M. (2003). Surface EMG electrodes do not accurately record from lumbar multifidus muscles. *Clinical Biomechanics*, *18*(1), 9–13. [https://doi.org/10.1016/S0268-0033\(02\)00140-7](https://doi.org/10.1016/S0268-0033(02)00140-7)
- Strommen, J. A., & Daube, J. R. (2001). Determinants of pain in needle electromyography. *Clinical Neurophysiology*, *112*(8), 1414–1418. [https://doi.org/10.1016/S1388-2457\(01\)00552-1](https://doi.org/10.1016/S1388-2457(01)00552-1)
- Tibshirani, R., Walther, G., & Hastie, T. (2001). Estimating the number of clusters in a data set via the gap statistic. *Journal of the Royal Statistical Society: Series B (Statistical Methodology)*, *63*(2), 411–423.
- Troni, W., DeMattei, M., & Contegiacomo, V. (1991). The effect of temperature on conduction velocity in human muscle fibers. *Journal of Electromyography and Kinesiology*, *1*(4), 281–287.
- Van Cutsem, M., Feiereisen, P., Duchateau, J., & Hainaut, K. (1997). Mechanical properties and behaviour of motor units in the tibialis anterior during voluntary contractions. *Journal of Applied Physiology*, *22*(6), 585–597.

- van Eijden, T. M. G. J., & Raadsheer, M. C. (1992). Heterogeneity of fiber and sarcomere length in the human masseter muscle. *The Anatomical Record*, 232(1), 78–84.
<https://doi.org/10.1002/ar.1092320109>
- Victor, J. D., & Purpura, K. P. (1996). Nature and precision of temporal coding in visual cortex: A metric-space analysis. *Journal of Neurophysiology*, 76(2), 1310–1326.
<https://doi.org/10.1152/jn.1996.76.2.1310>
- Vieira, T. M. M., Loram, I. D., Muceli, S., Merletti, R., & Farina, D. (2011). Postural activation of the human medial gastrocnemius muscle: Are the muscle units spatially localised? *The Journal of Physiology*, 589(Pt 2), 431–443.
<https://doi.org/10.1113/jphysiol.2010.201806>
- Westerblad, H., Allen, D. G., & Lännergren, J. (2002). Muscle fatigue: Lactic acid or inorganic phosphate the major cause? *News in Physiological Sciences: An International Journal of Physiology Produced Jointly by the International Union of Physiological Sciences and the American Physiological Society*, 17, 17–21.
- Winkel, J., & Jørgensen, K. (1991). Significance of skin temperature changes in surface electromyography. *European Journal of Applied Physiology and Occupational Physiology*, 63(5), 345–348. <https://doi.org/10.1007/BF00364460>
- Winter, D. A. (1990). *Biomechanics and motor control of human movement*. John Wiley & Sons.
- Winter, D. A., Fuglevand, A. J., & Archer, S. E. (1994). Crosstalk in surface electromyography: Theoretical and practical estimates. *Journal of Electromyography and Kinesiology*, 4(1), 15–26.

- Yaar, I., & Niles, L. (1992). Muscle fiber conduction velocity and mean power spectrum frequency in neuromuscular disorders and in fatigue. *Muscle & Nerve*, *15*(7), 780–787. <https://doi.org/10.1002/mus.880150706>
- Zaheer, F., Roy, S. H., & De Luca, C. J. (2012). Preferred sensor sites for surface EMG signal decomposition. *Physiological Measurement*, *33*(2), 195–206. <https://doi.org/10.1088/0967-3334/33/2/195>
- Zennaro, D., Läubli, T., Wellig, P., Krebs, D., Schnoz, M., Klipstein, A., & Krueger, H. (2002). A method to test reliability and accuracy of the decomposition of multi-channel long-term intramuscular EMG signal recordings. *International Journal of Industrial Ergonomics*, *30*(4), 211–224. [https://doi.org/10.1016/S0169-8141\(02\)00126-9](https://doi.org/10.1016/S0169-8141(02)00126-9)
- Zwarts, M. J., & Stegeman, D. F. (2003). Multichannel surface EMG: Basic aspects and clinical utility. *Muscle & Nerve*, *28*(1), 1–17. <https://doi.org/10.1002/mus.10358>

Appendix 1 – Piloting the Denoising Algorithm

Abstract

The purpose of this pilot work was to determine a systematic approach for removing erroneous motor unit (MU) discharge times obtained by the dEMG surface electromyographic (sEMG) decomposition technique. Motor unit discharge times were obtained from the flexor carpi radialis (FCR) and tibialis anterior (TA) during ramp isometric contractions, held at 60% of maximal voluntary contraction (MVC). The dominant and non-dominant, upper and lower limbs of 20 participants were tested. A total of 920 MUs were analyzed. The discharge times for each MU were used to spike trigger average the sEMG signal to calculate its template.

A custom graphical user interface in MATLAB (MathWorks Inc., Natick, MA) was used to denoise the surface electromyographic (sEMG) signal from the Delsys dEMG system (Natick, MA). The algorithm for inclusion of an individual motor unit potential (MUP) and its associated discharge time was the following, based on observations: (1) a positive correlation ($r > 0.0$) with the template; (2) a signal-to-noise ratio (SNR) greater than 0.5 dB; and (3) a peak that was located within the 68% confidence interval for the MU template peak location. Additional ‘tuning’ of these three parameters was required for only 30% of the MUPTs. Waveforms falling outside the boundaries of these three criteria were considered as a noise and the erroneous discharge time was removed. Thus, the term ‘denoising’.

Efficacy of the denoising routine was evaluated by changes in the variance ratio (VR) and SNR of MUPs contributing to each template. A three-way (4-Limb \times 4-

Channels \times 2-Denoise) randomized block factorial (RBF) analysis of variance (ANOVA) was therefore used to evaluate significant differences in the VR and SNR. On average, 33.07% of the discharge times were removed from MUPTs ($p < 0.05$). There was a significant decrease in the VR across limbs (23.05%, $p < 0.05$). Likewise, the SNR exhibited a significant increase across limbs (11.67%, $p < 0.05$). Denoising also resulted in a significant increase in the correlation between the VR and SNR across all limbs ($p < 0.05$). The variability in the shape of MUPs contributing to a MU template and increased its SNR, supporting the validity of the remaining MU discharge times.

Introduction

The gold standard for motor unit (MU) identification is through the use of needle or fine wire electrodes, where the recording surface is in close proximity to the muscle fibers (Farina, Merletti, & Enoka, 2015). Advances in decomposition of the surface electromyographic (sEMG) decomposition has led to a dramatic increase in neurophysiological studies that record MUs from the skin surface (De Luca, Adam, Wotiz, Gilmore, & Nawab, 2006; Farina & Holobar, 2016; Holobar & Farina, 2014; Nawab, Chang, & De Luca, 2010). At present, there are two main computational approaches to decomposing the sEMG signal into its individual MU potentials (MUPs). The computational approaches are also linked with different recording methodologies: high-density sEMG (HD-sEMG) grid electrodes (Farina, Holobar, Merletti, & Enoka, 2010), or the dEMG system with a five-pin recording sensor (Delsys, Natick, MA) (De Luca et al., 2006; Nawab et al., 2010). As a result, there is debate about the best approach for decomposing the sEMG signal and validating the results (De Luca, Nawab, & Kline, 2015; Farina et al., 2015),

The most direct validation technique compares the MU templates obtained from indwelling and surface signals, called the ‘two-source’ method. Originally, the amplitude of an indwelling MUP is used to trigger data collection and averaging of the surface signal, which is termed the ‘spike-triggered averaging’ (STA) technique (Stashuk, 2001). The discharge time of the MU is unambiguously linked with the MUP recorded on the skin surface. Hu, Rymer, and Suresh (2014) employed the two-source technique by comparing the MU template obtained by traditional STA to that with a MU template generated by using the discharge times obtained through sEMG decomposition. This version of the two-source technique was used to validate MU discharge times up to 15% MVC. The same research group more recently demonstrated that even slight errors in MU discharge times result in an unrecognizable template (Hu, Rymer, & Suresh, 2013b). As a result, STA of the sEMG signal using only the MU discharge times obtained by sEMG decomposition has been used to validate MU data up to 50% MVC (Hu et al., 2013b).

The purpose of this pilot work was to determine the feasibility of using the STA technique to extract MU discharge times for which there is a ‘high confidence’ of their validity. The validity of a MU discharge time was assessed on the basis of how its associated MUPs contributed to the final MU template. There were three criteria whose specific parameters were determined heuristically as part of the pilot work: (1) a positive correlation with the template, at least greater than zero; (2) a minimum signal-to-noise ratio (SNR) greater than 0 dB; and (3) a peak that was located within ‘at least’ the 95% confidence interval for that of the MU template. Otherwise, the discharge time was removed, and a MU template was recalculated based on MUPs with lower variability and

a greater signal-to-noise ratio (SNR). Removal of MUPs is hereafter referred to as “**denoising**”. If proven feasible, the next step is to use the remaining discharge times to calculate MU peak-to-peak (P-P) amplitude, P-P duration, and discharge rate with ‘high confidence’. The term ‘high confidence’ is derived from the notion that all MUPs within a MUPT having the same shape, confer a degree of validity to the discharge times (Parsaei & Stashuk, 2009, 2011).

Methods

The data that was used in this study was part of an intervention study on cross-education in the upper and lower limbs (Green & Gabriel, 2018). The dominant and non-dominant, upper and lower limbs were assessed for unilateral maximal isometric strength of the wrist flexors and ankle dorsiflexors. Motor unit discharge rate (MUDR) of the flexor carpi radialis (FCR) and tibialis anterior (TA) were then measured at 60% maximal voluntary contraction (MVC).

Participants. The force and sEMG data from 20 participants (10 males and 10 females) were used for analysis. Participants were free from neurological or musculoskeletal disorders of the upper and lower limbs and all within the age range of 18-35 years. The study was cleared by Brock University Research Ethics Board (REB: #16-313, Appendix 2).

Experimental Design. On each of the four days of testing, participants were required to complete 3 MVCs for dominant and non-dominant upper and lower limbs, in a randomized order. Electromyographic recordings were then taken from the FCR and TA during a 60% MVC force tracking task. There were three trials per limb, and the

order of testing was also randomized. A total of 48 trials per participant were used for this study.

Apparatus and Subject Test Position. For the sake of brevity, please see the same apparatus and test position for wrist flexion and ankle dorsiflexion depicted in the Green, McGuire, and Gabriel (2015) and Lenhardt and Gabriel (2009), respectively. Subjects were familiarized with the protocol on the first day. For the dorsiflexion trials, the participants were seated in a custom-made chair that allowed for isolation of dorsiflexion of the ankle. The participant's knees, hips and ankles were at an angle of 90°. The other leg was placed on a foot rest for the duration of the trials. Dorsiflexion force was recorded through a load cell that was secured to the foot plate (JR3 Inc., Woodland, CA). Forearm flexion trials were completed with the hand inserted into the custom jig. The arm rested at 160° elbow flexion. The device included a load cell (MB-100, Interface, Scottsdale, AZ) to measure flexion force at the wrist. Two metal bars were located on either side of the wrist reduce the amount of contribution from elbow and shoulder as much as possible.

Instrumentation. The participant's FCR and TA were located through palpation and flexion of the wrist and dorsiflexion of the ankle, respectively. The motor point was located through low-level, repeated percutaneous electrical stimulation at 1.5 pulses/s (Christie, Lester, LaPierre, & Gabriel, 2004). Once identified, motor point was marked using indelible ink so that the dEMG electrode was placed away from the location (Green et al., 2015). Skin preparation involved shaving a desired amount of hair off the skin surface over the muscle, cleaning the skin surface with alcohol, using a light abrasive

cream (NuPrep, Weaver and Co., Aurora, CO) to remove dead skin from the skin surface and then using alcohol to clean it once more.

The 5-pin dEMG electrode was placed approximately 2 cm distally from the identified motor point, taped on and secured with a Velcro strap. The dEMG electrode has an interelectrode distance of 5 mm resulting in four channels of differential EMG. The ground electrode was placed over the olecranon process of the ulna for FCR EMG and on the patella for the TA EMG. The EMG signal and force signals were collected through the Delsys Bagnoli-16 (Delsys, Natick, MA). Force was sampled without any amplification or filtering at 20,000 Hz. The EMG signals were amplified 1000 times and the signal was filtered between 20 and 450 Hz and digitized at 20 kHz.

Force Tracking. Participants had a computer screen in front of them that provided visual feedback of the force they exerted on the load cell. There were 3 maximal isometric contractions, each 4 seconds in duration with a 2-minute inter-trial rest interval, to determine the submaximal (20 and 60%) forces (Gabriel, Lester, Lenhardt, & Cambridge, 2007). Participants were asked to trace a ramp on the screen that represented 20% MVC, which was used as a signal quality check for the dEMG electrode to ensure low skin impedance, acceptable SNR and low line interference. Three ramp contractions to 60% MVC were completed after verification of signal quality. The ramp increased by 10% MVC/s for six seconds, then was maintained at 60% MVC for six seconds and then decreased by 10% MVC/s for six seconds (see Figure 1).

Preliminary Analysis

Since the proposed work represents our first attempt to use discharge times outside of the dEMG system to STA the identified MUs, shimmer plots of each identified MU at 60% MVC were created for all participants using MATLAB (The Mathworks, Inc., Natick, MA). The STA templates were 25 ms in length (12.5 ms on either side of the trigger time). The series of discharge times associated with a specific MU constitutes its MUPT. Since a MUP is recorded at each discharge time, the shimmer plot is the overlay of all the individual MUPs within the MUPT. The quality of the MU data was first assessed by visual inspection (see Figures 2, 3, and 4), which resulted in six classifications based on the variability of waveforms within the MUPT:

- (1) Few discharges (≈ 50) with a well-defined shape because there were no obvious errors in discharge times as revealed by waveforms that do not obscure the peaks and valley of the MUPT (Figure 2, top panel).
- (2) Few discharges (≈ 50) with a poorly-defined shape because there were obvious errors in discharge times as revealed by waveforms that obscure the peaks and valley of the MUPs (Figure 2, bottom panel).
- (3) Sufficient discharges (>50) with a high SNR. The definition of a high SNR was a peak-to-peak (P-P) amplitude for baseline noise that was roughly less than half the P-P amplitude for the MUPs. Additionally, there were no obvious errors in discharge times as revealed by waveforms that obscure the peaks and valley of the MUPs (Figure 3, top panel).

- (4) Sufficient discharges (>50) with a high SNR, with obvious errors in discharge times as revealed by waveforms that obscure the peaks and valley of the MUPs (Figure 3, bottom panel).
- (5) Sufficient discharges (>50) with a moderate SNR. The definition of a moderate SNR was a P-P amplitude for baseline noise that was approximately greater than half the P-P amplitude for the MUPs. There were no obvious errors in discharge times as revealed by waveforms that do not obscure the peaks and valley of the MUPs (Figure 4, top panel).
- (6) Sufficient discharges (>50) with a moderate SNR, and there were obvious errors in discharge times as revealed by waveforms that obscure the peaks and valleys of the MUPs (Figure 4, bottom panel).

The next step was to calculate the VR for MUPs associated with each MUPT, to determine if the six categories may be characterized by VRs of specific magnitudes. MUPTs with a SNR less than 0.5 with no obvious errors in discharge times had VRs less than 0.75. If the SNR was greater than 0.5 the VR was generally greater than 0.75. Errors in discharge times increased the VR even further as depicted in category 6. Linking the six categories to specific VRs allowed for the automatic selection of visually difficult to identify MUs (Lefever & De Luca, 1982) from which to develop a denoising routine. Therefore, MUPTs with a sufficient number of discharge times (>50) and a VR of 0.75 or greater were used for analysis.

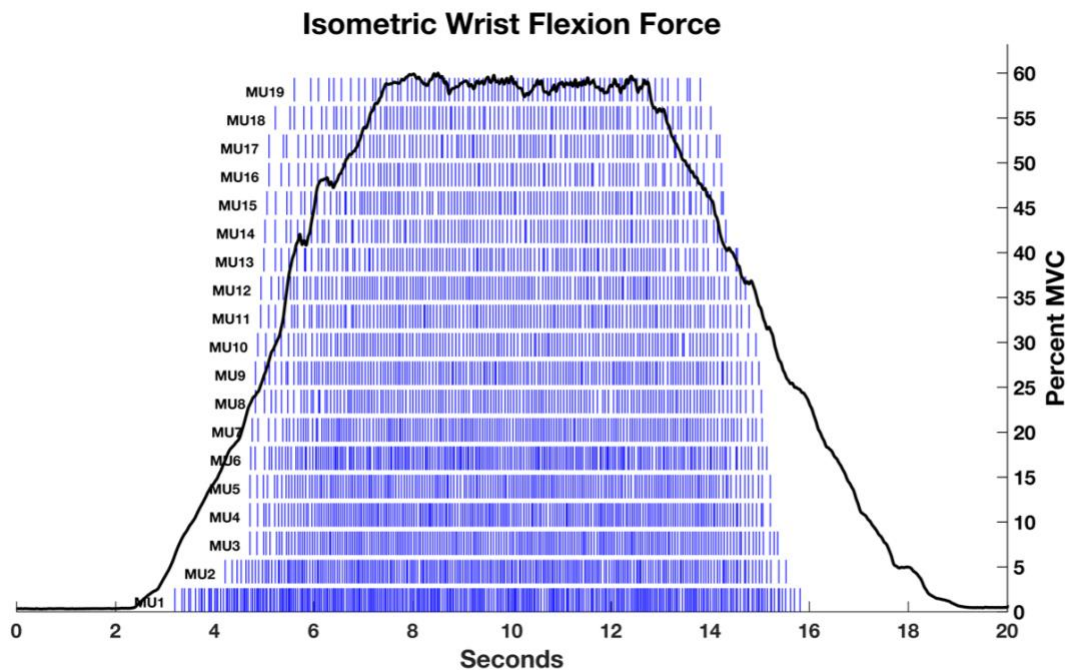


Figure 1. One decomposed ramp contraction from a representative participant. Along the left Y-axis is the MU number and the bar plot of its discharge times that was detected by dEMG with an accuracy rating of >90%. The right Y-axis is the force that the participant exerted during the 60% MVC ramp contraction.

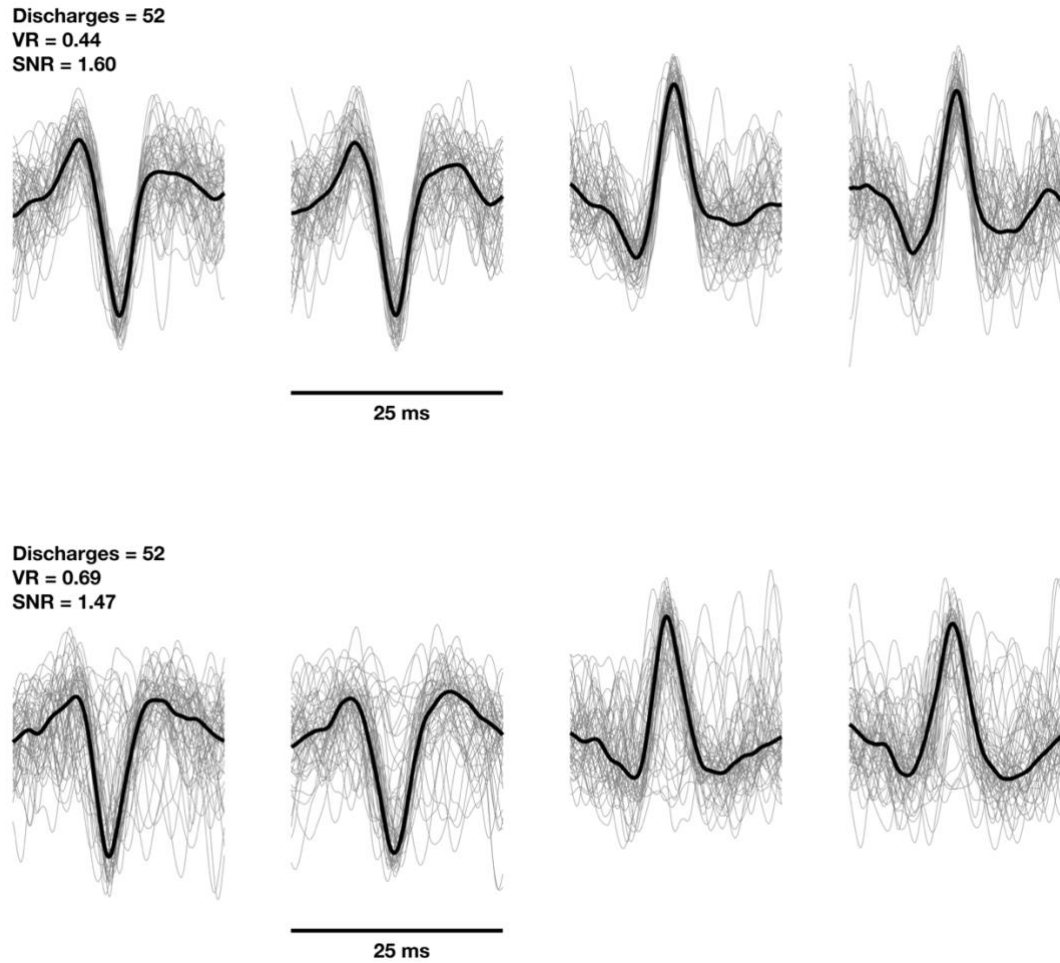


Figure 2. The shimmer plots for category 1 (top) and category 2 (bottom). The gray waveforms for the individual motor unit (MU) potentials with the motor unit potential train. The thick black line is the MU template for each channel. The total number of discharges is presented in the top left corner of channel 1 for each category. The variance ratio (VR) and signal-to-noise-ratio (SNR) are also presented in the top left corner of channel 1 for both categories, and they represent the mean across channels. The shimmer of each MUPT is plotted with the mean waveform overlaid (black line).

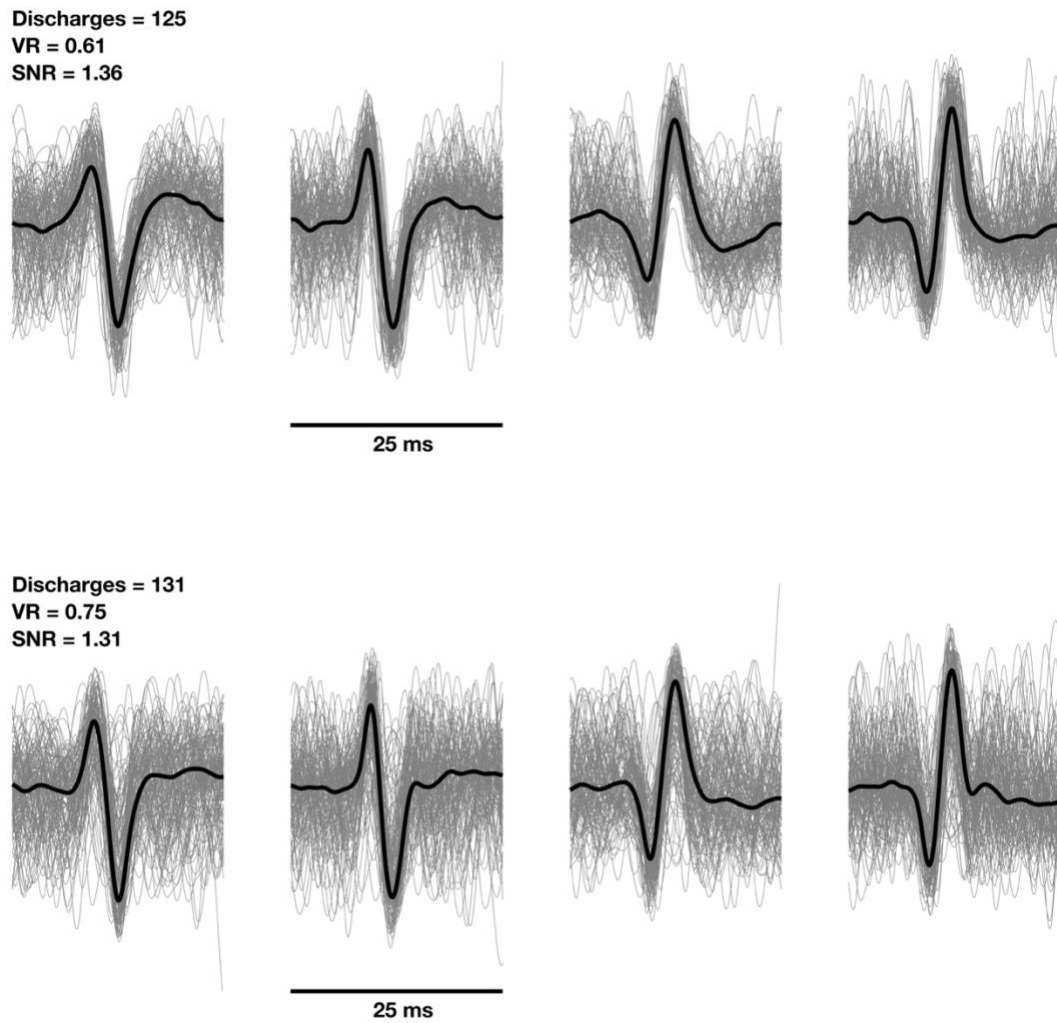


Figure 3. The shimmer plots for category 3 (top) and category 4 (bottom). The gray waveforms or the individual motor unit (MU) potentials with the motor unit potential train. The thick black line is the MU template for each channel. The total number of discharges is presented in the top left corner of channel 1 for each category. The variance ratio (VR) and signal-to-noise-ratio (SNR) are also presented in the top left corner of channel 1 for both categories, and they represent the mean across channels. The shimmer of each MUPT is plotted with the mean waveform overlaid (black line).

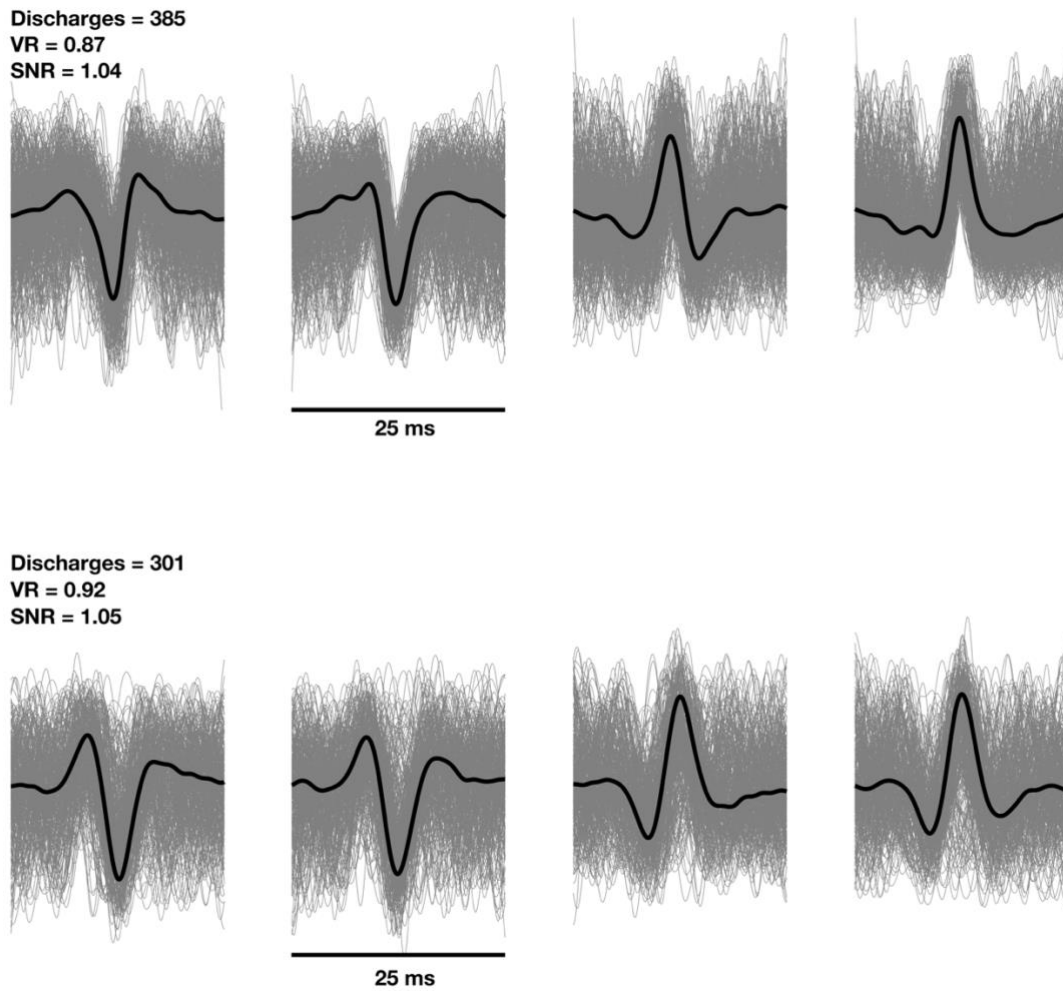


Figure 4. The shimmer plots for Category 5 (top) and category 6 (bottom). The gray waveforms or the individual motor unit (MU) potentials with the motor unit potential train. The thick black line is the MU template for each channel. The total number of discharges is presented in the top left corner of channel 1 for each category. The variance ratio (VR) and signal-to-noise-ratio (SNR) are also presented in the top left corner of channel 1 for both categories, and they represent the mean across channels. The shimmer of each MUPT is plotted with the mean waveform overlaid (black line).

Denoising. The denoising algorithm uses the correlation between an individual MUP and the extracted template that is calculated on the entire train identified by the dEMG discharge times. To start, the parameters were set such that the limits were not over-encumbering. The individual MUP must have a minimum correlation with the template of greater than zero ($r > 0$) (Davila & Mobin, 1992). The MUP also must have a SNR of the root-mean-square (RMS) amplitude that is greater than 0 to help identify an event (Florestal, Mathieu, & Malanda, 2006). Finally, the MUP peak has to occur within the 95% confidence interval of the location of that peak of the template (Dorfman, Howard, & McGill, 1989; Stålberg, Ekstedt, & Broman, 1971). These three criteria may be manually tuned using the feedback of how well the calculated template cross-correlates with the template provided by the dEMG system. The goal was to decrease the VR and increase the SNR with the following constraints: (1) the cross-correlation between the dEMG template and the recalculated template, after removing the erroneous discharge times, should not decrease more than 10% (Arendt-Nielsen & Zwarts, 1989), and (2) limit the loss of discharge times to approximately 30% of the entire train. The denoising steps are detailed below:

Step 1. Calculate the VR and SNR on each of the four channels.

Step 2. Calculate the template for the MUPT.

Step 3. Calculate the cross-correlation between the extracted template the dEMG template for that specific MU and channel.

Step 4. Denoise the MUPT using the following criteria:

- (1) The cross-correlation between the MUP and its template must be greater than 0.0;
- (2) The MUP peak location must be within the 68% confidence interval of those MUPs constituting the extracted template;
- (3) The MUP SNR must be greater than 0.5 dB.

Step 5. Recalculate the cross-correlation coefficient between the extracted template and that from dEMG.

Step 6. Recalculate the VR and SNR on the denoised MUPT.

Step 7. Calculate the percent change in the cross-correlation coefficient and discharge times.

Step 8. Plot the waveforms that have been removed (i.e., residuals) to verify that MUPs belonging to the MUPT have not been removed.

Step 9. Repeat steps 4 – 8, adjusting the three denoising criteria such that the cross-correlation between the updated extracted template and that from dEMG does not go below the 10% of the original value or the loss in the discharges does not exceed 30%.

Denoising was accomplished through a custom graphical user interface (GUI) in MATLAB (MathWorks, Natick, MA) that provided feedback on the impact of specific values for the denoising parameters: VR, SNR, and the cross-correlation coefficient (R_{xy}) between the calculated template using the dEMG discharge times and that provided by

the dEMG system. Figure 5 shows the information provided by the denoising GUI. The top panels plot the MUP shimmers, one for each of the four channels. The templates calculated from the discharge times (red) and that provided by the dEMG system (blue) are superimposed on the shimmer plots. Beneath each shimmer is a plot of the residual waveforms that have been removed from that particular channel as a result of denoising. Denoising was performed only on the channel with the lowest initial VR, termed the “target channel” (red title). The residual waveforms beneath the target channel are associated with the removed discharge times. Residual waveforms for the other three channels reflect the same removed discharge times.

The user adjusted the values for the denoising parameters so that the peaks and valleys of the target channel were clear, while the residuals waveforms had no distinct shape. The residual plots also include the percent decrease in the number of discharges (Δ FIR), which was the same across channels. The frequency-distribution curve for the inter-discharge intervals (IDIs) before denoising, along with the initial VR, SNR, and R_{xy} is presented in bottom left of Figure 5. The frequency-distribution curve for the remaining IDIs, and the VR, SNR, and R_{xy} after denoising is depicted in the bottom right of Figure 5. In this particular case, there was no change in R_{xy} but denoising effected a 6.3% decrease in VR and a 4.1% increase in the SNR.

The denoising parameters removed waveforms that were not positively correlated with the calculated MU templated. The discharge times with these waveforms were removed and “assumed” be noise. However, waveforms that were not positively correlated with the calculated MU templated could also be associated with another MU as would occur with superposition. Figure 6 shows the case of superposition which required

more “stringent” tuning of the denoising parameters to separate the two MU templates. Note, the residual waveforms resemble the MU template (blue) provided by the dEMG system.

The parameters of the denoising algorithm were specific enough to allow MUPTs to pass through unaltered (see Figure 7). Figures 6, 7, and 8 illustrates the necessity of calculating templates using the denoised motor unit discharge times. First, Figure 7 illustrates that it was not unusual for the MU templates provided by the dEMG system to include discontinuities, which would make the quantification of MU dimensions more difficult. Inspection of Figure 8 also shows that the calculated MU template has a better ‘fit’ with the underlying shimmer plot for each channel than the MU template provided by the dEMG system. The cross-correlation coefficient between the two templates is $R_{xy} = 0.88$, which is similar to that generally observed on Table 1. Finally, Figure 8, is an example of the difference in the calculated MU template before (red) and after (blue) denoising. In this case, the blue waveform is ‘not’ the MU template from the dEMG system. Rather, it is the MU template calculated on denoised data. The MU presented in Figure 8 (MU#2) is the same as the presented in Figure 6. Thus, denoising is expected to have a significant impact on the quantification of MU templates. The cross-correlation coefficient between the raw and denoised MU templates increased to $R_{xy} = 0.97$.

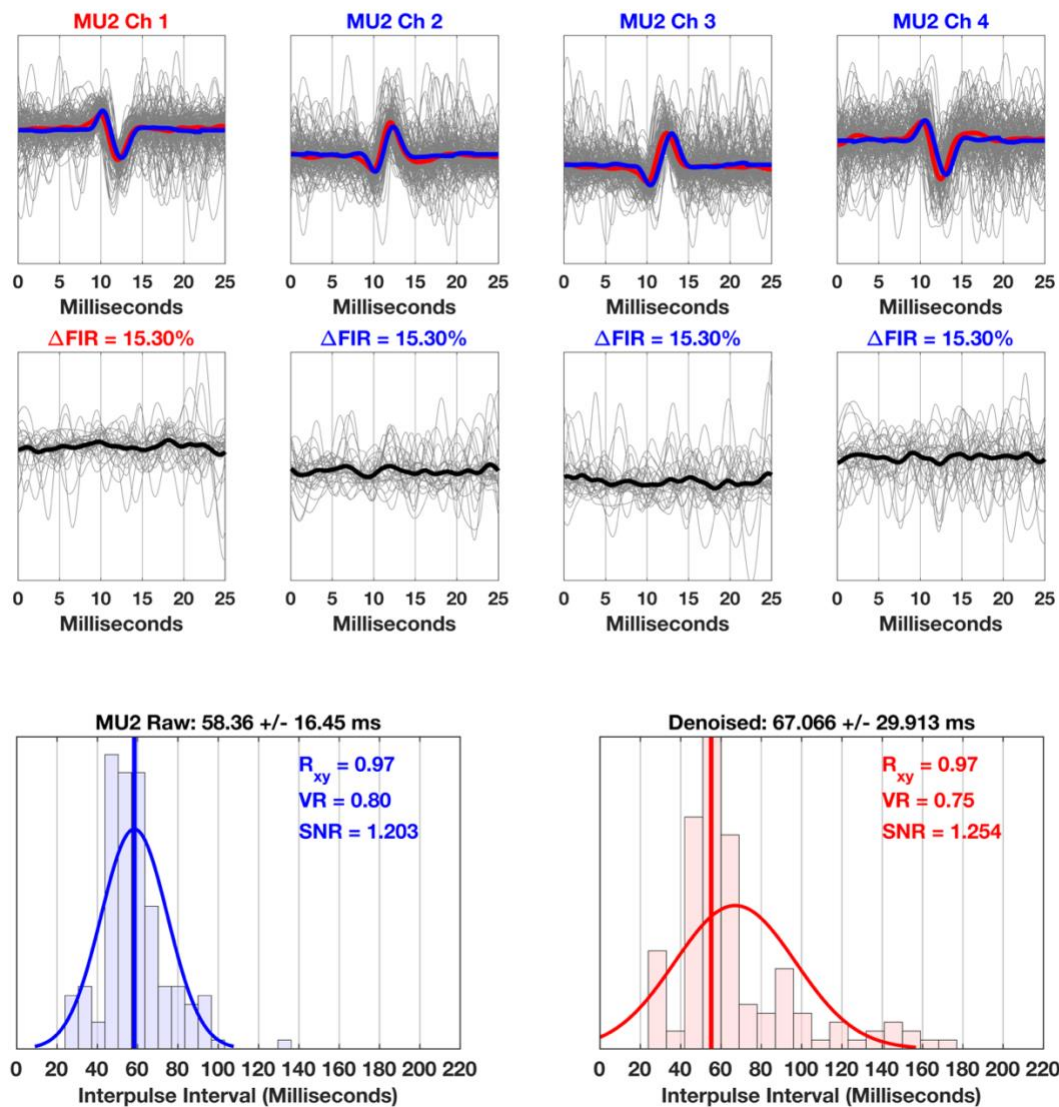


Figure 5. Representative example of denoising a motor unit potential train (MUPT). The top panels are the shimmer plots, one for each channel. The shimmer plots include the MU templates calculated from the discharge times (red) and that provided by the dEMG system (blue). The waveforms removed from each channel are plotted immediately below it, indicating the percent decrease in discharge times (Δ FIR). The bottom right and left graphs are the frequency-distributions curves of the inter-discharge intervals (IDIs) before and after denoising, respectively. Likewise, the variance ratio (VR), the signal-to-noise ratio (SNR), and the cross-correlation coefficient (R_{xy}) between the calculated MU template using the dEMG discharge times and that provided by the dEMG system.

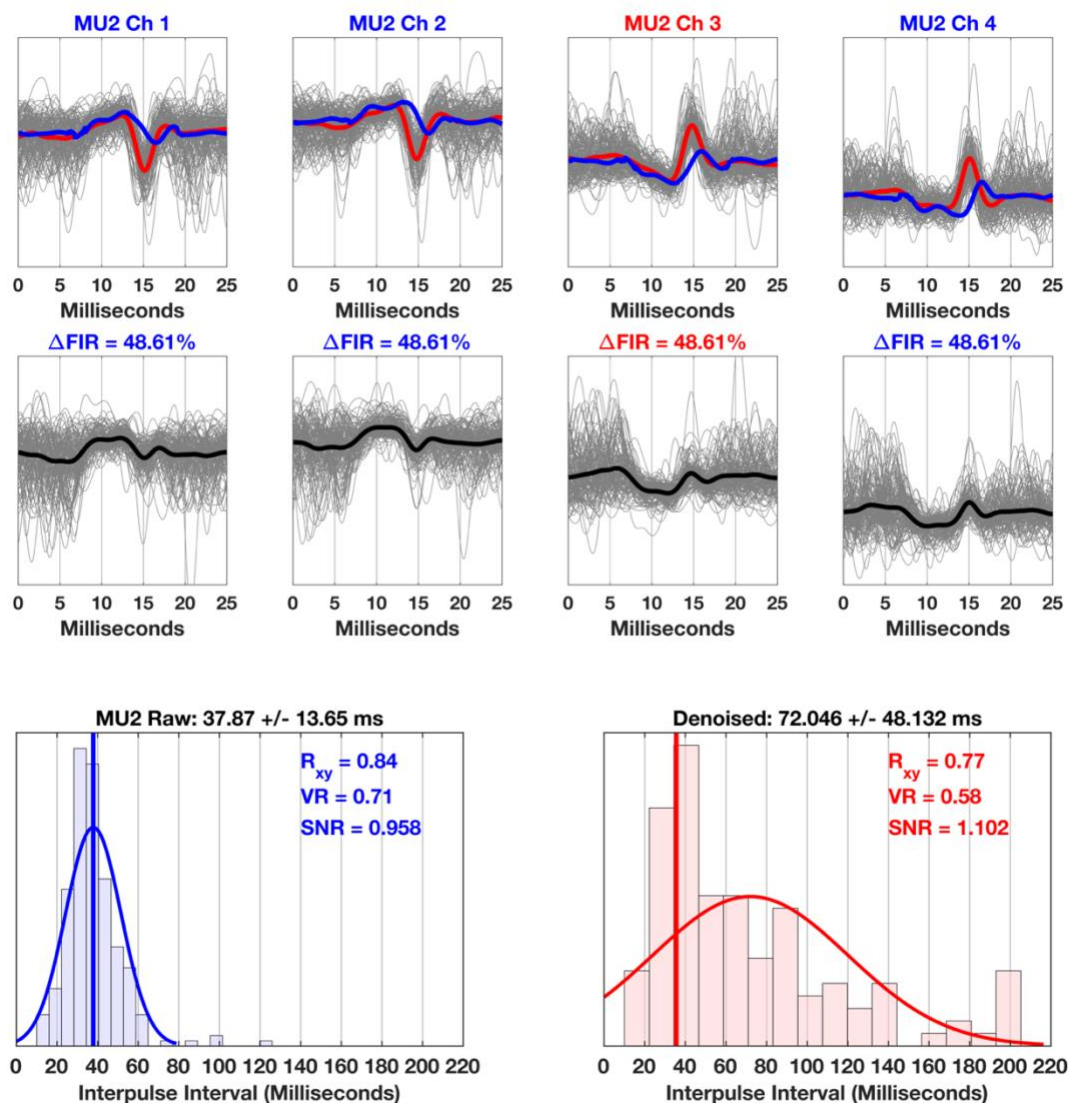


Figure 6. Representative example of superposition following denoising a motor unit potential train (MUPT). The top panels are the shimmer plots, one for each channel. The shimmer plots include the MU templates calculated from the discharge times (red) and that from the dEMG system (blue). The waveforms removed from each channel are plotted immediately below it, indicating the percent decrease in discharge times (Δ FIR). The bottom right and left graphs are the frequency-distributions curves of the interdischarge intervals (IDIs) before and after denoising, respectively. Likewise, the variance ratio (VR), the signal-to-noise ratio (SNR), and the cross-correlation coefficient (R_{xy}) between the calculated MU template using the dEMG discharge times and that from the dEMG system.

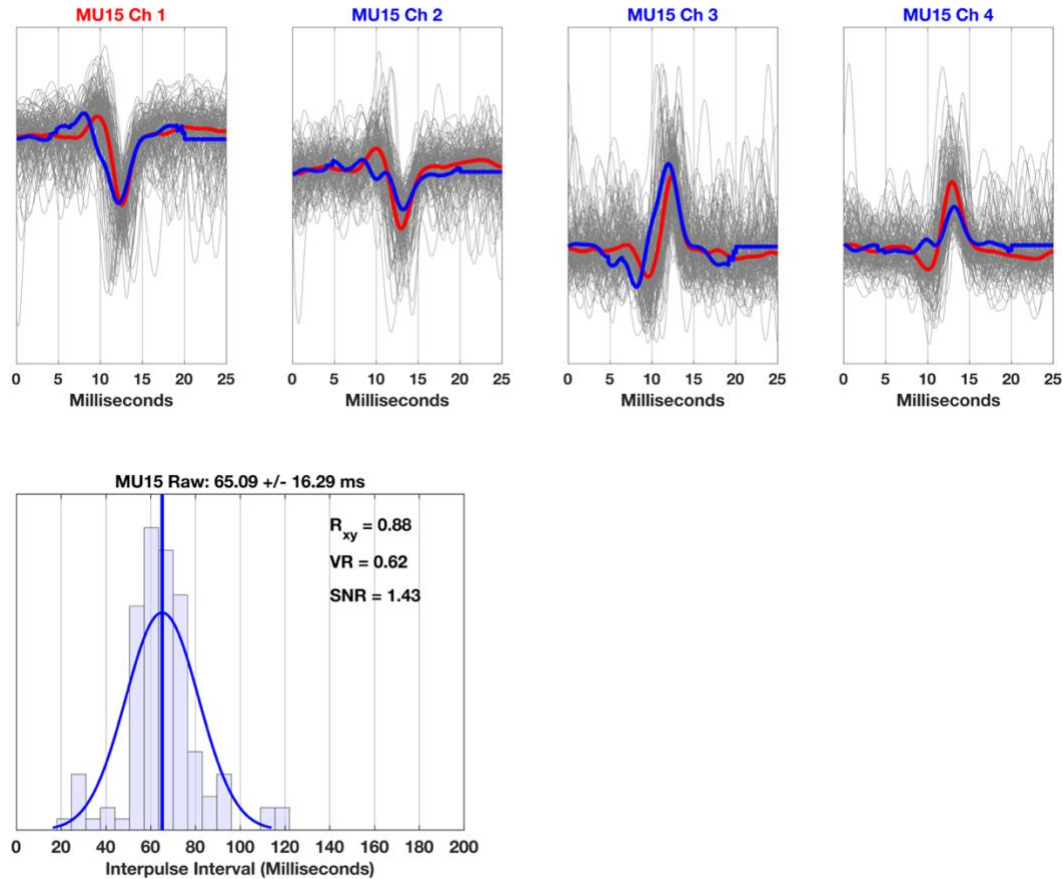


Figure 7. Representative example of the difference in shape between the calculated motor unit (MU) template using the dEMG discharge times and that from the dEMG system. The top panels are the shimmer plots, one for each channel. The shimmer plots include the MU templates calculated from the discharge times (red) and that from the dEMG system (blue). The bottom left graph is the frequency-distributions curve of the inter-discharge intervals (IDIs) before and after denoising, respectively. Likewise, the variance ratio (VR), the signal-to-noise ratio (SNR), and the cross-correlation coefficient (R_{xy}) between the calculated MU template using the dEMG discharge times and that from the dEMG system.

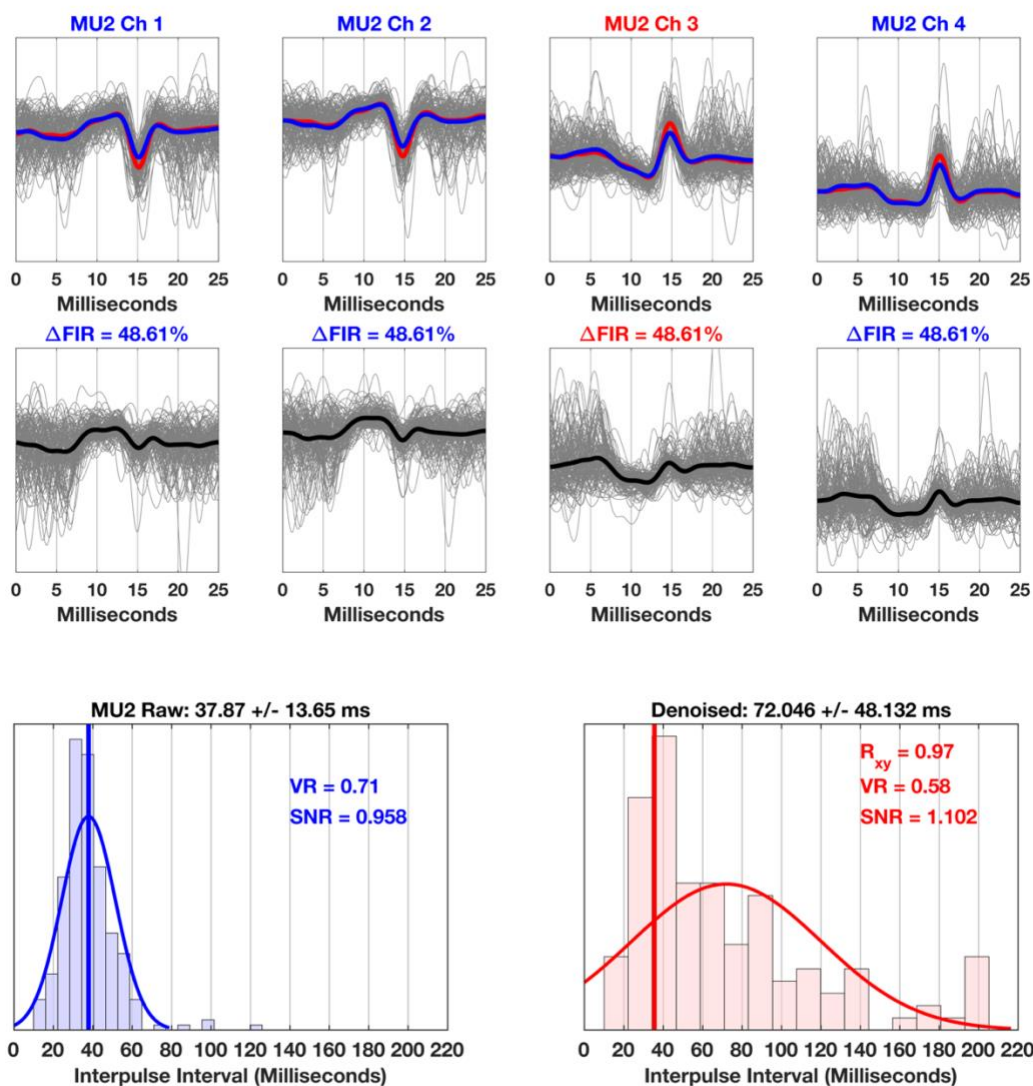


Figure 8. The effect of denoising on the calculated motor unit (MU) template. The top panels are the shimmer plots, one for each channel. The shimmer plots include the templates calculated from the ‘raw’ discharge times (red) and that after denoising (blue). The waveforms removed from each channel are plotted immediately below it, indicating the percent decrease in discharge times (Δ FIR). The bottom right and left graphs are the frequency-distribution curves of the interdischarge intervals (IDIs) before and after denoising, respectively. Likewise, the variance ratio (VR), the signal-to-noise ratio (SNR), and the cross-correlation coefficient (R_{xy}) between the calculated MU templates before and after denoising.

Study Variables

The following study variables were calculated on a two-second stable portion of the force trace, centered at the middle of the 60% contraction: (1) VR; (2) SNR, and (3) the cross-correlation (R_{xy}) between the calculate MU template and the template provide by the dEMG system (McManus, Hu, Rymer, Suresh, & Lowery, 2017). Across the 20 participants, there were 230 MUs per limb that met the criteria of having a VR of 0.75 or greater for a total of 920 MUs.

Statistics

Motor unit potential trains were studied in the dominant and non-dominant upper and lower limbs, across all four channels of the sEMG activity from the dEMG electrode, before and after denoising. A three-way (4-Limb \times 4-Channels \times 2-Denoise) randomized block factorial (RBF) analysis of variance (ANOVA) was therefore used to evaluate significant differences across limbs, channels, before and after denoising the MUPTs (Kirk, 2012). Orthogonal contrasts were used to further explore significant differences observed through the RBF ANOVA. The effect of denoising on the correlation between the VR and SNR was evaluated according to the procedures outlined by Raghunathan and colleagues (1996). When necessary, data transformations were applied to ensure normality and homogeneity of variances, as evaluated using probability plots and Levene's test, respectively (Bartlett, 1936; Berry, 1987; Hosken, Buss, & Hodgson, 2018). In the case of cross-correlation coefficients, Fisher's Z-transformations was applied prior to further statistical analysis (Silver & Dunlap, 1987).

Results

Figure 9 shows the cumulative probability curve for the three parameters used to denoise the MUPTs. In order, the frequency of adjustment from the initial values were: a standard deviation less than or equal to 1.0, a SNR of greater than 0.5 dB, and a cross-correlation coefficient greater than zero for 93% of the MUPTs. This parameter was highly sensitive to both noise and superpositions. When superpositions were identified in the residuals, the SNR and standard deviations were used to refine the inclusion criteria. In general, for denoising, the SNR for an individual MUP had to at least 0.5 for 70% of the MUPTs. The peak of an individual MUP had to be within 1.0 standard deviation of the location of the peak of the MUP template for 75% of the MUPTs. The dispersion of peaks within a MUPT was an average of 2.99 ± 3.76 ms, with a total range of 13.10 ms. These values were nearly identical across all four limbs, differing only in the second decimal place. There was a significant reduction in the overall number of firing times of 33.07% ($p < 0.05$), which was nearly identical across limbs.

The means and standard deviations for the criterion measures are presented in Table 1. There were no significant differences for changes in the VR across the four channels ($p < 0.05$). Denoising resulted in an overall 23.05% decrease in the variance ratio ($p < 0.05$). Although, the decrease in VR was greater for the upper limbs compared to the lower limbs ($p < 0.05$). The upper limbs had an average decrease of 21.07% while the lower limbs had a decrease of 16.35%. There was no significant difference for changes in the SNR across the four channels ($p > 0.05$). The SNR exhibited an overall increase of 11.67% ($p < 0.05$). There was, however, a significant difference in the increase in SNR between limbs ($p < 0.05$). Orthogonal contrasts revealed that the increase in SNR for the

dominant leg was 11.92% compared to 13.65% for the other three limbs, a difference which may be considered trivial.

A lower VR and a higher SNR for MUPs underlying a MU template should increase the quality of the template. It was there for interest to determine if denoising had an impact on the relationship between these two variables. Separate correlational analyses were performed for the upper and lower limbs on the relationship between the VR and the SNR due to the slight differential impact of denoising for the dominant leg. Figure 10 shows that the significant linear negative relationship between the VR and the SNR was observed for both upper ($r=-0.46$, $p<0.05$) and lower limbs ($r=-0.36$, $p<0.05$), as expected. Denoising resulted in a significant increase in the correlation ($r=-0.56$) for the FCR ($p<0.05$). In contrast, the increase to $r=-0.46$ for the TA failed to reach the 0.05 probability level ($p=0.26$).

The cross-correlation coefficient provided additional feedback when adjusting the parameters for the denoising algorithm. The goal was to prevent an appreciable reduction in the correlation between the calculated template and the dEMG template, or, if possible, to improve the correlation across all four channels. There were no significant differences for changes in the cross-correlation coefficient across the four channels ($p>0.05$). Inspection of the means and standard deviations in Table 1 shows alterations were not evident until the third decimal point. Overall, denoising resulted in a 0.15% change in the cross-correlation coefficient between the calculated MU template and that provided by the dEMG system ($p<0.05$). There also was a 1.33% difference in the overall cross-correlation coefficient for the upper versus lower limbs ($p<0.05$).

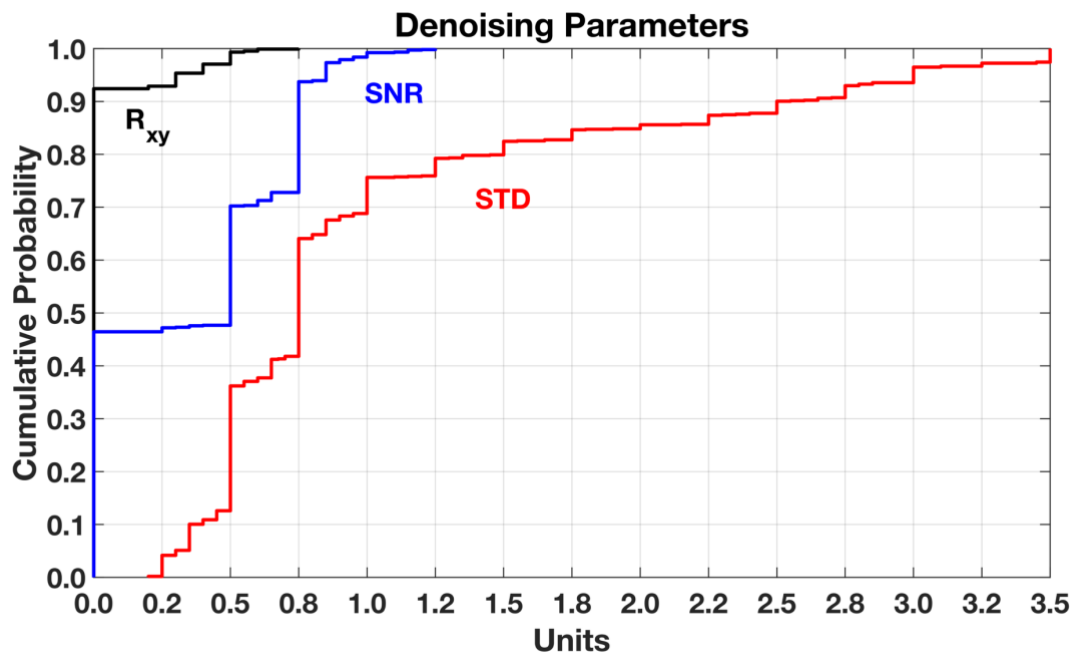


Figure 9. Cumulative probability curve for the denoising parameters used during the denoising process. Shown is cross-correlation (R_{xy}) between the individual motor unit potential (MUP) and the MUP template calculated by spike-trigger averaging the surface electromyographic signal from the discharge times (black), the signal-to-noise ratio (SNR) of the individual MUP (blue), and the standard deviation (STD) for the location of the MUP peaks contributing to the template ‘before’ denoising (red).

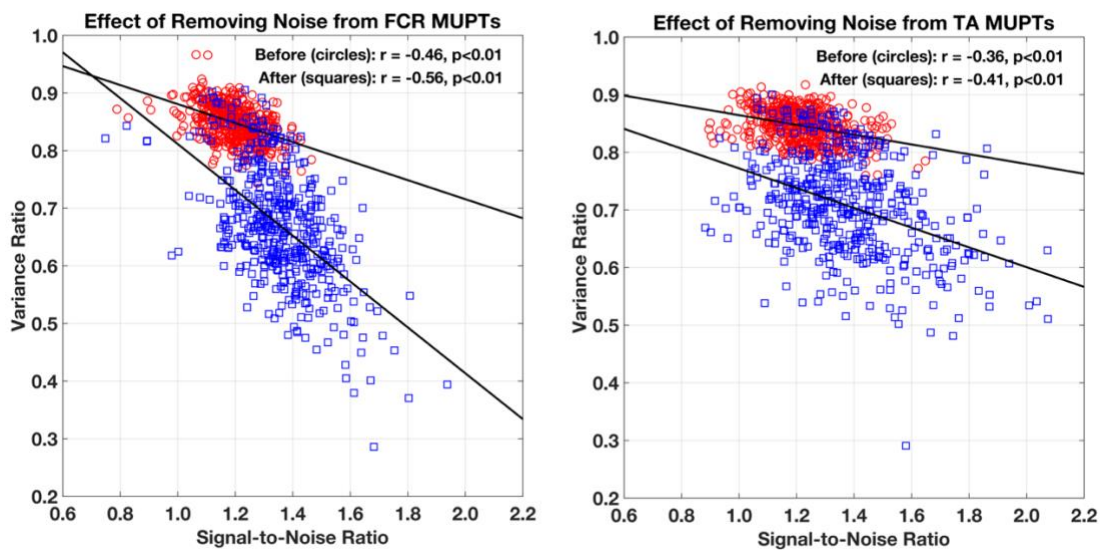


Figure 10. Relationship between the variance ratio (VR) and signal-to-noise ratio (SNR) before (red circles) and after denoising (blue squares), with the FCR on the left and the TA on the right.

Table 1. The means (M) and standard deviations (SD) for the variance ratio (VR), signal-to-noise ratio (SNR), the cross-correlation coefficient (R_{xy}) between the calculated motor unit template and that from the dEMG system, and the number of discharges (FIR) for each motor unit potential train for the dominant arm (D. Arm), non-dominant arm (N.D. Arm), dominant leg (D. Leg), and non-dominant (N.D Leg), before and after denoising. There were 230 motor units (MUs) per limb, for a total of N=920.

		D. Arm	N.D. Arm	D. Leg	N.D. Leg
		M \pm SD	M \pm SD	M \pm SD	M \pm SD
VR	Before	0.847 \pm 0.042	0.851 \pm 0.039	0.844 \pm 0.038	0.848 \pm 0.038
	After	0.666 \pm 0.116	0.673 \pm 0.118	0.703 \pm 0.106	0.712 \pm 0.111
SNR	Before	1.195 \pm 0.116	1.194 \pm 0.090	1.220 \pm 0.147	1.218 \pm 0.136
	After	1.359 \pm 0.188	1.353 \pm 0.151	1.365 \pm 0.240	1.388 \pm 0.258
R_{xy}	Before	0.898 \pm 0.073	0.892 \pm 0.080	0.879 \pm 0.085	0.887 \pm 0.083
	After	0.896 \pm 0.074	0.891 \pm 0.081	0.878 \pm 0.086	0.886 \pm 0.081
FIR	Before	122.25 \pm 56.92	122.14 \pm 48.85	122.70 \pm 46.96	124.27 \pm 47.75
	After	81.10 \pm 41.43	81.64 \pm 39.06	82.57 \pm 34.59	83.70 \pm 34.85

Discussion

Decomposition of the sEMG signal has been under constant scrutiny since its introduction. One reason is that the specific algorithms and software code are proprietary and part of commercially available system (Farina & Holobar, 2016; Nawab et al., 2010). In the absence of the original source code, emphasis has been placed on validating the MU discharge times obtained by sEMG decomposition methods (Farina & Enoka, 2011). The current approach was motivated by the work by Parsaei and Stashuk (2009) where validation of the MU discharge times associated with a MUPT is based on the shapes of the individual contributing MUPs. Parsaei and Stashuk (2009) perform their analysis *a priori* as part of their initial MU identification and creation of the calculation of its template. In contrast, the discharge times of MUPs contributing to the MUPT and its MU template are already provided. The denoising routine is a *posteriori* determination of validity based on removing discharge times associated with MUPs that do not ‘fit’ a data driven confidence interval for the specific MU template.

The data-driven confidence interval was based on the STA technique to create a MU template for the MUPT. First, MUP waveforms that were not positively correlated with the calculated template were removed. The waveform may be random noise or belong to another MU. In the case of superposition, the cross-correlation coefficient could be increased to separate the MUPs from two different MUPTs. Based on the present analysis, a cross-correlation coefficient of $R_{xy} > 0.0$ was sufficient for over 90% of the MUPTs. More recently McManus and colleagues (2017) remove firings from MUPs if they did not have an average correlation of 0.7 with the respective MU template. Their earlier work demonstrated that the a cross-correlation coefficient between the MU template obtained by discharge times versus STA was sensitive to errors in the discharge times (Hu, Rymer, & Suresh, 2013a). The cross-correlation coefficient was deemphasized

in the present work as it does not ‘entirely’ capture different aspects MUP variability, which is more than just shape.

Originally, it was thought that the SNR of the MU template could be used to set a threshold for MUPs belonging to a particular MUPT, however, this was not the case. The SNR has been used by other investigators for event detection during segmentation, where the EMG signal is broken down into non-overlapping segments of varying length to determine if a MUP exists against background noise (Florestal et al., 2006). Additionally, the SNR also determines the number of MUs that can be detected (Holobar, Farina, Gazzoni, Merletti, & Zazula, 2009). The ranges of SNRs reported are similar to values reported by Holobar and colleagues (2009), specifically for the sEMG signal decomposition but at much lower isometric force levels ($\approx 10\text{-}20\%$ MVC). The SNR was highly sensitive for the inclusion or exclusion of MUPs within a MUPT. Once a threshold was set, small increases would remove too many valid discharges. The 0.5 level was sufficient for 70% of the MUPTs.

The location of the MUP peak relative to that of the STA MU template was the most effective parameter for tuning the denoising process. The dispersion of peak locations within a MUPT is related to the variability in motor unit discharge times. Motor unit discharge statistics are a critical component of MU identification routines where the algorithm estimates the probability of MUP occurring at a specific location in the sEMG signal (De Luca et al., 2006). This may be one source of error in the observed discharge times. Motor unit discharge statistics are also used in an *a posteriori* fashion to determine the validity of MU identification technique, based on MUPT stability (Holobar, Minetto, Botter, Negro, & Farina, 2010). Once an event has been detected, an epoch of time (20 – 30 ms for sEMG signals) is used to determine whether the observed MUP belongs to a particular MUPT (Florestal et al., 2006). Errors in event detection, location of the MUP within the epoch, and normal physiologic variability in MU discharge rates interact to

contribute to scatter of MUP peaks contributing a template. It was observed that a 68% confidence interval (1 standard deviation) allowed for a high degree of selectivity for 75% of the MUPTs and was the most ‘tunable’ parameter, continually being adjusted thereafter (see Figure 8).

The scatter of peaks contributing to a MU template is related to the dispersion of waveforms which has a partial impact on the VR. The origins of this source of variability in MUP shape is different than the jiggle measure, which is used clinically to assess the integrity of the neuromuscular system (Campos et al., 2000). Computationally, the VR and jiggle are quite similar. While not a main focus of this pilot work, jiggle was calculated to determine its relationship with the VR. As expected, there was a correlation of $r=0.99$ ($p<0.05$). Thus, jiggle is another measure of MUP variability but is more directly linked with variability in motor unit discharge statistics (Abdelmaseeh, Smith, & Stashuk, 2014; Stålberg & Sonoo, 1994). Jiggle is also affected by variability in the innervation of muscle fibers contributing to the MU, termed “jitter”. Neuromuscular disorders can affect the innervation of individual muscle fibers within a MU, resulting in a large time difference ($>20 \mu\text{s}$) in the appearance of individual muscle fiber action potentials (Miralles, 2001)

It was expected and shown that denoising would have a significant impact on the VR and SNR, which are important variables for MU identification techniques (Florestal et al., 2006; Holobar et al., 2010; Parsaei & Stashuk, 2011, 2013). It is expected that MU templates associated with MUPs with that have lower VR and higher SNR, would facilitate the *a posteriori* classification of MU templates obtained by sEMG decomposition because motor units shapes can be quite similar (Holobar et al., 2009; Parsaei & Stashuk, 2009, 2011). The lack of significant differences across channels validates the strategy of using a single ‘target channel’ for denoising.

The impact of denoising on the SNR was slightly less for the dominant lower leg than the other three limbs. It is possible that the difference is not of practical significance due to the large sample size ($N=230$). However, it may reflect the fact that SNR for the TA of both legs was already significantly greater than that for the FCR of both arms, before denoising (2.0%, $p<0.05$). Regression analysis clearly showed that a higher initial SNR played a role on the impact of denoising on the relationship between VR and SNR. The change was not as great as that observed for the upper limb. One reason for the slightly higher SNR in the TA, may be due to a lower amount of subcutaneous tissue. Significant negative correlations have been observed between skin-fold thickness and root-mean-square sEMG amplitude (Gabriel & Kamen, 2009; Nordander et al., 2003). The literature is scant on this specific topic but there is evidence that, in males, the amount of subcutaneous tissue over the TA is slightly less (≈ 1 mm) than that over the FCR (Borkan & Norris, 1977; Garn, 1954). Difference in the distribution of subcutaneous tissue may be a factor to consider in future efforts.

References

- Abdelmaseeh, M., Smith, B., & Stashuk, D. (2014). Feature selection for motor unit potential train characterization: Feature Selection for MUPT Characterization. *Muscle & Nerve*, *49*(5), 680–690. <https://doi.org/10.1002/mus.23977>
- Arendt-Nielsen, L., & Zwarts, M. (1989). Measurement of muscle fiber conduction velocity in humans: techniques and applications. *Journal of Clinical Neurophysiology: Official Publication of the American Electroencephalographic Society*, *6*(2), 173–190.
- Bartlett, M. S. (1936). The Square Root Transformation in Analysis of Variance. *Supplement to the Journal of the Royal Statistical Society*, *3*(1), 68–78. <https://doi.org/10.2307/2983678>
- Berry, D. A. (1987). Logarithmic Transformations in ANOVA. *Biometrics*, *43*(2), 439–456. <https://doi.org/10.2307/2531826>
- Borkan, G. A., & Norris, A. H. (1977). Fat Redistribution and the Changing Body Dimensions of the Adult Male. *Human Biology; Baltimore*, *49*(3), 495–514.
- Campos, C., Malanda, A., Gila, L., Segura, V., Lasanta, I., & Artieda, J. (2000). Quantification of jiggle in real electromyographic signals. *Muscle & Nerve*, *23*(7), 1022–1034. [https://doi.org/10.1002/1097-4598\(200007\)23:7<1022::AID-MUS4>3.0.CO;2-3](https://doi.org/10.1002/1097-4598(200007)23:7<1022::AID-MUS4>3.0.CO;2-3)
- Christie, A., Lester, S., LaPierre, D., & Gabriel, D. A. (2004). Reliability of a new measure of H-reflex excitability. *Clinical Neurophysiology: Official Journal of the International Federation of Clinical Neurophysiology*, *115*(1), 116–123.

- Davila, C. E., & Mobin, M. S. (1992). Weighted averaging of evoked potentials. *IEEE Transactions on Biomedical Engineering*, *39*(4), 338–345.
- De Luca, C. J., Adam, A., Wotiz, R., Gilmore, L. D., & Nawab, S. H. (2006). Decomposition of Surface EMG Signals. *Journal of Neurophysiology*, *96*(3), 1646–1657. <https://doi.org/10.1152/jn.00009.2006>
- De Luca, C. J., Nawab, S. H., & Kline, J. C. (2015). Clarification of methods used to validate surface EMG decomposition algorithms as described by Farina et al. (2014). *Journal of Applied Physiology*, *118*(8), 1084–1084. <https://doi.org/10.1152/jappphysiol.00061.2015>
- Dorfman, L. J., Howard, J. E., & McGill, K. C. (1989). Motor unit firing rates and firing rate variability in the detection of neuromuscular disorders. *Electroencephalography and Clinical Neurophysiology*, *73*(3), 215–224. [https://doi.org/10.1016/0013-4694\(89\)90122-3](https://doi.org/10.1016/0013-4694(89)90122-3)
- Farina, D., & Enoka, R. M. (2011). Surface EMG decomposition requires an appropriate validation. *Journal of Neurophysiology*, *105*(2), 981–982.
- Farina, D., & Holobar, A. (2016). Characterization of Human Motor Units From Surface EMG Decomposition. *Proceedings of the IEEE*, *104*(2), 353–373. <https://doi.org/10.1109/JPROC.2015.2498665>
- Farina, D., Holobar, A., Merletti, R., & Enoka, R. M. (2010). Decoding the neural drive to muscles from the surface electromyogram. *Clinical Neurophysiology*, *121*(10), 1616–1623. <https://doi.org/10.1016/j.clinph.2009.10.040>
- Farina, D., Merletti, R., & Enoka, R. M. (2015). Reply to De Luca, Nawab, and Kline: The proposed method to validate surface EMG signal decomposition remains

problematic. *Journal of Applied Physiology*, 118(8), 1085–1085.

<https://doi.org/10.1152/jappphysiol.00107.2015>

Florestal, J. R., Mathieu, P. A., & Malanda, A. (2006). Automated decomposition of intramuscular electromyographic signals. *IEEE Transactions on Biomedical Engineering*, 53(5), 832–839. <https://doi.org/10.1109/TBME.2005.863893>

Gabriel, D. A., & Kamen, G. (2009). Experimental and modeling investigation of spectral compression of biceps brachii SEMG activity with increasing force levels. *Journal of Electromyography and Kinesiology: Official Journal of the International Society of Electrophysiological Kinesiology*, 19(3), 437–448. <https://doi.org/10.1016/j.jelekin.2007.10.009>

Gabriel, D. A., Lester, S. M., Lenhardt, S. A., & Cambridge, E. D. J. (2007). Analysis of surface EMG spike shape across different levels of isometric force. *Journal of Neuroscience Methods*, 159(1), 146–152. <https://doi.org/10.1016/j.jneumeth.2006.07.004>

Garn, S. M. (1954). Fat Patterning and Fat Intercorrelations in the Adult Male. *Human Biology; Baltimore*, 26(1), 59–69.

Green, L. A., & Gabriel, D. A. (2018). The cross education of strength and skill following unilateral strength training in the upper and lower limbs. *Journal of Neurophysiology*, 120(2), 468–479. <https://doi.org/10.1152/jn.00116.2018>

Green, L. A., McGuire, J., & Gabriel, D. A. (2015). Flexor carpi radialis surface electromyography electrode placement for evoked and voluntary measures. *Muscle & Nerve*, 52(5), 818–825. <https://doi.org/10.1002/mus.24631>

- Holobar, A., & Farina, D. (2014). Blind source identification from the multichannel surface electromyogram. *Physiological Measurement*, *35*(7), R143–R165.
<https://doi.org/10.1088/0967-3334/35/7/R143>
- Holobar, A., Farina, D., Gazzoni, M., Merletti, R., & Zazula, D. (2009). Estimating motor unit discharge patterns from high-density surface electromyogram. *Clinical Neurophysiology*, *120*(3), 551–562.
- Holobar, A., Minetto, M. A., Botter, A., Negro, F., & Farina, D. (2010). Experimental Analysis of Accuracy in the Identification of Motor Unit Spike Trains From High-Density Surface EMG. *IEEE Transactions on Neural Systems and Rehabilitation Engineering*, *18*(3), 221–229. <https://doi.org/10.1109/TNSRE.2010.2041593>
- Hosken, D. J., Buss, D. L., & Hodgson, D. J. (2018). Beware the F test (or, how to compare variances). *Animal Behaviour*, *136*, 119–126.
<https://doi.org/10.1016/j.anbehav.2017.12.014>
- Hu, X., Rymer, W. Z., & Suresh, N. L. (2013a). Assessment of validity of a high-yield surface electromyogram decomposition. *Journal of Neuroengineering and Rehabilitation*, *10*, 99. <https://doi.org/10.1186/1743-0003-10-99>
- Hu, X., Rymer, W. Z., & Suresh, N. L. (2013b). Motor unit pool organization examined via spike-triggered averaging of the surface electromyogram. *Journal of Neurophysiology*, *110*(5), 1205–1220. <https://doi.org/10.1152/jn.00301.2012>
- Hu, X., Rymer, W. Z., & Suresh, N. L. (2014). Accuracy assessment of a surface electromyogram decomposition system in human first dorsal interosseus muscle. *Journal of Neural Engineering*, *11*(2), 026007. <https://doi.org/10.1088/1741-2560/11/2/026007>

- Kirk, R. E. (2012). *Experimental Design: Procedures for the Behavioral Sciences: Procedures for the Behavioral Sciences*. SAGE.
- Lefever, R. S., & De Luca, C. J. (1982). A Procedure for Decomposing the Myoelectric Signal Into Its Constituent Action Potentials - Part I: Technique, Theory, and Implementation. *IEEE Transactions on Biomedical Engineering, BME-29*(3), 149.
- Lenhardt, S. A. (2009). *The surface electromyography-force relationship during isometric dorsiflexion in males and females*. Retrieved from <http://dr.library.brocku.ca/handle/10464/1630>
- McManus, L., Hu, X., Rymer, W. Z., Suresh, N. L., & Lowery, M. M. (2017). Motor Unit Activity during Fatiguing Isometric Muscle Contraction in Hemispheric Stroke Survivors. *Frontiers in Human Neuroscience, 11*.
<https://doi.org/10.3389/fnhum.2017.00569>
- Miralles, F. (2001). Computer simulation of jitter phenomenon in neuromuscular transmission disorders. *Muscle & Nerve, 24*(12), 1635–1646.
<https://doi.org/10.1002/mus.1199>
- Nawab, S. H., Chang, S.-S., & De Luca, C. J. (2010). High-yield decomposition of surface EMG signals. *Clinical Neurophysiology, 121*(10), 1602–1615.
<https://doi.org/10.1016/j.clinph.2009.11.092>
- Nawab, S. H., Wotiz, R. P., & De Luca, C. J. (2008). Decomposition of indwelling EMG signals. *Journal of Applied Physiology (Bethesda, Md.: 1985), 105*(2), 700–710.
<https://doi.org/10.1152/jappphysiol.00170.2007>

- Nordander, C., Willner, J., Hansson, G., Larsson, B., Unge, J., Granquist, L., & Skerfving, S. (2003). Influence of the subcutaneous fat layer, as measured by ultrasound, skinfold calipers and BMI, on the EMG amplitude. *European Journal of Applied Physiology*, *89*(6), 514–519. <https://doi.org/10.1007/s00421-003-0819-1>
- Parsaei, H., & Stashuk, D. W. (2009, September). *MUP shape-based validation of a motor unit potential train*. 2551–2554. <https://doi.org/10.1109/IEMBS.2009.5334758>
- Parsaei, H., & Stashuk, D. W. (2011). Adaptive motor unit potential train validation using MUP shape information. *Medical Engineering & Physics*, *33*(5), 581–589. <https://doi.org/10.1016/j.medengphy.2010.12.012>
- Parsaei, H., & Stashuk, D. W. (2013). EMG Signal Decomposition Using Motor Unit Potential Train Validity. *IEEE Transactions on Neural Systems and Rehabilitation Engineering*, *21*(2), 265–274. <https://doi.org/10.1109/TNSRE.2012.2218287>
- Raghuathan, T. E., Rosenthal, R., & Rubin, D. B. (1996). Comparing correlated but nonoverlapping correlations. *Psychological Methods*, *1*(2), 178–183. <https://doi.org/10.1037/1082-989X.1.2.178>
- Silver, N. C., & Dunlap, W. P. (1987). Averaging correlation coefficients: should Fisher's z transformation be used? *Journal of Applied Psychology*, *72*(1), 146.
- Stålberg, E., Ekstedt, J., & Broman, A. (1971). The electromyographic jitter in normal human muscles. *Electroencephalography and Clinical Neurophysiology*, *31*(5), 429–438. [https://doi.org/10.1016/0013-4694\(71\)90164-7](https://doi.org/10.1016/0013-4694(71)90164-7)

- Stålberg, E. V., & Sonoo, M. (1994). Assessment of variability in the shape of the motor unit action potential, the “jiggle,” at consecutive discharges. *Muscle & Nerve*, *17*(10), 1135–1144. <https://doi.org/10.1002/mus.880171003>
- Stashuk, D. W. (2001). EMG signal decomposition: how can it be accomplished and used? *Journal of Electromyography and Kinesiology*, *11*(3), 151–173.

Appendix 2 – Ethics Clearance



Brock University
 Research Ethics Office
 Tel: 905-688-5550 ext. 3035
 Email: reb@brocku.ca

Bioscience Research Ethics Board

Certificate of Ethics Clearance for Human Participant Research

DATE: 5/1/2018
 PRINCIPAL INVESTIGATOR: GABRIEL, David - Kinesiology
 FILE: 16-313 - GABRIEL
 TYPE: Masters Thesis/Project STUDENT: SUPERVISOR: David Gabriel
 TITLE: Validation of a surface EMG decomposition algorithm for motor unit identification

ETHICS CLEARANCE GRANTED

Type of Clearance: RENEWAL Initial Clearance Date: 5/24/2017
 Expiry Date: 5/1/2019

The Brock University Bioscience Research Ethics Board has reviewed the above named research proposal and considers the procedures, as described by the applicant, to conform to the University's ethical standards and the Tri-Council Policy Statement.

Renewed certificate valid from **5/1/2018 to 5/1/2019**.

The Tri-Council Policy Statement requires that ongoing research be monitored by, at a minimum, an annual report. Should your project extend beyond the expiry date, you are required to submit a Renewal form before **5/1/2019**. Continued clearance is contingent on timely submission of reports.

To comply with the Tri-Council Policy Statement, you must also submit a final report upon completion of your project. All report forms can be found on the Research Ethics web page at <http://www.brocku.ca/research/policies-and-forms/research-forms>.

In addition, throughout your research, you must report promptly to the REB:

- a) Changes increasing the risk to the participant(s) and/or affecting significantly the conduct of the study;
- b) All adverse and/or unanticipated experiences or events that may have real or potential unfavourable implications for participants;
- c) New information that may adversely affect the safety of the participants or the conduct of the study;
- d) Any changes in your source of funding or new funding to a previously unfunded project.

We wish you success with your research.

Approved:

 Stephen Cheung, Chair
 Bioscience Research Ethics Board

Note: Brock University is accountable for the research carried out in its own jurisdiction or under its auspices and may refuse certain research even though the REB has found it ethically acceptable.

If research participants are in the care of a health facility, at a school, or other institution or community organization, it is the responsibility of the Principal Investigator to ensure that the ethical guidelines and clearance of those facilities or institutions are obtained and filed with the REB prior to the initiation of research at that site.



Brock University
 Research Ethics Office
 Tel: 905-688-5550 ext. 3035
 Email: reb@brocku.ca

Bioscience Research Ethics Board

Certificate of Ethics Clearance for Human Participant Research

DATE: 5/1/2018
 PRINCIPAL INVESTIGATOR: GABRIEL, David - Kinesiology
 FILE: 16-313 - GABRIEL
 TYPE: Masters Thesis/Project STUDENT: David Gabriel
 SUPERVISOR: David Gabriel
 TITLE: Validation of a surface EMG decomposition algorithm for motor unit identification

ETHICS CLEARANCE GRANTED

Type of Clearance: RENEWAL	Initial Clearance Date: 5/24/2017 Expiry Date: 5/1/2019
----------------------------	--

The Brock University Bioscience Research Ethics Board has reviewed the above named research proposal and considers the procedures, as described by the applicant, to conform to the University's ethical standards and the Tri-Council Policy Statement.

Renewed certificate valid from **5/1/2018 to 5/1/2019**.

The Tri-Council Policy Statement requires that ongoing research be monitored by, at a minimum, an annual report. Should your project extend beyond the expiry date, you are required to submit a Renewal form before **5/1/2019**. Continued clearance is contingent on timely submission of reports.

To comply with the Tri-Council Policy Statement, you must also submit a final report upon completion of your project. All report forms can be found on the Research Ethics web page at <http://www.brocku.ca/research/policies-and-forms/research-forms>.

In addition, throughout your research, you must report promptly to the REB:

- a) Changes increasing the risk to the participant(s) and/or affecting significantly the conduct of the study;
- b) All adverse and/or unanticipated experiences or events that may have real or potential unfavourable implications for participants;
- c) New information that may adversely affect the safety of the participants or the conduct of the study;
- d) Any changes in your source of funding or new funding to a previously unfunded project.

We wish you success with your research.

Approved:

 Stephen Cheung, Chair
 Bioscience Research Ethics Board

Note: Brock University is accountable for the research carried out in its own jurisdiction or under its auspices and may refuse certain research even though the REB has found it ethically acceptable.

If research participants are in the care of a health facility, at a school, or other institution or community organization, it is the responsibility of the Principal Investigator to ensure that the ethical guidelines and clearance of those facilities or institutions are obtained and filed with the REB prior to the initiation of research at that site.